

**POLITECNICO DI MILANO**

**Corso di Laurea Specialistica in  
Ingegneria Aeronautica**



**Development of a simplified rotor model  
and integration in a flight simulator code**

Relatore: Prof. Lorenzo Trainelli

Correlatore: Ing. Riccardo Bianco Mengotti

Tesi di laurea di

Lorenzo MASELLIS  
matr. 724782

Anno Accademico 2010 - 2011

2011 © *Lorenzo Masellis* - [lorenzo@masellis.eu](mailto:lorenzo@masellis.eu)

Masellis, Lorenzo <1981>

Development of a simplified rotor model and integration in a flight simulator code / Lorenzo Masellis ; rel. Lorenzo Trainelli ; correl. Riccardo Bianco Mengotti. Milano : Politecnico di Milano, 2010/11. - 1 v. : xiii, 118 pag., ill., 30 cm

(Scuola di Ingegneria Industriale - Bovisa - Corso di laurea specialistica in ingegneria aeronautica - Sessione Dicembre 2011)

CDD 629.133352

*Non chi comincia  
ma quel che persevera*



Vorrei ringraziare il Prof. Lorenzo Trainelli e l'Ing. Riccardo Bianco Mengotti per avermi dato l'opportunità di realizzare questo lavoro, permettendomi al contempo di sperimentare, durante il periodo di *stage* presso *AgustaWestland*, la piú valida esperienza formativa di tutta la mia carriera universitaria. Spero di aver dimostrato di meritare la fiducia che mi é stata accordata.

Al Dr. Ing. Francesco Scorcelletti é riservato un ringraziamento speciale per la competenza, la costanza e soprattutto la pazienza con cui ha quotidianamente indirizzato e seguito il mio lavoro durante lo *stage* e per l'attenzione dedicata durante la redazione della tesi e dell'articolo presentato alla *Pegasus-AIAA Student Conference*.

A tutte le ragazze ed i ragazzi degli uffici *Meccanica del Volo* e *Carichi* di *AgustaWestland*, grazie della simpatia con cui mi avete accolto; in particolare ringrazio l'Ing. Valentina Giuliani, la cui disponibilitá fin dai primi contatti mi ha aiutato a fare il primo passo per la realizzazione di questo lavoro.

Un sincero ringraziamento per avermi accompagnato nella lunga stagione formativa della mia vita va ai miei genitori ed a mia sorella, ed anche al piccolo Matteo che, inconsapevole, mi ha insegnato a guardare al futuro.

Ma il contributo piú grande al percorso che si conclude con questa tesi é stato sicuramente quello della persona che, piú di tutti, ne ha condiviso giorno per giorno fatiche e soddisfazioni, senza mai farmi mancare il suo sostegno: a lei, ad Anita, é dedicato questo lavoro.



# Contents

<b>Contents</b>	<b>vii</b>
<b>List of Figures</b>	<b>ix</b>
<b>Abstract</b>	<b>xiii</b>
<b>Introduction</b>	<b>1</b>
<b>1 Review of NFpath formulations</b>	<b>3</b>
1.1 Code description and assumptions . . . . .	3
1.2 Formulation of model components . . . . .	4
1.3 Trim procedure . . . . .	15
1.4 Direct snapshot procedure . . . . .	22
1.5 Simplified re-implementation of the model . . . . .	24
<b>2 Implementation of an algebraic rotor model</b>	<b>37</b>
2.1 Scope . . . . .	37
2.2 Methodology and tools . . . . .	38
2.3 Model description . . . . .	38
2.4 Limitations and foreseen developments . . . . .	54
<b>3 Integration of a complete rotorcraft model</b>	<b>57</b>
3.1 Scope . . . . .	57
3.2 Methodology and tools . . . . .	57
3.3 Model description . . . . .	58
3.4 Implementation . . . . .	64
3.5 Limitations and foreseen developments . . . . .	66
<b>4 Numerical results</b>	<b>69</b>
4.1 Trim analysis . . . . .	70
4.2 Validation of components . . . . .	73
4.3 Analysis of the ground effect model . . . . .	79

<b>Conclusions</b>	<b>97</b>
<b>A Numerical methods</b>	<b>99</b>
A.1 Polynomial solution for the inflow . . . . .	99
A.2 Broyden's method . . . . .	104
<b>B Reference systems</b>	<b>107</b>
B.1 Inertial frame . . . . .	107
B.2 Design frame . . . . .	107
B.3 Body frame . . . . .	107
B.4 Shaft-body frame . . . . .	110
B.5 Shaft-wind frame . . . . .	111
B.6 Shaft frame . . . . .	111
B.7 Tip-path plane frame, flapping and blade pitch . . . . .	111
<b>Nomenclature</b>	<b>113</b>
Symbols . . . . .	113
Acronyms and abbreviations . . . . .	114
<b>Bibliography</b>	<b>117</b>



# List of Figures

1.1	Overview of forces, lateral view . . . . .	15
1.2	Overview of forces, rear view . . . . .	16
1.3	Trim procedure algorithm overview . . . . .	16
1.4	Direct snapshot algorithm overview . . . . .	23
1.5	Overview of the reimplemented algorithm for the rotor model . . . . .	26
1.6	Overview of the reimplemented algorithm for the rotorcraft model . . . . .	26
1.7	Control time history, hover test case . . . . .	29
1.8	Coning, hover test case . . . . .	29
1.9	Longitudinal flapping, hover test case . . . . .	30
1.10	Lateral flapping, hover test case . . . . .	30
1.11	Thrust, hover test case . . . . .	31
1.12	H-force, hover test case . . . . .	31
1.13	Pitching control moment, hover test case . . . . .	32
1.14	Induced velocity, hover test case . . . . .	32
1.15	Control time history, $\mu = 0.34$ test case . . . . .	33
1.16	Coning, $\mu = 0.34$ test case . . . . .	33
1.17	Longitudinal flapping, $\mu = 0.34$ test case . . . . .	34
1.18	Lateral flapping, $\mu = 0.34$ test case . . . . .	34
1.19	Thrust, $\mu = 0.34$ test case . . . . .	35
1.20	H-force, $\mu = 0.34$ test case . . . . .	35
1.21	Pitching control moment, $\mu = 0.34$ test case . . . . .	36
1.22	Induced velocity, $\mu = 0.34$ test case . . . . .	36
2.1	Overview of the rotor model algorithm . . . . .	39
2.2	Induced velocity from actuator disc theory . . . . .	45
2.3	Induced velocity with vortex ring state . . . . .	45
2.4	Vortex ring state: difference with NFpath . . . . .	46
2.5	Vortex ring state: difference with actuator disc . . . . .	46
2.6	Experimental Curtiss-Sun diagram with interpolations . . . . .	48
2.7	Ground effect coefficient . . . . .	49
3.1	Rotorcraft model architecture . . . . .	64

3.2	Framework architecture . . . . .	66
4.1	Attitude Euler's angles in trim as a function of horizontal speed . . . . .	71
4.2	Control angles in trim as a function of horizontal speed . . . . .	71
4.3	Flapping angles in trim as a function of horizontal speed . . . . .	72
4.4	Shaft power in trim as a function of horizontal speed . . . . .	72
4.5	Main rotor forces resulting from NFpath trimmed attitude and controls . . . . .	74
4.6	Main rotor moments resulting from NFpath trimmed attitude and controls . . . . .	74
4.7	Main rotor flapping angles resulting from Camrad trimmed attitude and controls . . . . .	75
4.8	Main rotor torque required resulting from Camrad trimmed attitude and controls . . . . .	75
4.9	Main rotor forces resulting from Camrad trimmed attitude and controls . . . . .	76
4.10	Main rotor moments resulting from Camrad trimmed attitude and controls . . . . .	76
4.11	Tail rotor flapping angles resulting from Camrad trimmed attitude and controls . . . . .	77
4.12	Tail rotor torque required resulting from Camrad trimmed attitude and controls . . . . .	77
4.13	Tail rotor forces resulting from Camrad trimmed attitude and controls . . . . .	78
4.14	Tail rotor moments resulting from Camrad trimmed attitude and controls . . . . .	78
4.15	Gravity forces resulting from Camrad trimmed attitude and controls . . . . .	80
4.16	Gravity moments resulting from Camrad trimmed attitude and controls . . . . .	80
4.17	Fuselage angle of attack resulting from NFpath trimmed attitude and controls . . . . .	81
4.18	Fuselage forces resulting from NFpath trimmed attitude and controls . . . . .	81
4.19	Fuselage moments resulting from NFpath trimmed attitude and controls . . . . .	82
4.20	Fuselage Angle of attack resulting from Camrad trimmed attitude and controls . . . . .	82
4.21	Fuselage forces resulting from Camrad trimmed attitude and controls . . . . .	83
4.22	Fuselage moments resulting from Camrad trimmed attitude and controls . . . . .	83

4.23	Horizontal tail angle of attack resulting from NFpath trimmed attitude and controls . . . . .	84
4.24	Horizontal tail lift and drag resulting from NFpath trimmed attitude and controls . . . . .	84
4.25	Horizontal tail forces resulting from NFpath trimmed attitude and controls . . . . .	85
4.26	Horizontal tail moments resulting from NFpath trimmed attitude and controls . . . . .	85
4.27	Horizontal and vertical tail angle of attack resulting from Camrad trimmed attitude and controls . . . . .	86
4.28	Horizontal tail forces resulting from Camrad trimmed attitude and controls . . . . .	86
4.29	Horizontal tail moments resulting from Camrad trimmed attitude and controls . . . . .	87
4.30	Vertical tail forces resulting from Camrad trimmed attitude and controls . . . . .	87
4.31	Vertical tail moments resulting from Camrad trimmed attitude and controls . . . . .	89
4.32	Thrust coefficient versus advance ratio at constant attitude and controls . . . . .	89
4.33	Trimmed attitude versus horizontal speed in ground effect . . . . .	90
4.34	Trimmed flapping angles versus horizontal speed in ground effect . . . . .	90
4.35	Trimmed shaft power versus horizontal speed in ground effect . . . . .	91
4.36	Trimmed controls versus horizontal speed in ground effect . . . . .	91
4.37	Trimmed induced velocity versus horizontal speed in ground effect . . . . .	93
4.38	Trimmed attitude versus ground altitude, hovering . . . . .	93
4.39	Trimmed flapping angles versus ground altitude, hovering . . . . .	94
4.40	Trimmed shaft power versus ground altitude, hovering . . . . .	94
4.41	Trimmed controls versus ground altitude, hovering . . . . .	95
4.42	Trimmed induced velocity versus ground altitude, hovering . . . . .	95
A.1	Induced velocity polynomial residual for $\alpha_{\text{TPP}} = -\pi/2$ . . . . .	100
A.2	Induced velocity polynomial residual for $\alpha_{\text{TPP}} = -\pi/4$ . . . . .	100
A.3	Induced velocity polynomial residual for $\alpha_{\text{TPP}} = 0$ . . . . .	101
A.4	Induced velocity polynomial residual for $\alpha_{\text{TPP}} = \pi/4$ . . . . .	101
A.5	Induced velocity polynomial residual for $\alpha_{\text{TPP}} = \pi/2 - 0.1$ . . . . .	102
A.6	Induced velocity polynomial residual for $\alpha_{\text{TPP}} = \pi/2$ . . . . .	102
B.1	Overview of the main reference frames . . . . .	108
B.2	Main reference frames, lateral view . . . . .	108
B.3	Flapping angles, lateral view . . . . .	109

B.4	Flapping angles, rear view . . . . .	109
B.5	Relationship between shaft-body and shaft-wind reference systems	110

# Abstract

After extensive analysis of an existing rotorcraft simulation code, a new algebraic rotor model was developed, based on quasi-steady flapping motion, closed-form equations, and a polynomial expression of the induced velocity according to the actuator disc theory, also including empirical models of the vortex ring state and of the ground effect derived from experimental evidence. The model core reduces to a set of three non linear equations which are solved numerically. It includes coordinate transformations that extend the validity of the model for a generic three-dimensional orientation of the rotor with reference to the airspeed vector. The new rotor model was integrated in a comprehensive rotorcraft simulation framework and extensive testing and comparison against other codes was performed.

**Keywords:** Rotorcraft, Helicopter, Algebraic rotor model.

---

# Sommario

Dopo una dettagliata analisi di un codice di simulazione elicotteristica esistente, si è sviluppato un nuovo modello algebrico di rotore basato su un modello di flappeggio quasi-stazionario, su equazioni in forma chiusa e su un'espressione polinomiale della velocità indotta, secondo la teoria del disco attuatore, includendo anche modelli empirici della condizione di anello vorticoso e dell'effetto suolo, derivati da evidenze sperimentali. Il nucleo del modello si riduce ad un sistema di tre equazioni non lineari, risolvibili numericamente. Sono incluse le trasformazioni di coordinate che estendono la validità del modello per una generica orientazione tridimensionale del rotore rispetto al vettore della velocità relativa all'aria. Il nuovo modello è stato integrato in un ambiente di simulazione per velivoli ad ala rotante ed è stato sottoposto ad una estesa campagna di prove, anche comparative rispetto ad altri codici.

**Parole chiave:** Ala rotante, Elicottero, Rotore algebrico.



# Introduction

Flight mechanics modelling is an essential task in the aerospace design process and rotorcraft make no exception. In the case of fixed-wing aircraft, it is possible to analytically describe flight mechanics with relative ease and, under appropriate hypotheses, simplify and decouple the equations, while preserving a significant fidelity level. Rotorcraft, unfortunately, are much more complex and their behaviour shows tight couplings, so that they are less prone to be described accurately by the means of simple analytical relationships. As a consequence of this complexity, numerical modelling and simulation are very important even in the early stages of the design process and enable basic tasks such as trim calculation.

It is easy to understand that the main challenge in modelling a rotorcraft is obtaining an accurate estimate of forces produced by the rotor as a function of flight conditions and rotor controls. An accurate description of a rotor implies in-depth mechanics and aerodynamic concepts in order to represent on one hand the blade relative DOFs (i.e. flapping and lead-lag motions), as well as its flexibility properties, while reproducing, on the other hand, the complex fully unsteady aerodynamic flow-field around the rotor. Moreover, the two problems, mechanics and aerodynamics, need typically to be solved iteratively due to aero-elastic couplings. This description, of course, must be significantly simplified in order to be of any practical use in the field of flight mechanics.

Several different approaches are possible for aerodynamic modelling: the first and simplest option involves the use of an inflow model derived from the *actuator disc theory*, the description of the blade trajectory in terms of a truncated Fourier series, the spanwise analytical integration of aerodynamic loads and the averaging along the rotation, that result in closed-form algebraic expressions for rotor forces [23]. A more detailed model can be obtained by using the *blade element theory* [21] in order to numerically integrate the aerodynamic loads, thus allowing complex blade geometries and the reproduction of non linear effects and blade vortex interaction. Beyond this level, methods are available, that can widely vary in sophistication and can reach the complexity of a full-blown CFD model.

The latter approach is generally too complex for the purposes of flight dynamics modelling, due to the combined requirements of a very high computational cost and of a detailed description of the problem. Of the first two approaches, the one based on the *blade element theory* is nowadays considered as the state-of-art and widely used, due to the increased availability of computational resources.

The main scope of the work here presented is to recover the first, simpler approach of an algebraic rotor model, reimplement it in a generalised form and show that it can be efficiently and effectively used for modelling rotor forces. This model would provide a useful tool for flight mechanics analysis, especially in the early design phases, when only a small subset of parameters are considered in order to describe the rotor.

As described in chapter 1, modelling formulations used in the *Agusta-Westland* in-house flight mechanics code *NFpath* were reviewed. These formulations were traced to their sources in literature in order to establish a clear system of algebraic expressions, together with the hypotheses they are rely on, which represent a proven model, well suited as a starting point for further development.

Chapter 2 describes a new implementation of a rotor model mainly based on the previously reviewed formulations; the model was generalised in order to relax some of the hypotheses, especially by removing the previous limitation to longitudinal motion. This resulted in a general purpose rotor model for three-dimensional motion [14]. Also the modelling of ground effect was the object of further attention. A significant effort was dedicated to ensuring the numerical robustness of the solver.

The so obtained rotor model was then integrated into a wider framework for full rotorcraft simulation, which includes models for fuselage and aerodynamic appendages. This part of the work is described in chapter 3.

Both the rotor model and the complete rotorcraft model were the object of extensive test that allowed an evaluation of their performance in comparison to the original *NFpath* code and to the more complex *CAMRAD* code. These evaluations are described in chapter 4.



# Chapter 1

## Review of NFpath formulations

### 1.1 Code description and assumptions

*NFpath* is a proprietary helicopter flight mechanics code, developed and used by *AgustaWestland* for almost three decades for the purpose of performing several different kinds of flight mechanics analyses. In the beginning of the 80s the code was initially conceived as a trim calculation tool; since then it was extended and largely rewritten several times, adding a large number of new features.

In the latest release, coded in *Fortran 77*, the code is able to carry out the following main tasks:

- trim;
- direct simulation (calculate trajectory from a given control time history);
- inverse simulation (calculate controls from a given trajectory time history);
- stability analysis.

During the long timespan since its introduction, the code has proven very reliable and models running on this code are routinely used in the Flight Mechanics office at *AgustaWestland*.

The code was conceived on the basis of simplified assumptions [18] with the aim of :

- reducing the computational cost, taking into account the constrained computing resources that were available at the time of initial development;

- providing a simulation tool oriented to the preliminary design phase, when typically many configuration details are still unknown and specialists focus their analysis on a relatively small number of parameters.

The main assumption in the model is that the motion of the vehicle is limited to the longitudinal plane; this implies that yaw angle and yaw rate are always null.

Based on this assumption, the problem of solving dynamic equilibrium equations of the vehicle still retains one ambiguous degree of freedom because either roll or sideslip angle need to be fixed. The choice was to assume that sideslip always equals zero. Because of this assumption the roll angle can be calculated at each time step by imposing that it must satisfy dynamic equilibrium; roll rate is instead assumed to be negligible.

As a consequence of restricting the motion to the longitudinal plane and imposing null sideslip, the lateral cyclic pitch and the tail rotor collective pitch are implicitly determined, since they must satisfy latero-directional equilibrium.

Coherently with the simplified assumptions described above, transformations between different reference frames are not performed by using complete rotation tensors, but instead by the means of approximate trigonometric relationships. This implies that the validity of the model is restricted to small attitude angles.

Definitions of reference frames, as listed in appendix B, are always implied in the following description.

## 1.2 Formulation of model components

The core model formulations are the ones conceived for the trim procedure, originally implemented as the stand-alone program *NFtrim*; theoretical documentation is supplied in [16] and [17]. Additional up-to-date information was gathered by source code analysis and comparison to the user manual [13].

### 1.2.1 Main rotor model

The main rotor is represented by an algebraic model, constituted by a set of closed-form, linear and non-linear equations.

One assumption that is common to all the equations is that rotor blades are untwisted; that means, pitch angle is assumed constant along the radius. As reported in [5], such a model is, as first approximation, equivalent to modelling a rotor with linearly twisted blades, provided that constant pitch

along the blade in the untwisted model is set equal to the pitch at the 75% radial station in the twisted rotor. Thus, for the collective pitch we consider:

$$\theta_0 = \theta_{75, \text{twisted}} . \quad (1.1)$$

Some other common quantities are defined, such as the advance parameter with reference to the non-feathering plane  $\mu_{\text{NF}}$ , the inflow parameter with reference to the tip path plane  $\lambda_{\text{TPP}}$  and the induced inflow parameter  $\lambda_i$ :

$$\mu_{\text{NF}} = \frac{V \cos(\alpha_{\text{TPP}} - a_{1\text{NF}})}{v_{\text{tip}}} , \quad (1.2a)$$

$$\lambda_{\text{TPP}} = \frac{V \sin(\alpha_{\text{TPP}} - u)}{v_{\text{tip}}} , \quad (1.2b)$$

$$\lambda_i = \frac{u}{v_{\text{tip}}} , \quad (1.2c)$$

where  $\alpha_{\text{TPP}}$  is the tip-path plane angle of attack,  $a_{1\text{NF}}$  is the longitudinal flapping angle with reference to the non-feathering plane,  $u$  is the uniform induced velocity and  $V_{\text{tip}}$  is the tip speed.

### 1.2.1.1 Induced velocity model

In the calculation of induced velocity over the rotor, absolute value of the thrust  $T_{\text{TPP}}$ , referring to the TPP reference frame, will be used. In order to account for the negative thrust case, the sign of the resulting induced velocity will be adjusted according to the sign of the thrust. Because of momentum conservation considerations, uniform induced velocity vector will always be opposite to the thrust; since in our convention induced velocity is positive downwards (downwash) and thrust is positive upwards, their values will always have the same sign.

Hovering induced velocity is calculated according to actuator disc theory [21]:

$$u_h = \sqrt{\frac{|T_{\text{TPP}}|}{2\rho A_{\text{MR}}}} . \quad (1.3)$$

When horizontal speed doesn't exceed an empirical horizontal threshold, the classical equations for axial flight, derived from the actuator disc theory, are applied:

$$\frac{v_v}{u_h} > -1 : u_{\text{OGE}} = -\frac{1}{2}v_v + \frac{1}{2}\sqrt{v_v^2 + 4u_h^2} , \quad (1.4a)$$

$$\frac{v_v}{u_h} < -2 : u_{\text{OGE}} = -\frac{1}{2}v_v - \frac{1}{2}\sqrt{v_v^2 - 4u_h^2}, \quad (1.4b)$$

where  $v_v$  is the vertical speed (positive upwards, with reference to the inertial frame).

The vertical speed range not covered by these equations is the moderate descent condition, in which the disc actuator theory loses its validity because of the vortex ring state phenomenon. The algorithm uses a proprietary empirical formula, derived from experimental data, to provide the induced speed value in this speed interval<sup>1</sup>.

Above the aforementioned horizontal speed threshold, induced velocity is calculated as solution to the polynomial:

$$u_{\text{OGE}}^4 - 2u_{\text{OGE}}^3 \sin \alpha_{\text{TPP}} + u_{\text{OGE}}^2 V^2 - u_h^4 = 0. \quad (1.5)$$

The physical solution to this equation is the minimum real positive root; this root is found numerically.

Ground effect is introduced in the model by applying a correction to the previously calculated induced velocity; a ground effect coefficient for axial flight is calculated as a function of height over ground<sup>2</sup>:

$$k_{\text{IGE},0} = k_{\text{IGE},0}(z_g). \quad (1.6)$$

In order to account for the reduction of ground effect at high speed, a coefficient  $k_{\text{IGE}}$  is calculated as a linear interpolation between  $k_{\text{IGE},0}$  at zero horizontal speed and unity at a given transition speed.

Finally, the value for uniform induced speed can be written as:

$$u = \frac{T_{\text{TPP}}}{|T_{\text{TPP}}|} k_{\text{IGE}} u_{\text{OGE}}. \quad (1.7)$$

### 1.2.1.2 Closed-form equations for flapping

Closed form equations are used for flapping angles. These equations are derived using the classical azimuth-averaged approach [23], with the addition of a non-uniform induced velocity distribution based on the theory by Mangler and Squire [12], as laid out by Bramwell [5], with the ordinary hypotheses and assumptions described in [21] (*Rotor flapping characteristics, Flapping equations in forward flight*).

<sup>1</sup>Company confidentiality restrictions apply: detailed information about this topic cannot be disclosed.

<sup>2</sup>Company confidentiality restrictions apply: detailed information about this topic cannot be disclosed. A public reference for this kind of approach can be found in [21] (*Aerodynamics of hovering flight, Ground effect*).

This approach leads to the closed form equation for the coning angle as it appears in [21]:

$$a_0 = \frac{2}{3} \frac{\rho c R^4 t_{cd} (1 - e)}{I_\beta + e R \frac{M_b}{g}} - \frac{M_b}{\Omega^2 \left( I_\beta + e R \frac{M_b}{g} \right)}, \quad (1.8)$$

and to the longitudinal flapping coefficient  $a_{1NF}$  and the lateral flapping coefficient  $b_{1NF}$  as they appear in [5], with the addition of the pitch-rate contribution from [21]:

$$a_{1NF} = \frac{2\mu_{NF} \left( \frac{4}{3}\theta_0 + \lambda_{NF} \right) - \frac{16\dot{\Theta}}{\Omega\gamma(1-e)^2} + \frac{8}{\gamma}\epsilon b_{1NF}}{1 - \frac{1}{2}\mu_{NF}^2}, \quad (1.9a)$$

$$b_{1NF} = \frac{\frac{4}{3} \left( \mu_{NF} a_0 + 1.1\nu^{\frac{1}{2}} \lambda_i \right) - \frac{8}{\gamma}\epsilon a_{1NF}}{1 - \frac{1}{2}\mu_{NF}^2}. \quad (1.9b)$$

In both equations we can substitute:

$$\lambda_{NF} \approx \lambda_{TPP} - \mu_{NF} a_{1NF}. \quad (1.10)$$

The second equation is readily substituted in the first and solved for  $a_{1NF}$ , then substituted back in the second.

The non-uniform inflow model according to Mangler and Squire is introduced by the function:

$$\nu = \frac{1 - \sin(-\alpha_{TPP})}{1 + \sin(-\alpha_{TPP})}. \quad (1.11)$$

The cited model for non-uniform inflow model is valid based on the hypothesis that airspeed is considerably larger than average induced velocity, thus it is not applicable to the near-hover and low speed part of the flight envelope. The code accounts for this limitation by setting  $\nu$  to zero when  $\mu_{NF}$  is lower than an empirical threshold; setting  $\nu$  to zero has the effect of reducing the equations to the uniform-inflow form.

Other quantities introduced in the equations above are the blade mean aerodynamic chord  $c$  and radius  $R$ , the air density  $\rho$ , the non dimensional eccentricity of the flapping hinge  $e$ , the blade mass  $M_b$ , the blade moment of inertia with reference to the flapping hinge  $I_\beta$ , the pitch  $\Theta$  and its time derivative and the rotor angular speed  $\Omega$ . Additionally, the Lock's number is defined as:

$$\gamma = \frac{\rho C_{l/\alpha} c R^4}{I_\beta}, \quad (1.12)$$

while the blade hinge offset factor is:

$$\epsilon = \frac{M_\beta}{I_\beta} x_{cg} e R^2 , \quad (1.13)$$

and the thrust coefficient for the thrust  $T_{\text{TPP}}$  with reference to the TPP is defined as:

$$t_{cd} = \frac{C_T}{\sigma} = \frac{T_{\text{TPP}}}{\rho \sigma A_{\text{MR}} v_{\text{tip}}^2} . \quad (1.14)$$

Moreover we define the lift coefficient/angle of attack slope  $C_{l/\alpha}$  for the blade profile, the non-dimensional radial station of the blade centre of gravity  $x_{cg}$ , which is given as a ratio of  $R$ , and the solidity ratio:

$$\sigma = \frac{N_b c R}{A_{\text{MR}}} \quad (1.15)$$

where  $N_b$  is the number of blades.

### 1.2.1.3 Evaluation of drag coefficient

The blade drag coefficient is assumed to be constant over the whole rotor disc; the value to be used is calculated using a proprietary algorithm based on averaging the drag coefficient calculated for for the azimuth  $\psi = 90^\circ$  (advancing blade) and  $\psi = 270^\circ$  (retreating blade) at a fixed radial station.

The reasons for this approach are based on the empirical consideration that the advancing blade is representative of high speed phenomena involving compressibility, while the retreating blade is representative of low speed conditions, where the angle of attack is the dominating factor.

The foundations of the algorithm, as described in [2], involve calculating the total airspeed at the two azimuths (including translation and rotation contributions) and the respective angles of attack.

The tangential and normal components of the asymptotic airspeed, with reference to the plane normal to the shaft, are:

$$v_{S,t} = V \cos \alpha_S , \quad (1.16a)$$

$$v_{S,n} = V \sin \alpha_S , \quad (1.16b)$$

where  $\alpha_S$  is the angle of attack of the plane normal to the shaft; then, assuming that conditions at a given radial station  $x_{C_d}$  are representative of the whole rotor, the total relative speed at the two considered azimuths are:

$$v_{90} = \Omega x_{C_d} + v_{S,t} , \quad (1.17a)$$

$$v_{270} = \Omega x_{C_d} - v_{S,t} , \quad (1.17b)$$

while the normal component due to rotation is:

$$v_{\Omega,n} = \Omega x_{C_d} R a_{1S} . \quad (1.18)$$

The angles of attack are then calculated as:

$$\alpha_{90} = \theta_0 - B_1 + \tan^{-1} \left( \frac{v_{S,n} - u - v_{\Omega,n}}{v_{90}} \right) , \quad (1.19a)$$

$$\alpha_{270} = \theta_0 - B_1 + \tan^{-1} \left( \frac{v_{S,n} - u - v_{\Omega,n}}{v_{270}} \right) , \quad (1.19b)$$

where  $B_1$  is the longitudinal cyclic pitch.

Once the angle of attack is known, the incidence contribution to the drag coefficient can be calculated for each azimuth as a function of the angle of attack, using experimental profile data (e.g. polynomial interpolations):

$$C_{d,\alpha,\psi} = C_{d,\alpha,\psi}(\alpha_\psi); \quad \psi = 90^\circ, 270^\circ . \quad (1.20)$$

The compressibility contribution is calculated using a proprietary model as a function of the difference between the local Mach number and a critical Mach number  $M_{cr}$ <sup>3</sup>:

$$M_\psi = \frac{v_p s i}{a} , \quad (1.21a)$$

$$\Delta M_\psi = M_\psi - M_{cr} , \quad (1.21b)$$

$$C_{d,M,\psi} = C_{d,M,\psi}(\Delta M_\psi); \quad \psi = 90^\circ, 270^\circ , \quad (1.21c)$$

where  $M_{cr}$  is calculated using a proprietary formulation and  $a$  is the speed of sound.

Then the two contributions can be added and the resulting values at the two considered azimuths can be averaged:

$$C_d = \frac{C_{d,\alpha,90} + C_{d,M,90} + C_{d,\alpha,270} + C_{d,M,270}}{2} \quad (1.22)$$

---

<sup>3</sup>Company confidentiality restrictions apply: detailed information about this topic cannot be disclosed.

### 1.2.1.4 Closed form equations for forces and torque

The closed form equations for the thrust coefficient  $t_{cd}$ , the H-force coefficient  $h_{cd}$  and the torque coefficient  $q_C$ , as in [5], are<sup>4</sup>:

$$t_{cd} = \frac{C_T}{\sigma} = \frac{C_{l/\alpha}}{4} \left( \frac{2}{3} \theta_0 \frac{1 - \mu_{NF}^2 + \frac{9}{4} \mu_{NF}^4}{1 + \frac{3}{2} \mu_{NF}^2} + \lambda_{TPP} \frac{1 - \frac{1}{2} \mu_{NF}^2}{1 + \frac{3}{2} \mu_{NF}^2} \right), \quad (1.23a)$$

$$h_{cd} = \frac{C_H}{\sigma} = \frac{1}{4} \mu_{NF} \left( C_d + C_{l/\alpha} \lambda_{TPP} \frac{\frac{1}{3} \theta_0 (1 - \frac{9}{2} \mu_{NF}^2) + \lambda_{TPP}}{1 + \frac{3}{2} \mu_{NF}^2} \right), \quad (1.23b)$$

$$q_C = \frac{1}{8} C_d (1 + k_B \mu_{NF}^2) - \lambda_{TPP} t_{cd} - \mu_{NF} h_{cd} + K_i t_{cd} \lambda_i; \quad (1.23c)$$

where  $k_B$  is known as the Bennet's number (typically 4.7) and  $K_i$  as the "induced K".

Dimensional quantities, including also the power required  $P_{MR}$ , are defined as:

$$T_{TPP,MR} = t_{cd} \rho \sigma A v_{tip}^2, \quad (1.24a)$$

$$H_{TPP,MR} = h_{cd} \rho \sigma A v_{tip}^2, \quad (1.24b)$$

$$Q_{MR} = q_C \rho \sigma A R v_{tip}^2, \quad (1.24c)$$

$$P_{MR} = q_{cd} \rho \sigma A v_{tip}^3. \quad (1.24d)$$

### 1.2.1.5 Reverse flow correction

The closed form equations described above are obtained by integration on a full azimuth turn, neglecting that, in this way, the lift in the area interested by the reverse flow is accounted for with the wrong sign [21].

The code implements a correction for this error only for the H-force. Reverse flow effect on other quantities is neglected.

The correction is performed by numerically integrating the lift contribution to the H-force on the reverse flow region and making this contribution non-dimensional:

$$h_{cd,corr} = \frac{1}{\rho \sigma A v_{tip}^2} \frac{N_b}{2\pi} \int_{\pi}^{2\pi} \int_0^{-\mu_{NF} R \sin \psi} \frac{1}{2} U_T^2 C_l(\phi) \sin \phi \sin \psi \phi c \, dr \, d\psi, \quad (1.25)$$

where:

$$v_1 = \Omega r + v \sin \psi, \quad (1.26a)$$

<sup>4</sup>In the calculation of required torque coefficient the code uses also proprietary corrective contributions which are subject to company confidentiality restrictions.



$$v_2 = v \sin \alpha_{\text{TPP}} - u , \quad (1.26b)$$

$$\phi = \tan^{-1} \left( \frac{v_2}{v_1} \right) , \quad (1.26c)$$

$$U_T = \sqrt{v_1^2 + v_2^2} . \quad (1.26d)$$

Special considerations are dedicated to the lift coefficient; since the angle of attack in the reverse flow region is generally outside the range of applicability of linearised aerodynamics, an empirical analytical expression that approximates the lift coefficient at high angle of attack is used. A public source of an empirical expression of the lift coefficient for high angles can be found in [8] and in [21] (*Airfoils for rotor blades, Representing airfoil data with equations*).

Once the coefficient for the lift contribution to H-force in the reverse flow area  $h_{\text{cd,corr}}$  is known, the error in the closed form H-force coefficient is compensated by summing two times  $h_{\text{cd,corr}}$ ; this implies the assumption that the wrong contribution of lift to the closed form H-force coefficient approximately equals  $h_{\text{cd,corr}}$  with the opposite sign. This is an approximation because the two contributions are calculated in different ways, one analytically and one numerically, and because the first relies on linearised aerodynamics, while the second on a high-angle model.

### 1.2.1.6 Control moments

Control moments are directly proportional to flapping angles with reference to the shaft reference frame:

$$M_{\Theta,C} = \frac{1}{2} N_b M_b x_{\text{cg}} e v_{\text{tip}}^2 a_{1S} , \quad (1.27a)$$

$$M_{\Phi,C} = -\frac{1}{2} N_b M_b x_{\text{cg}} e v_{\text{tip}}^2 b_{1S} , \quad (1.27b)$$

### 1.2.2 Fuselage model

Fuselage angle of attack is calculated as difference between pitch and climb angle:

$$\alpha_{\text{fus}} = \Theta - \tau , \quad (1.28)$$

where the climb angle is defined as:

$$\tau = \tan^{-1} \left( \frac{v_v}{v_h} \right) , \quad (1.29)$$

with  $v_v$  and  $v_h$  being the vertical (positive upwards) and horizontal speed with reference to the inertial reference frame.

Because of rotor wake contraction, airspeed induced by the main rotor on the fuselage will be in general  $k_{IB}$  times the uniform induced velocity on the rotor disc, with:

$$1 \leq k_{IB} \leq 2 . \quad (1.30)$$

If this coefficient is known, assuming that induced velocity is directed downwards parallel to  $z_{TPP}$ , total airspeed acting on the fuselage is the vector sum of induced velocity and asymptotic airspeed:

$$\mathbf{v}_{fus} = \mathbf{v} - k_{IB} u \mathbf{k}_{TPP} . \quad (1.31)$$

The rotor-fuselage influence angle  $\epsilon_{fus}$  is the angle between  $\mathbf{v}$  and  $\mathbf{v}_{fus}$ , defined as negative for downwash.

Values of the flat plate area  $f$ , of the lift coefficient  $C_{l,fus}$  and of the pitching moment coefficient  $C_{m,fus}$  are calculated as a function of the angle of attack, either through a linearised model, or through interpolation of tabulated values:

$$f = f(\alpha_{fus} + \epsilon_{fus}) ; , \quad (1.32a)$$

$$C_{l,fus} = C_{l,fus}(\alpha_{fus} + \epsilon_{fus}) ; , \quad (1.32b)$$

$$C_{m,fus} = C_{m,fus}(\alpha_{fus} + \epsilon_{fus}) ; , \quad (1.32c)$$

Consequently we obtain the related dimensional quantities for fuselage drag, lift and moment:

$$D_{fus} = \frac{1}{2} \rho f v_{fus}^2 , \quad (1.33a)$$

$$L_{fus} = \frac{1}{2} \rho C_{l,fus} A v_{fus}^2 , \quad (1.33b)$$

$$M_{fus} = \frac{1}{2} \rho C_{l,fus} A R v_{fus}^2 . \quad (1.33c)$$

### 1.2.3 Horizontal tail model

The influence angle on the horizontal tail  $\epsilon_{ht}$  is defined as positive for an increase of the angle of attack (upwash); it is obtained as a sum of the contributions of fuselage and main rotor:

$$\epsilon_{ht} = \epsilon_{MR,ht} + \epsilon_{fus,ht} . \quad (1.34)$$

The fuselage contribution is directly proportional to fuselage lift by an empirical constant:

$$\epsilon_{fus,ht} = -k_{l,fus} C_{l,fus} , \quad (1.35)$$

where  $k_{I,\text{fus}}$  is normally positive; a positive lift deflects the flow downwards, thus decreasing the angle of attack at the tail plane.

A proprietary algorithm evaluates the effect of the main rotor on the horizontal tail plane, accomplishing different tasks<sup>5</sup>:

- determine whether or not the tail plane is in the wake of the rotor;
- evaluate the main rotor induced velocity contribution to airspeed at the tail plane;
- evaluate the influence angle  $\epsilon_{\text{fus,ht}}$ .

Pitch-rate contribution to local airspeed and angle of attack is also considered.

Values of the lift and drag coefficients are obtained as a function of the angle of attack, either through a linearised model, either through interpolation of tabulated values:

$$C_{l,\text{ht}} = C_{l,\text{ht}}(\alpha_{\text{fus}} + \iota_{\text{ht}} + \epsilon_{\text{ht}}); \quad , \quad (1.36a)$$

$$C_{d,\text{ht}} = C_{d,\text{ht}}(\alpha_{\text{fus}} + \iota_{\text{ht}} + \epsilon_{\text{ht}}); \quad , \quad (1.36b)$$

where  $\iota_{\text{ht}}$  is the setting angle of the tail plane, which is assumed to be controlled proportionally to the main rotor collective through a given constant:

$$\iota_{\text{ht}} = \iota_{\text{ht},0} + \iota_{\text{ht},1}\theta_0 . \quad (1.37)$$

Forces are calculated as:

$$L_{\text{ht}} = \frac{1}{2}\rho A_{\text{ht}} C_{l,\text{fus}} v_{\text{ht}}^2 , \quad (1.38a)$$

$$D_{\text{ht}} = \frac{1}{2}\rho A_{\text{ht}} C_{d,\text{fus}} v_{\text{ht}}^2 , \quad (1.38b)$$

where  $A_{\text{ht}}$  is the reference area.

Moments are then defined as:

$$M_{\Theta,\text{ht}} = - (L_{\text{ht}} \cos(\alpha_{\text{fus}} + \epsilon_{\text{ht}}) + D_{\text{ht}} \sin(\alpha_{\text{ht}} + \epsilon_{\text{ht}})) d_{\text{ht}} , \quad (1.39a)$$

$$M_{\Phi,\text{ht}} = - (L_{\text{ht}} \cos(\alpha_{\text{fus}} + \epsilon_{\text{ht}}) + D_{\text{ht}} \sin(\alpha_{\text{ht}} + \epsilon_{\text{ht}})) l_{\text{ht}} , \quad (1.39b)$$

where  $d_{\text{ht}}$  is the longitudinal distance between the horizontal tail aerodynamic computational point and the moments reference point and  $l_{\text{ht}}$  is the lateral distance.

---

<sup>5</sup>Company confidentiality restrictions apply: detailed information about this topic cannot be disclosed.

### 1.2.4 Vertical tail and tail rotor model

The vertical tail is modelled as a simple lifting surface; since sideslip is zero by hypothesis, aerodynamic coefficients are assumed to be constant, thus neglecting the contribution of combined pitch and roll to vertical plane angle of attack:

$$L_{vt} = \frac{1}{2} \rho A_{vt} C_{l,ht} v_{ht}^2, \quad (1.40a)$$

$$D_{vt} = \frac{1}{2} \rho A_{vt} C_{d,ht} v_{ht}^2, \quad (1.40b)$$

Since tail rotor thrust  $T_{TR}$  is calculated by imposing yaw equilibrium, modelling of the tail rotor is limited to the calculation of other relevant quantities as functions of thrust, using closed form equations analogous to the ones used for the main rotor:

$$\mu_{TR} = \frac{V}{\Omega_{TR} R_{TR}}, \quad (1.41a)$$

$$t_{cd,TR} = \frac{T_{TR}}{\rho (\Omega_{TR} R_{TR})^2 \sigma_{TR} A_{TR}}, \quad (1.41b)$$

$$h_{cd,TR} = \frac{1}{4} C_{d,TR} \mu_{TR}, \quad (1.41c)$$

$$u_{TR} = \frac{T_{TR}}{|T_{TR}|} \sqrt{\frac{|T_{TR}|}{2\rho A_{TR}}}. \quad (1.41d)$$

$$\lambda_{TR} = \frac{u_{TR}}{\Omega_{TR} R_{TR}}, \quad (1.41e)$$

$$\theta_{0,TR} = \frac{\left( t_{cd,TR} - \lambda_{TR} \frac{C_{l/\alpha,TR} (1 - \frac{1}{2} \mu_{TR}^2)}{1 + \frac{3}{2} \mu_{TR}^2} \right) \left( 1 + \frac{3}{2} \mu_{TR}^2 \right)}{\frac{C_{l/\alpha,TR}}{6} \left( 1 - \mu_{TR}^2 + \frac{9}{4} \mu_{TR}^4 \right)}, \quad (1.41f)$$

$$q_{C,TR} = \frac{1}{8} C_{d,TR} (1 + k_B \mu_{TR}^2) - \lambda_{TR} t_{cd,TR} - \mu_{TR} h_{cd,TR}. \quad (1.41g)$$

$$Q_{TR} = q_{C,TR} \rho \sigma A_{TR} R_{TR} (\Omega_{TR} R_{TR})^2, \quad (1.41h)$$

$$P_{TR} = q_{C,TR} \rho \sigma A_{TR} (\Omega_{TR} R_{TR})^3, \quad (1.41i)$$

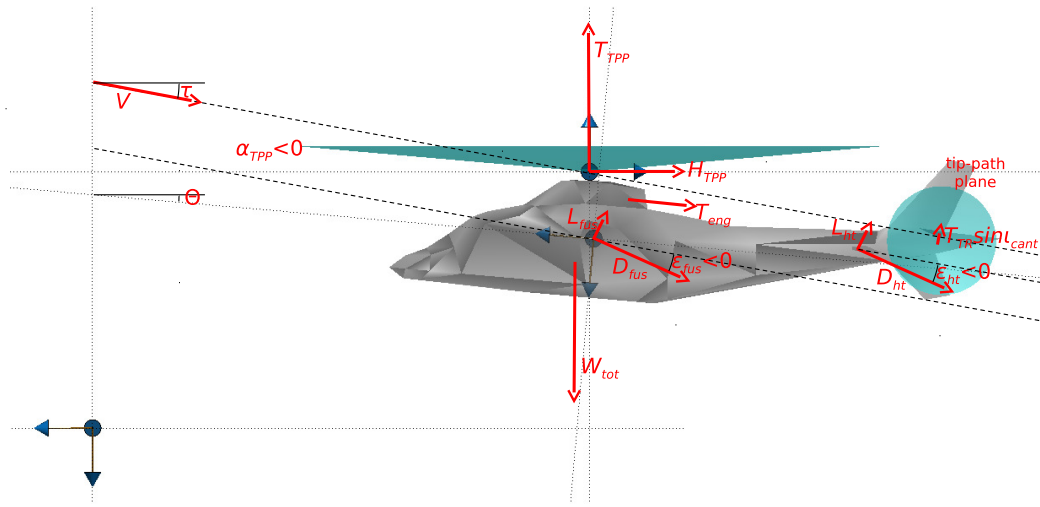


Figure 1.1: Overview of forces, lateral view

### 1.3 Trim procedure

Historically the trim procedure was the first to be implemented in what would later become the *NFpath* code; for this reason it can be considered the core of the code, since all the assumptions and formulations were defined bearing in mind the classical trim approach described in the literature (see [2] and [21]) based on solving the inverse problem for the rotor: given forces, required controls are calculated using closed form equations. At present time, this approach is generally deprecated, since increased availability of computational resources allows obtaining trim conditions by applying numerical gradient methods to direct simulation models, with the advantage of using the same formulation for both direct and inverse problems. The *NFpath* code actually includes also a second trim procedure for using this alternative approach, but the description of this procedure goes beyond the scope of our discussion.

In short, the algorithm used in *NFpath* for the classical trim procedure is based on the following main steps:

- obtain estimates of unknown quantities required for the solution of the inverse problem (e.g. forces, attitude), either using approximated formulation, or values from the previous iteration, or guess values;
- calculate required controls, while imposing equilibrium constraints;
- update other unknown quantities;
- iterate.

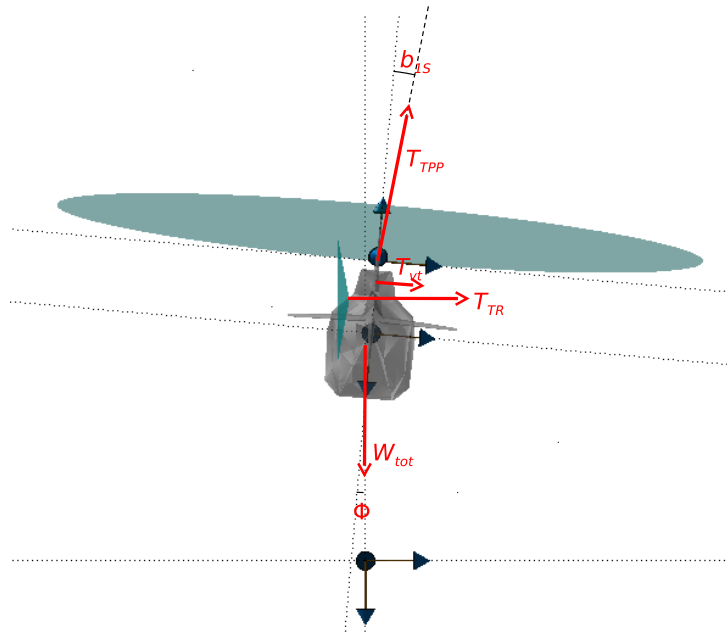


Figure 1.2: Overview of forces, rear view

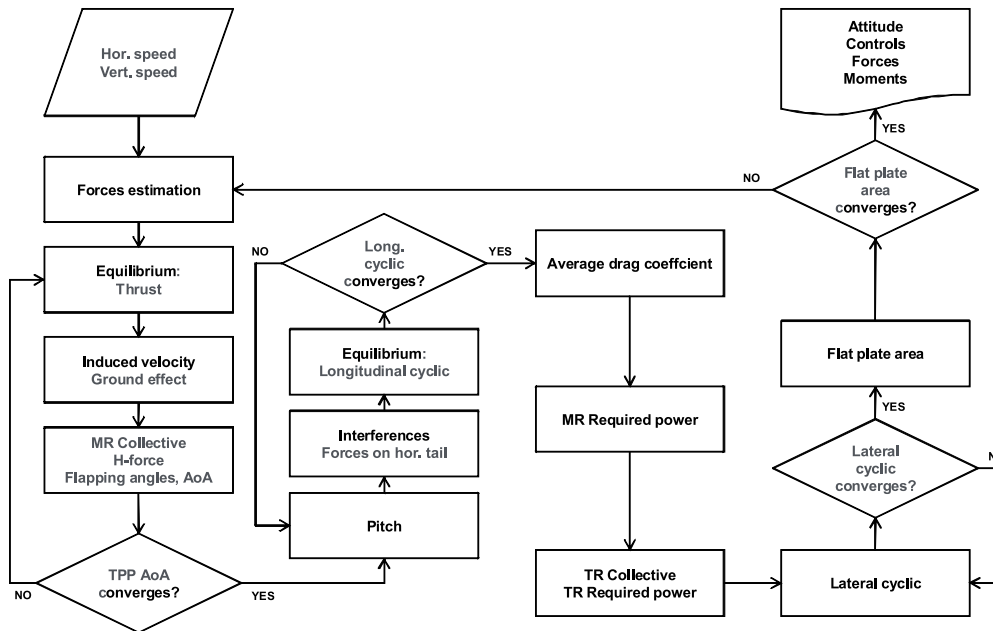


Figure 1.3: Trim procedure algorithm overview

As can be seen in figure 1.3, the algorithm is actually implemented in the form of many nested iterative calculations, with the outer one being the update of flat plate area. This approach requires the use of relaxation factors in the update of quantities for each iteration in order to ensure convergence.

### 1.3.1 Preliminary calculations

The trim procedure starts with the calculation of constants defined only by parameters, such as tip speed  $v_{\text{tip}}$  and area  $A$  for both the main and the tail rotor, the Lock number  $\gamma$  for the main rotor and so on.

Also the climb angle  $\tau$  and the advance parameter (with reference to inertial frame) for the considered horizontal and vertical speeds with reference to the inertial frame are calculated:

$$\mu = \frac{v_h}{v_{\text{tip}}} . \quad (1.42)$$

All unknown quantities such as the longitudinal non-feathering flapping angle  $a_{1\text{NF}}$ , the fuselage angle of attack  $\alpha_{\text{fus}}$  and the horizontal component of the main rotor equilibrating force  $D_O$  are set to zero, while a guess value is assumed for the average drag coefficient  $C_d$  of the main rotor.

### 1.3.2 Evaluation of main rotor forces, angle of attack and required collective pitch

From here on, the iteration on the flat plate are begins. By considering only the first term in eq. 3.39 in [5], a rough estimate for the H-force can be obtained:

$$H_{\text{TPP}} \approx \frac{1}{4} \mu \rho A v_{\text{tip}}^2 C_d , \quad (1.43)$$

and from this we can easily estimate angle of attack of the rotor disc:

$$\alpha_{\text{TPP}} \approx -\tan^{-1} \left( \frac{D_0 + H_{\text{TPP}}}{W_{\text{tot}}} \right) , \quad (1.44)$$

Starting the TPP angle of attack iteration, the first value to be calculated is the advance parameter with reference to the non-feathering plane, which is obtained using eq. 1.2a.

Horizontal equilibrium is imposed by:

$$\begin{aligned} & T_{\text{TPP}} \sin(\alpha_{\text{TPP}} + \tau) + H_{\text{TPP}} \cos(\alpha_{\text{TPP}} + \tau) + \\ & + \frac{1}{2} \rho f v_{\text{fus}}^2 \cos(\tau - \epsilon_{\text{fus}}) + D_{\text{ht}} \cos(\tau - \epsilon_{\text{ht}}) + L_{\text{ht}} \sin(\tau - \epsilon_{\text{ht}}) + \\ & - T_{\text{eng}} \cos \Theta + L_{\text{fus}} \sin(\tau - \epsilon_{\text{fus}}) + T_{\text{TR}} \sin \iota_{\text{cant}} \sin \Theta = 0 , \end{aligned} \quad (1.45)$$

where  $T_{\text{eng}}$  is the residual thrust generated by the engine, assumed to be directed longitudinally aftwards.

From this equation an expression of the horizontal component of the main rotor equilibrating force can be written:

$$\begin{aligned} D_0 &= -T_{\text{TPP}} \sin(\alpha_{\text{TPP}} + \tau) - H_{\text{TPP}} \cos(\alpha_{\text{TPP}} + \tau) = \\ &= \frac{1}{2} \rho f v_{\text{fus}}^2 \cos(\tau - \epsilon_{\text{fus}}) + D_{\text{ht}} \cos(\tau - \epsilon_{\text{ht}}) + L_{\text{ht}} \sin(\tau - \epsilon_{\text{ht}}) + \\ &\quad - T_{\text{eng}} \cos \Theta + L_{\text{fus}} \sin(\tau - \epsilon_{\text{fus}}) + T_{\text{TR}} \sin \iota_{\text{cant}} \sin \Theta, \end{aligned} \quad (1.46)$$

where all quantities that are still unknown at the first iteration are set to zero.

Similarly, vertical equilibrium can be imposed by:

$$\begin{aligned} T_{\text{TPP}} \cos(\alpha_{\text{TPP}} + \tau) - H_{\text{TPP}} \sin(\alpha_{\text{TPP}} + \tau) + \\ - \frac{1}{2} \rho f v_{\text{fus}}^2 \sin(\tau - \epsilon_{\text{fus}}) - D_{\text{ht}} \sin(\tau - \epsilon_{\text{ht}}) + L_{\text{ht}} \cos(\tau - \epsilon_{\text{ht}}) + \\ + T_{\text{eng}} \sin \Theta + L_{\text{fus}} \cos(\tau - \epsilon_{\text{fus}}) + T_{\text{TR}} \sin \iota_{\text{cant}} \cos \Theta - W_{\text{tot}} = 0, \end{aligned} \quad (1.47)$$

that can be turned into an expression for the rotor thrust with reference to the TPP frame:

$$\begin{aligned} T_{\text{TPP}} &= \frac{1}{\cos(\alpha_{\text{TPP}} + \tau)} (H_{\text{TPP}} \sin(\alpha_{\text{TPP}} + \tau) + \\ &\quad + \frac{1}{2} \rho f v_{\text{fus}}^2 \sin(\tau - \epsilon_{\text{fus}}) + D_{\text{ht}} \sin(\tau - \epsilon_{\text{ht}}) - L_{\text{ht}} \cos(\tau - \epsilon_{\text{ht}}) + \\ &\quad - T_{\text{eng}} \sin \Theta - L_{\text{fus}} \cos(\tau - \epsilon_{\text{fus}}) - T_{\text{TR}} \sin \iota_{\text{cant}} \cos \Theta + W_{\text{tot}}), \end{aligned} \quad (1.48)$$

where  $W_{\text{tot}}$  is the weight force.

Now the average induced velocity can be determined as shown in section 1.2.1.1, and from this the inflow parameter with reference to the TPP frame  $\lambda_{\text{TPP}}$ , according to eq. 1.2b.

From previously estimated thrust, we can calculate the thrust coefficient:

$$t_{\text{cd}} = \frac{T_{\text{TPP}}}{\rho \sigma A v_{\text{tip}}^2}, \quad (1.49)$$

By manipulating eq. 1.23a we can now determine the required collective pitch:

$$\theta_0 = \left( t_{\text{cd}} - \lambda_{\text{TPP}} \frac{\frac{C_{l/\alpha}}{4} \left( 1 - \frac{1}{2} \mu_{\text{NF}}^2 \right)}{1 + \frac{3}{2} \mu_{\text{NF}}^2} \right) \frac{1 + \frac{3}{2} \mu_{\text{NF}}^2}{\frac{C_{l/\alpha}}{6} \left( 1 - \mu_{\text{NF}}^2 + \frac{9}{4} \mu_{\text{NF}}^4 \right)}, \quad (1.50)$$



and then the H-force as shown in sections 1.2.1.4 and 1.2.1.5.

By imposing again the horizontal equilibrium:

$$D_0 + T_{\text{TPP}} \sin(\alpha_{\text{TPP}} + \tau) + H_{\text{TPP}} \cos(\alpha_{\text{TPP}} + \tau) = 0 , \quad (1.51)$$

we can now update the value of the rotor disc angle of attack:

$$\alpha_{\text{TPP}}^{(k+1)} = \sin^{-1} \left( -\frac{H_{\text{TPP}} \cos(\alpha_{\text{TPP}}^{(k)} + \tau) + D_0}{T_{\text{TPP}}} \right) - \tau , \quad (1.52)$$

that, using an adequate relaxation, will be used to iterate from the beginning of section 1.3.2 until convergence on  $\alpha_{\text{TPP}}$  is reached.

### 1.3.3 Evaluation of flapping angles, fuselage angle of attack and horizontal plane angle of attack

Applying equations presented in section 1.2.1.2, coning angle  $a_0$ , longitudinal flapping coefficient  $a_{1\text{NF}}$  and lateral flapping coefficient  $b_{1\text{NF}}$  are determined; since the calculation is for a trimmed condition, the term proportional to pitch rate is absent.

Then the longitudinal flapping coefficient with reference to the shaft reference frame is calculated (using a tentative value for  $B_1$  at the first iteration):

$$a_{1\text{S}} = a_{1\text{NF}} - B_1 , \quad (1.53)$$

which, in turn, allows to find the angle of attack of the fuselage:

$$\alpha_{\text{S}} = \alpha_{\text{TPP}} - a_{1\text{S}} , \quad (1.54a)$$

$$\alpha_{\text{fus}} = \alpha_{\text{S}} - \iota_{\text{S}} , \quad (1.54b)$$

where  $\iota_{\text{S}}$  is the tilt angle of the main rotor mast (positive backwards).

From this the angle of attack on the tail plane can be found:

$$\alpha_{\text{ht}} = \alpha_{\text{fus}} + \iota_{\text{ht}} + \epsilon_{\text{ht}} , \quad (1.55)$$

where the tail plane influence angle is calculated as described in section 1.2.3, that also describes the calculation of tail plane forces that is performed at this stage.

The pitch angle is given by:

$$\Theta = \alpha_{\text{fus}} + \tau , \quad (1.56)$$

### 1.3.4 Pitching equilibrium

Now all the contributions to the pitching moment can be calculated; fuselage moment is described in section 1.2.2, horizontal tail in section 1.2.3, main rotor control moments in section 1.2.1.6. Moreover we have a tail rotor contribution (set to zero at the first iteration since not all the quantities are already known):

$$M_{\Theta,TR} = -q_{C,TR}\rho\sigma_{TR}A_{TR}(\Omega_{TR}R_{TR})^2R_{TR} - T_{TR}d_{TR}\sin\iota_{cant,TR}, \quad (1.57)$$

where  $\iota_{cant,TR}$  is the cant angle of the tail rotor rotor and  $d_{TR}$  is the distance between the tail rotor hub and the body frame origin along  $x_B$ .

An additional contribution due to residual thrust from engines (again assumed to be parallel to the longitudinal body axis at a distance  $h_{eng}$ ):

$$M_{\Theta,eng} = -T_{eng}h_{eng}, \quad (1.58)$$

Then pitching equilibrium can be imposed by:

$$M_{\Theta,C} + M_{\Theta,fus} + M_{\Theta,ht} + M_{\Theta,eng} + M_{\Theta,TR} + \\ - d_{cg}W_{tot}\cos\Theta + (H_{TPP}\cos a_{1S} + T_{TPP}\sin a_{1S})h_{cg}, \quad (1.59)$$

where  $d_{cg}$  is the longitudinal distance between the centre of gravity and the moment reference point, and  $h_{cg}$  is the distance along  $z_B$  between the moment reference point and the main rotor hub.

Explicitating  $M_{\Theta,C}$  we obtain the required longitudinal control moment; then, remembering the relation between cyclic pitch and flapping angle in eq. B.5 and the expression of the control moment in eq. 1.27a we can obtain an expression for updating the longitudinal cyclic pitch:

$$B_1 = a_{1NF} - a_{1S} = a_{1NF} - \frac{2M_{\Theta,C}}{N_b M_b x_{cg} ev_{tip}^2} \quad (1.60)$$

Until convergence is reached on  $B_1$ , a new value is obtained by using an adequate relaxation and this new value is used to iterate from section 1.3.2.

At this stage an average value for the drag coefficient on the main rotor is calculated using the model described in section 1.2.1.3; this value is then used for the purpose of evaluating forces and torque on the main rotor (see section 1.2.1.4).

### 1.3.5 Main rotor torque compensation

Considering a counter-clockwise rotating main rotor, the force, positive to the right, that must be applied at the tail to compensate the main rotor

torque is:

$$T_{\text{tail}} = \frac{P_{\text{MR}}}{\Omega d_{\text{TR}}} , \quad (1.61)$$

where  $d_{\text{TR}}$  is the longitudinal distance between the tail rotor hub and the moment reference point.

Then the part of this force that has to be generated by the tail rotor is  $T_{\text{TR}}$ , that is obtained subtracting the vertical tail force and accounting tail blockage and cant angle:

$$T_{\text{TR,eff}} = T_{\text{tail}} - \frac{L_{\text{vt}} d_{\text{vt}}}{d_{\text{TR}}} , \quad (1.62a)$$

$$T_{\text{TR}} = T_{\text{TR,eff}} \frac{k_{\text{bf}}}{\cos \iota_{\text{cant,TR}}} , \quad (1.62b)$$

where  $d_{\text{vt}}$  is the longitudinal distance between the vertical tail aerodynamic computational point and the moment reference point, and  $k_{\text{bf}}$  is the tail blockage factor.

Using the equations given in section 1.2.4, it is possible to calculate the required collective pitch at the tail rotor and the power required by it.

Then the total power required is:

$$P_{\text{tot}} = \frac{P_{\text{MR}} + P_{\text{TR}}}{\eta_{\text{tr}}} + P_{\text{acc}} + \frac{T_{\text{eng}} v \alpha_{\text{fus}}}{\eta_{\text{eng}}} , \quad (1.63)$$

where  $P_{\text{acc}}$  is the power required by accessories,  $\eta_{\text{tr}}$  is the transmission efficiency and  $\eta_{\text{eng}}$  is the efficiency related to the residual engine thrust at the nozzle.

Knowing the lateral cyclic pitch (or assuming a value for it at the first iteration), it is possible to calculate the lateral flapping coefficient:

$$b_{1S} = A_1 + b_{1\text{NF}} . \quad (1.64)$$

Imposing equilibrium of forces along  $x_S$ :

$$T_{\text{TPP}} \sin b_{1S} + T_{\text{tail}} - W_{\text{tot}} \sin \Phi = 0 , \quad (1.65)$$

it is then possible to calculate the roll angle:

$$\Phi = \sin^{-1} \left( \frac{T_{\text{TPP}} \sin b_{1S} + T_{\text{tail}}}{W_{\text{tot}}} \right) . \quad (1.66)$$

In the same way as already done for the pitching equilibrium, rolling moment for each component is calculated as described in the relevant paragraph; moreover, we have the moment produced by the vertical tail:

$$M_{\Phi, \text{tail}} = T_{\text{TR,eff}} h_{\text{TR}} + L_{\text{vt}} h_{\text{vt}} , \quad (1.67)$$

where  $h_{vt}$  is the distance along  $z_B$  between the moment reference point and the vertical tail aerodynamic computational point.

We can then write an equilibrium equation about the roll axis:

$$M_{\Phi,C} + M_{\Phi,tail} + M_{\Phi,ht} + W_{tot}l_{cg} \cos \Phi + H_{TPP}h_{cg} \sin b_{1S} = 0 , \quad (1.68)$$

where  $l_{cg}$  is the lateral displacement of the centre of gravity from the centerline; again, as it was done for the longitudinal cyclic pitch, the control moment  $M_{\Phi,C}$  resulting from the equilibrium equation can be used into an expression of the lateral cyclic pitch:

$$A_1 = -b_{1NF} + b_{1S} = -b_{1NF} - \frac{2M_{\Phi,C}}{N_b M_b x_{cg} e v_{tip}^2} \quad (1.69)$$

The so calculated value is then used for iterating from the calculation of  $b_{1S}$ , using an adequate relaxation to ensure stability and checking for convergence against a preset threshold.

Concluding the outer iteration, the flat plate area of the fuselage is evaluated as a function of the angle of attack (see section 1.2.2), checked for convergence and updated with adequate relaxation in order to iterate, if necessary, from section 1.3.2.

Upon convergence of the flat plate area, controls and attitude angles for the given flight condition are known, then the trim problem is solved.

## 1.4 Direct snapshot procedure

The direct snapshot procedure calculates forces and dependent controls (lateral cyclic and tail rotor collective pitch) for a given set of states (horizontal speed, vertical speed, pitch, pitch rate, ground distance) and independent controls (main rotor collective and longitudinal cyclic pitch). The reason for having two dependent controls resides in the constraints set by the hypotheses of longitudinal motion and zero sideslip.

The procedure itself doesn't implement nor the equations of motion nor the integration of them. These functions are implemented by an outer layer, outside of the scope of this description.

The procedure is largely based on the trim procedure already described; the details of the common parts will be omitted, as the reader can use the trim procedure description for reference.

The climb angle and the advance ratio are calculated as already shown in section 1.3.1. Then the angle of attack of the fuselage is readily obtained:

$$\alpha_{TPP} = \Theta - \tau , \quad (1.70)$$

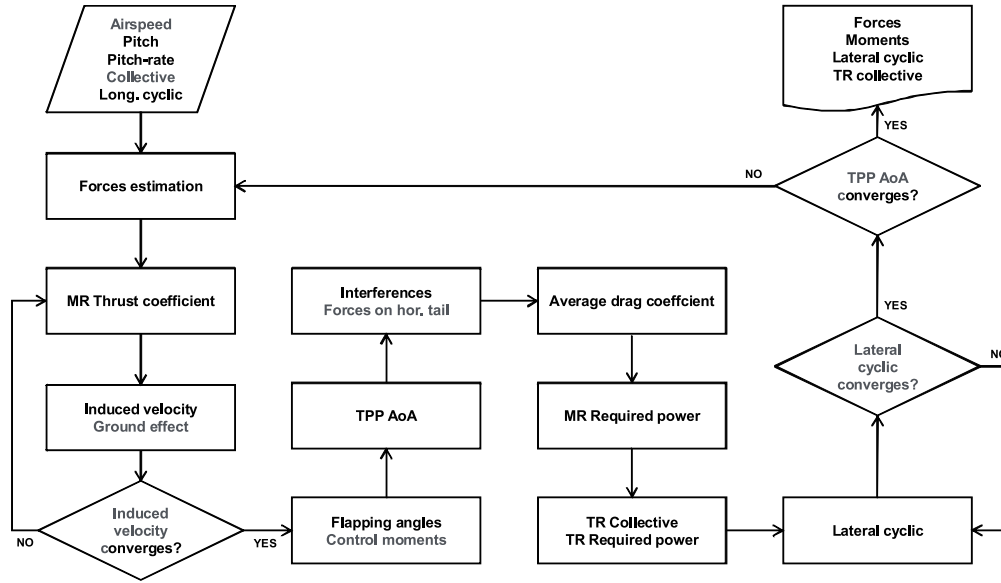


Figure 1.4: Direct snapshot algorithm overview

and the flat plate area can be calculated as a function of it; also the fuselage drag is readily calculated.

Then the fuselage lift coefficient and the fuselage moment coefficient are obtained as a function of the angle of attack, and from them the lift and moment themselves.

The advance parameter with reference to the non-feathering frame is calculated (using a tentative value for  $a_{1NF}$  at the first iteration) by eq. 1.2a.

Then using the latest value of the induced velocity (or a tentative value) also the inflow and induced inflow parameters get calculated according to eqs. 1.2b and 1.2c.

It is now possible to evaluate the equation given in section 1.2.1.4 for the main rotor thrust coefficient, and dimensional thrust is readily obtained from it. Once the thrust is known, a new value for induced velocity can be calculated as a function of it, using the model described in section 1.2.1.1, and then the value of the TPP angle of attack. After checking for convergence on the induced velocity, it is possible, if needed, to iterate with the usual relaxation technique from where the inflow and induced inflow parameters were calculated.

Once convergence on induced velocity is obtained, the H-force coefficient and its dimensional value are calculated as per section 1.2.1.4, as well as the flapping angles as described in section 1.2.1.2.

Then it is possible to calculate the longitudinal flapping with reference

to the shaft frame by eq. 1.53, and using it the TPP angle of attack can be updated updated:

$$\alpha_{\text{TPP}} = \alpha_{\text{fus}} + \iota_{\text{S}} + a_{1\text{S}} . \quad (1.71)$$

Also the main rotor longitudinal control moment, as defined in section 1.2.1.6, is now known.

Induced velocity on the fuselage and on the horizontal tail, as well as forces and moments acting on them, can be obtained as described in the relevant sections 1.2.1.2 and 1.2.3.

Then also the main rotor required power and torque are calculated as per section 1.2.1.4.

Duplicating the procedure described in 1.3.5, the forces and controls on the tail rotor are obtained; with appropriate inputs, in this calculation the code can also account for transmission limit, inoperative engines and rotor angular velocity dynamics, that requires one more nested level of iteration. Detailed description of this part of the algorithm is beyond the scope of this document.

The lateral cyclic pitch is iteratively calculated as described in section 1.3.5.

At this point convergence on TPP angle of attack is checked: if needed a new iteration is started with the calculation of  $\mu_{\text{NF}}$ , using an adequate relaxation for  $\alpha_{\text{TPP}}$ .

## 1.5 Simplified re-implementation of the model

### 1.5.1 Scope

Having gained a comprehensive understanding of the internals of some important parts of the *NFpath* code, it was decided to re-implement the direct snapshot procedure, using the same formulations as the original software in a new simplified model. There were many reasons for this intermediate step before further developments, the most important being:

- the original model is reproduced in a simplified form and in a higher level programming language, where formulations and algorithms are clearly understandable, sacrificing computational efficiency in exchange for readability;
- the simplified model can be tested for coherency of results against the original model, thus validating the correctness of the interpretation of the original model.

- the simplified model provides a safe and user-friendly sandbox environment for formulation analysis and development prototyping, where it is easier to modify, debug, test and run the source code.

An additional goal was added to the re-implementation task: the rotor model was isolated from the rest of the iterative procedure, decoupling it from other entities of the rotorcraft and implementing it in a module with well defined interfaces. In this fashion the rotor model receives states (speed, attitude, distance from ground) and complete controls (collective pitch, longitudinal and lateral cyclic pitch) and returns outputs (forces relative to the tip-path plane and tip-path plane attitude), while parameters are separated in a dedicated interface.

### 1.5.2 Methodology and tools

The simplified model was implemented using *Freemat v4.0*. *Freemat* is a calculation tool oriented to the matrix algebra [3] which provides a command line interface, a built-in function set, a programming language, diagram plotting routines and a graphical user interface that closely reproduce the basic functionality of the industry standard *Matlab* environment by *Mathworks Inc.* Even though not every feature in *Matlab* is exactly replicated in *Freemat*, programming syntax and basic functions are largely interoperable between the two environments.

The software is released as open source under the *GNU General Public Licence version 2*.

Apart from the free availability and industry standard (partial) compatibility, one of the strong points that supported the choice of *Freemat* was the availability of a very simple generic DLL interface, that provides a gateway to compiled code written in lower level languages (such as C). This interface enables easy testing of compiled program modules and will be discussed later.

### 1.5.3 Model structure

The heart of the re-implemented model is the routine that calculates forces, moments and flapping angles on the isolated rotor. An overview of the algorithm is shown in figure 1.5, which is self-explanatory, since the used formulations are identical to those used in the *NFpath* direct simulation algorithm and the concept itself is very similar. The most important differences are:

- all non-rotor related evaluations are moved outside of the core routine, which is supposed to deal only with the rotor;

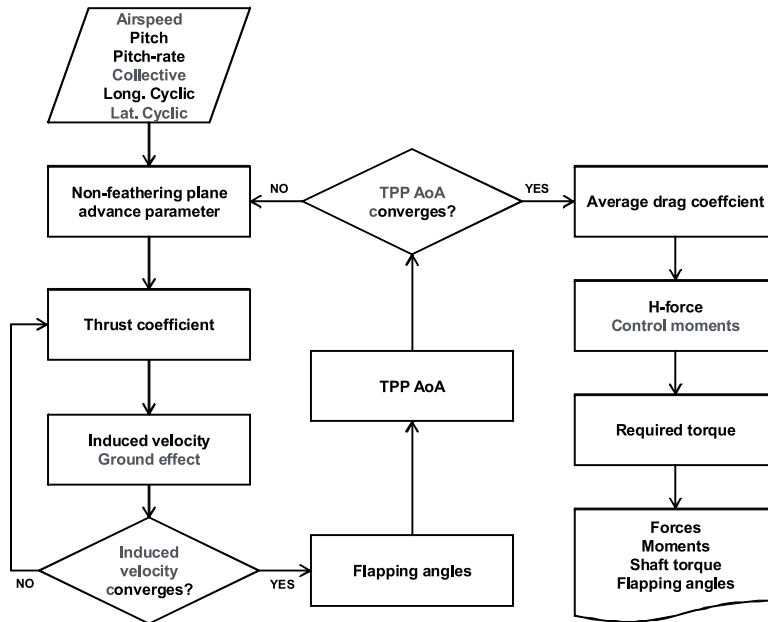


Figure 1.5: Overview of the reimplemented algorithm for the rotor model

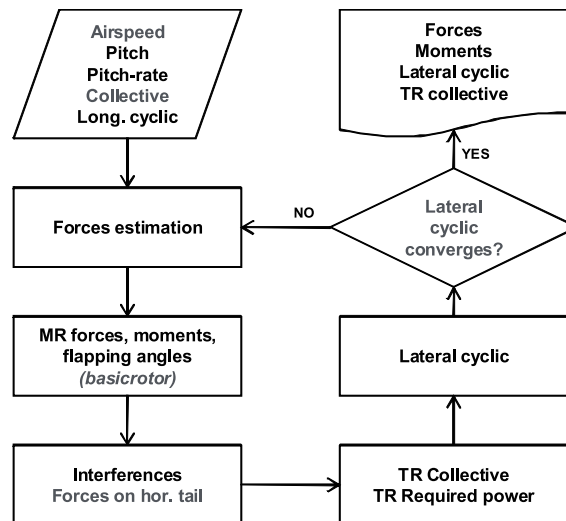


Figure 1.6: Overview of the reimplemented algorithm for the rotorcraft model



- all the calculations that are not needed in the iterative calculations are moved outside of the iteration cycles, in order to minimize computational cost;
- all the internal calculations are performed using only SI units (as opposed to *NFpath*, which uses mainly the MKS system, with some non-coherent additions such as degrees and horsepower);
- the routine outputs forces with reference to the TPP reference frame, control moments with reference to the body frame, the required power at the shaft and the flapping angles; since the flapping angles define the attitude of the TPP, it is possible to compute adequate transformations in order to express all the forces and moments with reference to the body frame;
- the remainder calculations required to emulate the *NFpath* direct simulation procedure for a complete helicopter are implemented into an outer layer that calls the rotor model inside its loop in order to evaluate rotor forces; the procedure implements an iteration on the lateral cyclic pitch, which is looped until the partial trim condition is satisfied (lateral equilibrium, zero sideslip); an overview of the algorithm is illustrated in figure 1.6.

#### 1.5.4 Model validation

The re-implemented model was validated against the original *NFpath* code in order to ensure that formulations used in *NFpath* were correctly understood and that the modified algorithm is equivalent to the original. This validation consisted in performing the following steps in different flight conditions:

1. an arbitrary time history for controls is defined;
2. *NFpath* simulation is run starting from trimmed condition;
3. for each time step in *NFpath* simulation, attitude, velocities and controls are used as input for the re-implemented simulation;
4. results are compared.

It should be noted that no time integration is performed in the newly implemented code and comparison is made on a snapshot-by-snapshot basis: this procedure avoids the time integration of errors, so that the validation is specific to the correctness of the evaluation of forces and other relevant quantities at each instant of time.

The comparison was performed using for both codes the same parameter set, representative of a light twin helicopter comparable to the *AW109*, partly derived from the example helicopter in [2].

The result of the comparison, as shown in the figures<sup>6</sup> from 1.7 to 1.22, is substantially an overplot, with some minor discrepancies which are considered to be due chiefly on the effect of preset tolerance on the differently nested iterations, which control convergence on different variables, and, in a minor way, to numerical truncation.

---

<sup>6</sup>Results from the reimplemented model are indicated as *direct2d* in the figures.

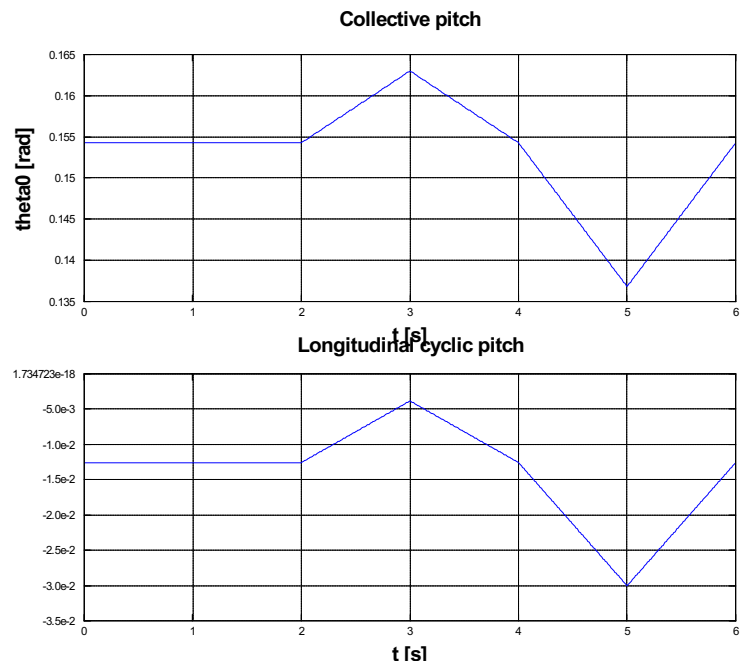


Figure 1.7: Control time history, hover test case

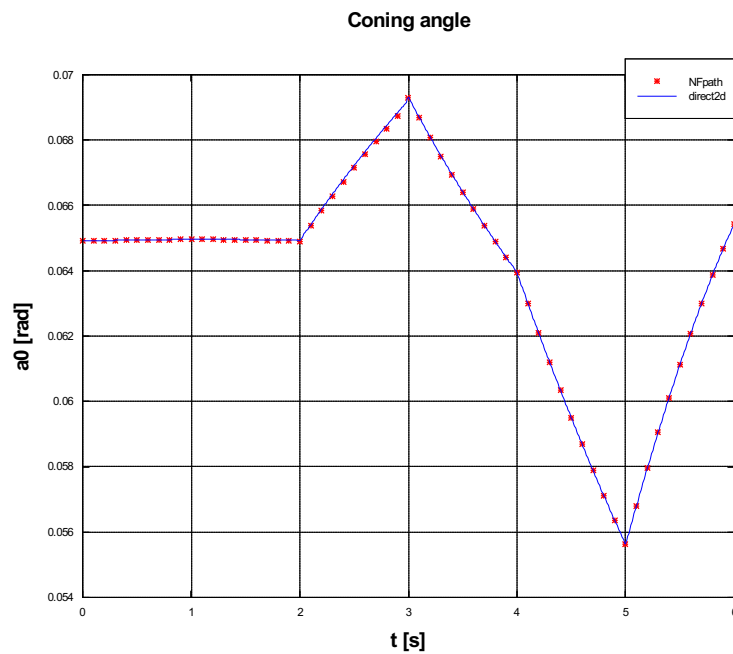


Figure 1.8: Coning, hover test case

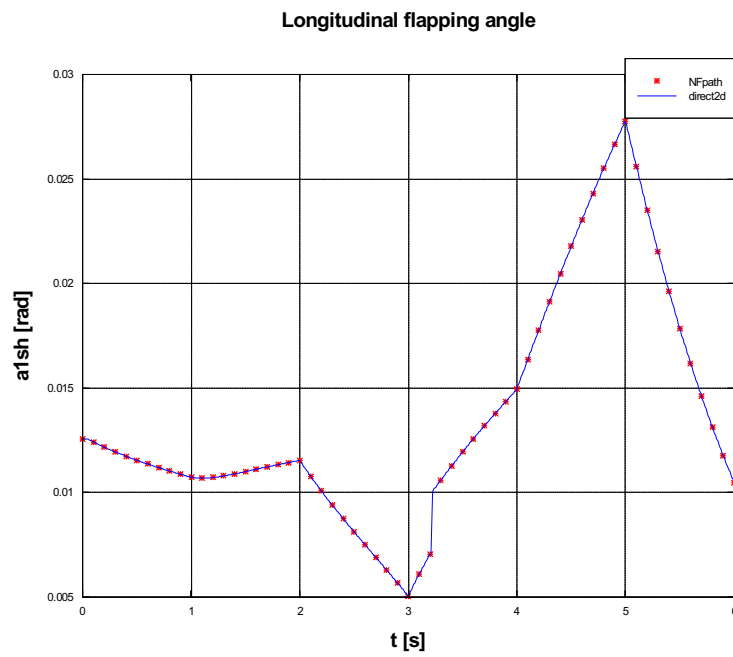


Figure 1.9: Longitudinal flapping, hover test case

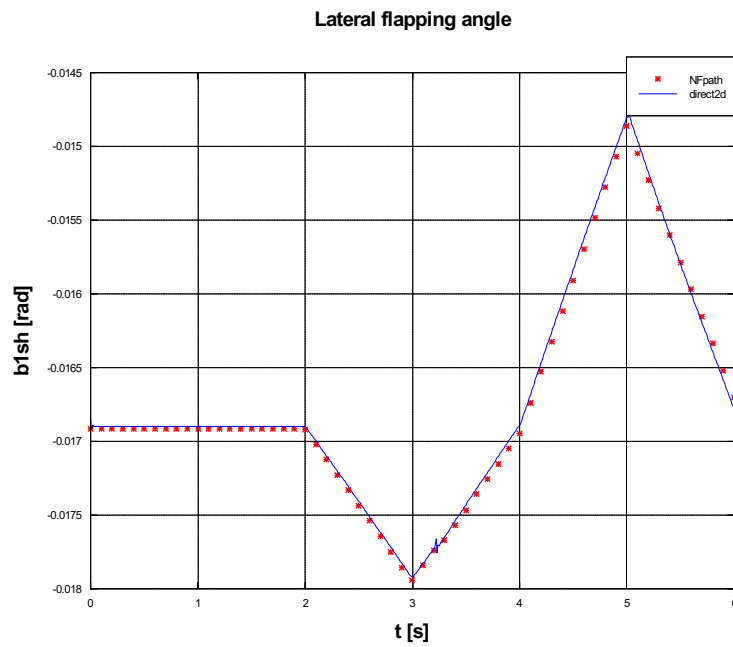


Figure 1.10: Lateral flapping, hover test case

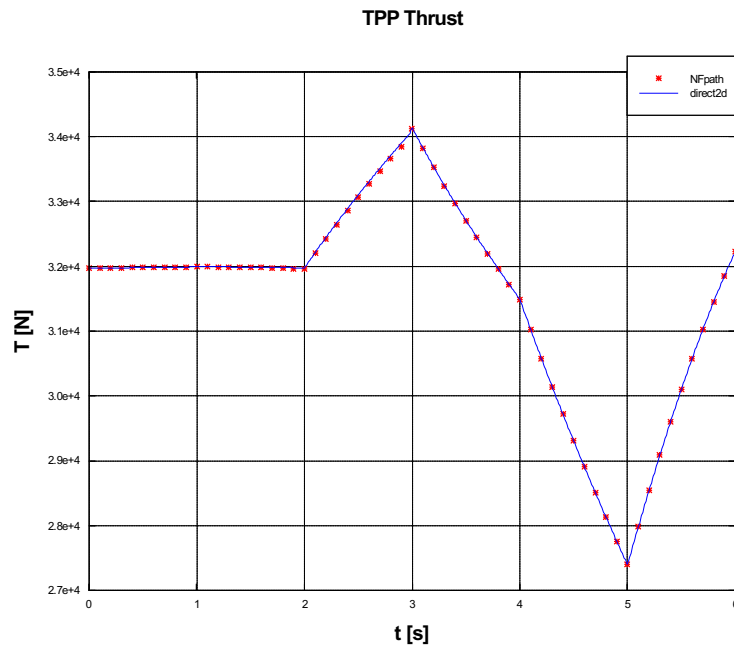


Figure 1.11: Thrust, hover test case

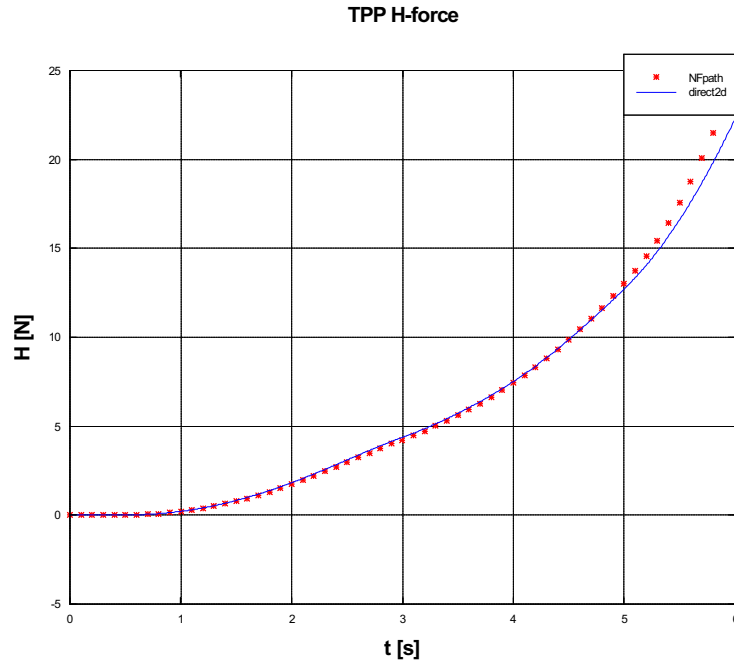


Figure 1.12: H-force, hover test case

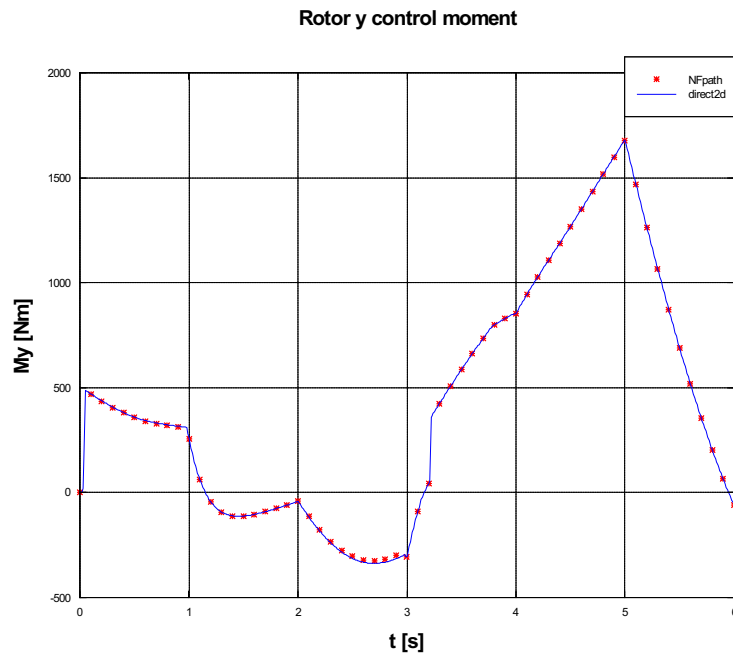


Figure 1.13: Pitching control moment, hover test case

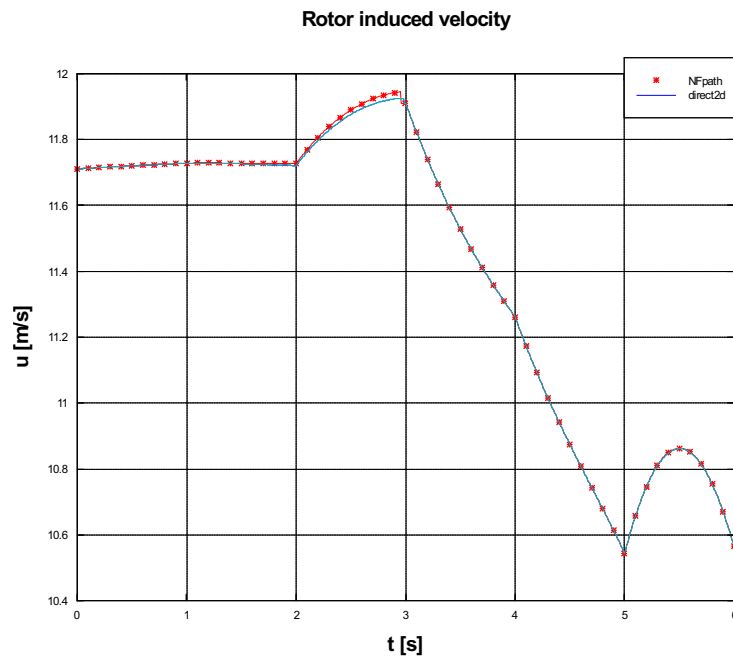


Figure 1.14: Induced velocity, hover test case

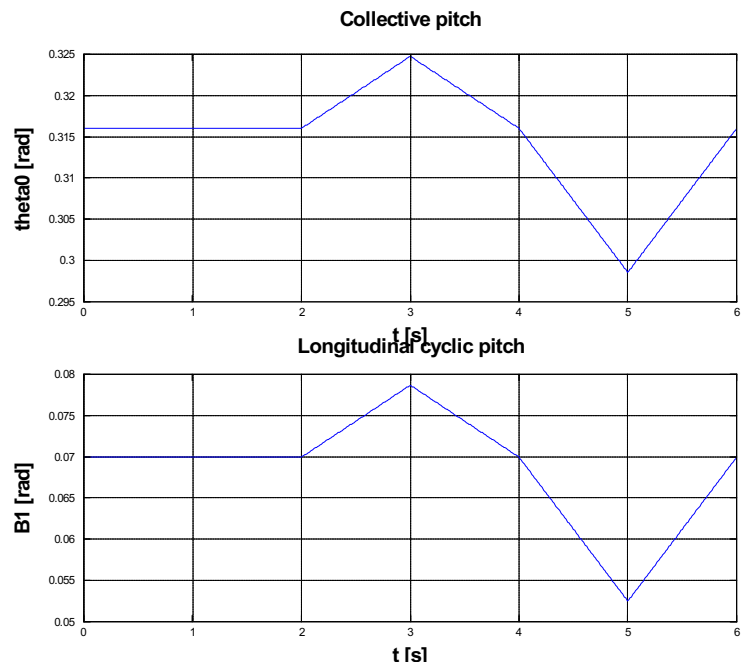


Figure 1.15: Control time history,  $\mu = 0.34$  test case

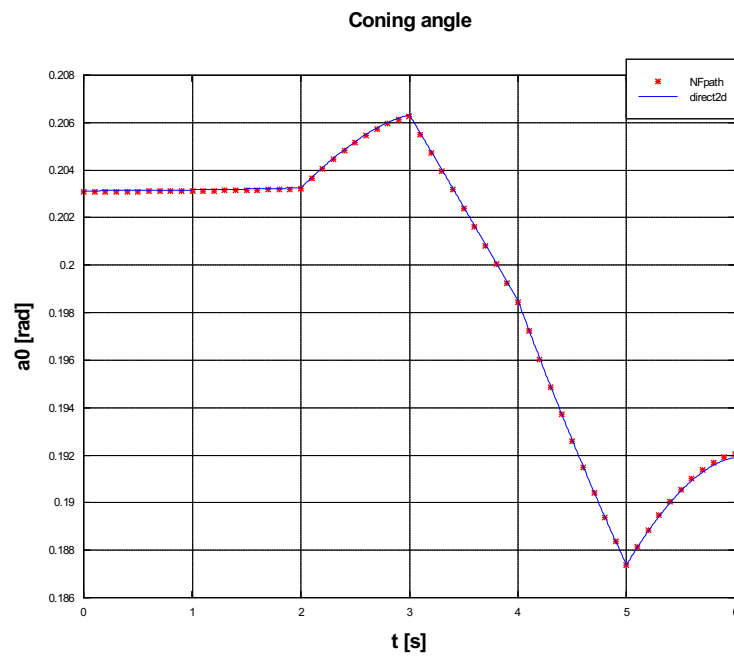


Figure 1.16: Coning,  $\mu = 0.34$  test case

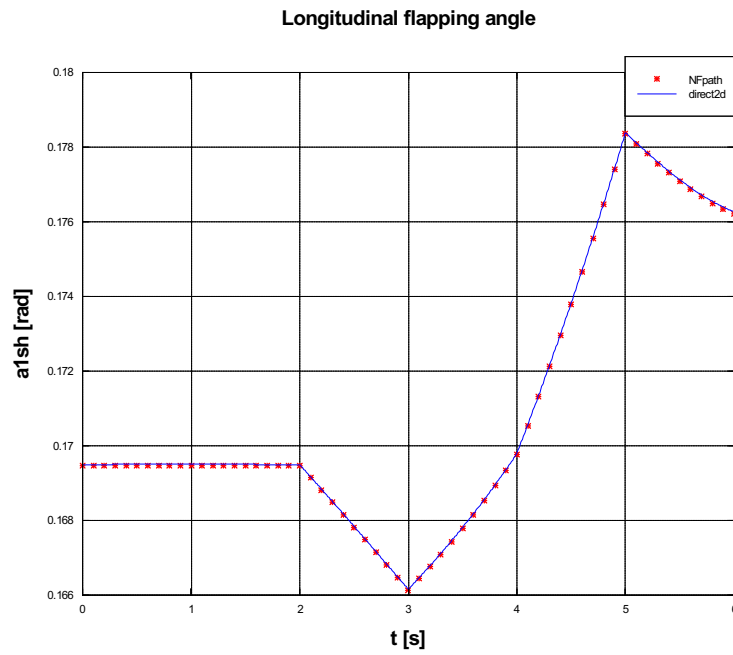


Figure 1.17: Longitudinal flapping,  $\mu = 0.34$  test case

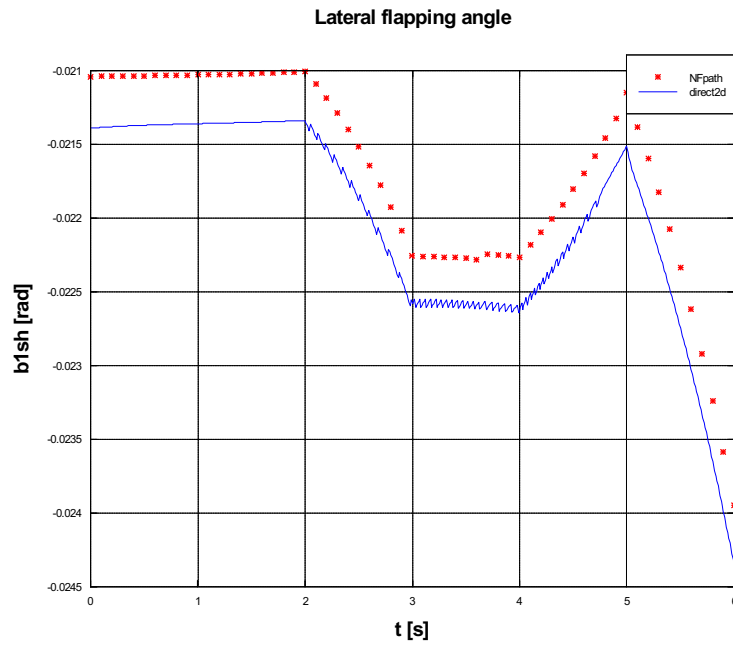


Figure 1.18: Lateral flapping,  $\mu = 0.34$  test case



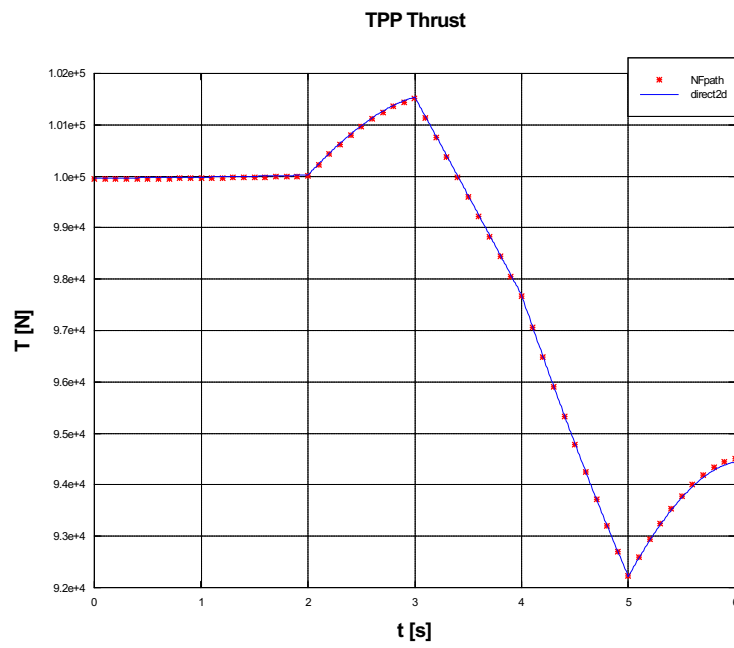


Figure 1.19: Thrust,  $\mu = 0.34$  test case

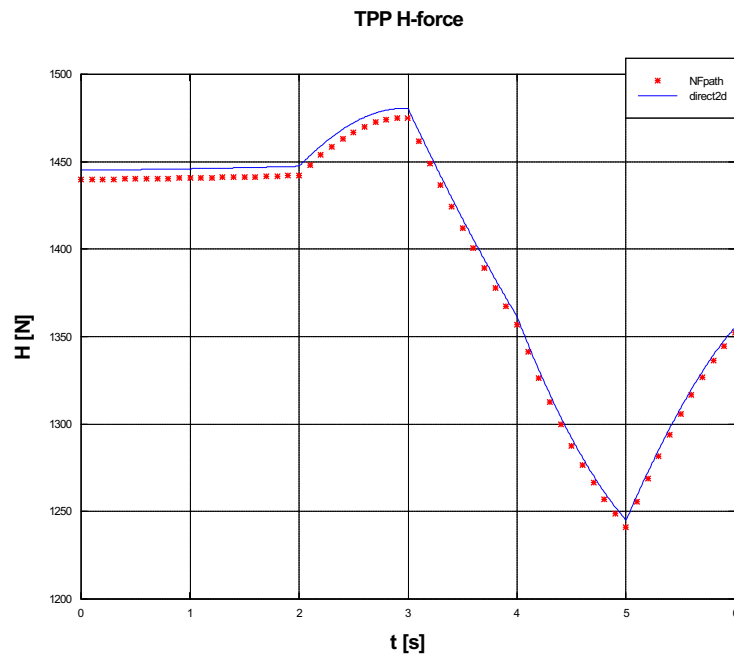


Figure 1.20: H-force,  $\mu = 0.34$  test case

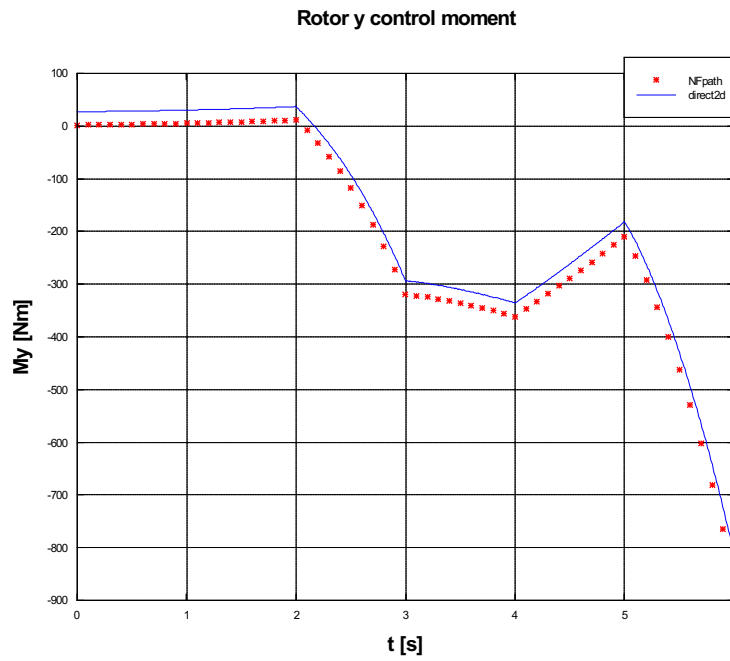


Figure 1.21: Pitching control moment,  $\mu = 0.34$  test case

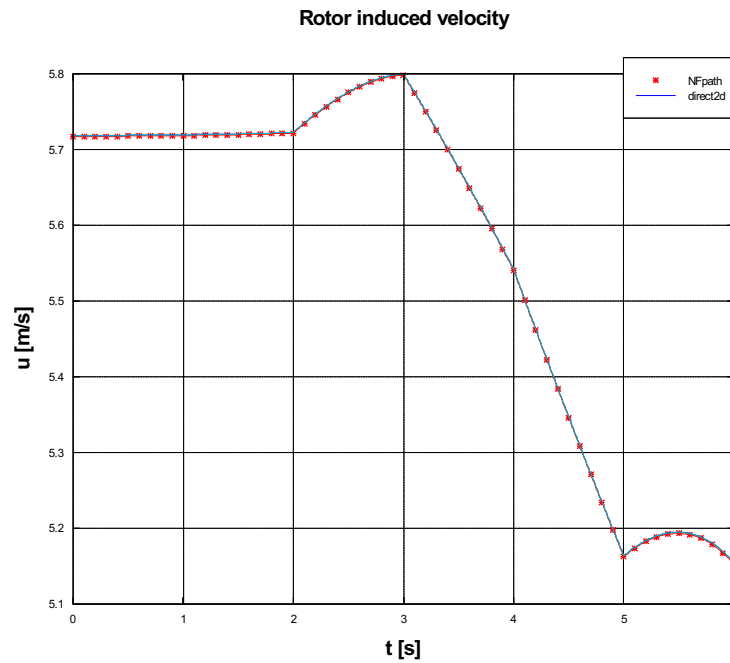


Figure 1.22: Induced velocity,  $\mu = 0.34$  test case

## Chapter 2

# Implementation of an algebraic rotor model

### 2.1 Scope

Once the needed formulations were extrapolated from *NFpath* code and validated, the isolated rotor model was re-implemented in a relatively lower level language in order to obtain a software module supposed to serve as rotor forces evaluator for a new rotorcraft simulation framework.

The objectives of this task were to:

- isolate the rotor model for the direct snapshot (for given parameters and controls, the module calculates forces generated by the rotor) while preserving the underlying proven formulations;
- extend the domain of the model to a fully three-dimensional motion;
- formulate rigorous transformations between couples of different reference frames, accounting for rigid body kinematics;
- introduce the effect of roll-rate (analogous to pitch-rate effect already modelled);
- improve the implementation with particular focus on ensuring continuity of the outputs, that is of primary importance when the model is called by gradient-based numerical methods (e.g. trim procedure);
- improve the inflow model with regard to:
  - continuity;
  - robustness;
  - computational efficiency;

- algorithm simplification;
- improve the ground effect model with regard to:
  - continuity;
  - new formulation of the ground speed influence on ground effect;
- use a single non linear solver as substitute to the nested iterations.

## 2.2 Methodology and tools

The model was implemented in *ANSI C* language, taking particular care in the use of only standard portable language features and best programming practices [11]. A considerable effort was applied in ensuring readability and maintainability of the code through code modularity, consistent indentation and a systematic use of comments and meaningful variable names.

The code was written, compiled, debugged and tested using the *Integrated Development Environment* provided by *Microsoft Visual C++ 2008 Express Edition* [15].

Since the rotor model is intended to be a software library and not a stand alone application, in order to simplify testing of the model it was compiled as a *Dynamic Loading Library* (DLL), which in turn was loaded by the previously described software *Freemat*; the latter provided an easy-to-use interface for supplying data to the library and for post-processing results.

## 2.3 Model description

### 2.3.1 Structure

An overview of the rotor model is presented in figure 2.1. It is immediate to see that the model is made up of two nested tiers: the innermost performs the calculations in the shaft-wind reference frame, where the formulations described in the previous chapters have their validity, while the outermost tier takes care of all the necessary changes of basis to and from other reference frames for inputs and outputs.

It can be seen, also, that all the nested iterations present in the legacy algorithm have been replaced by a single set of three equations, which is solved by the means of a numerical non linear solver. The inflow module, including the ground effect model, is implemented as a separate model, which is seen by the solver as a non-linear function.

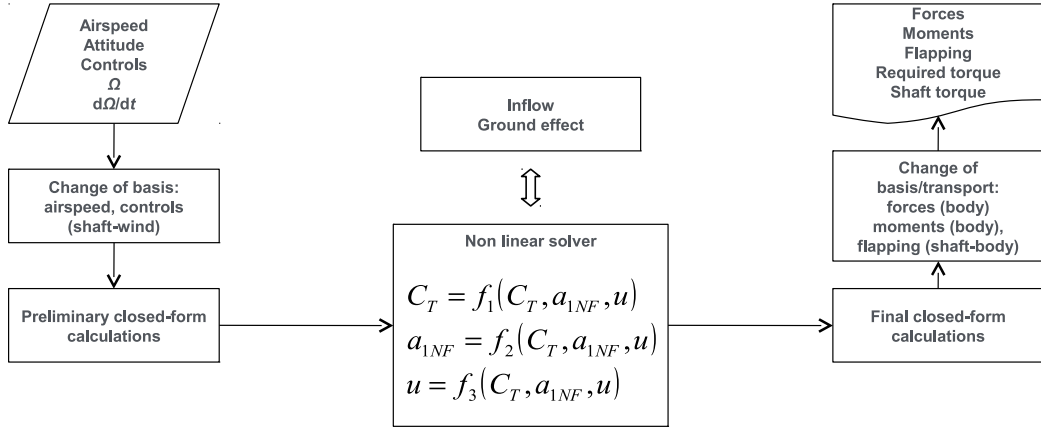


Figure 2.1: Overview of the rotor model algorithm

## 2.3.2 Rotations

### 2.3.2.1 Rotation from inertial triad to body triad

The rotation tensor from inertial triad to body triad, expressed in the inertial reference frame, and its inverse rotation tensor, can be written as a function of Eulers attitude angles in 3-2-1 sequence, in the form of a DCM (Direction Cosine Matrix):

$$\mathbf{R}_{I \rightarrow B}^I = \begin{bmatrix} c_\Psi c_\Theta & c_\Psi s_\Theta s_\Phi - s_\Psi c_\Phi & c_\Psi s_\Theta c_\Phi + s_\Psi s_\Phi \\ s_\Psi c_\Theta & s_\Psi s_\Theta s_\Phi + c_\Psi c_\Phi & s_\Psi s_\Theta c_\Phi - c_\Psi s_\Phi \\ -s_\Theta & c_\Theta s_\Phi & c_\Theta c_\Phi \end{bmatrix}, \quad (2.1a)$$

$$\mathbf{R}_{B \rightarrow I}^B = (\mathbf{R}_{I \rightarrow B}^I)^T, \quad (2.1b)$$

where, for the sake of compactness  $c_\Phi = \cos \Phi$ ,  $s_\Phi = \sin \Phi$ ,  $c_\Theta = \cos \Theta$ ,  $s_\Theta = \sin \Theta$ ,  $c_\Psi = \cos \Psi$ ,  $s_\Psi = \sin \Psi$ , and  $\Phi$ ,  $\Theta$  and  $\Psi$  are the angles of roll, pitch and yaw.

From here on, rotation tensors notation uses the subscript to indicate the initial and final triads of the transformation, and the superscript to indicate the triad used to express the tensor itself.

### 2.3.2.2 Rotation from design triad to body triad

The rotation tensor from design triad (STA-BL-WL frame) to body triad, expressed in the design reference frame, and its inverse rotation tensor, can

be written in the form of a DCM (Direction Cosine Matrix):

$$\mathbf{R}_{D \rightarrow B}^D = \begin{bmatrix} -1 & 0 & 0 \\ 0 & 1 & 0 \\ 0 & 0 & -1 \end{bmatrix}, \quad (2.2a)$$

$$\mathbf{R}_{B \rightarrow D}^B = (\mathbf{R}_{D \rightarrow B}^D)^T, \quad (2.2b)$$

### 2.3.2.3 Rotation from body triad to shaft-body triad

According to Eulers theorem, a rotation between two reference systems can be always described as a single rotation of a certain amount about a well defined axis. In this fashion, a rotation tensor can be written as a function of an angle and a unity vector defining the rotation axis, expressed in the initial frame; this function is known as *Euler-Rodrigues* formula [4]:

$$\mathbf{R}_{A \rightarrow B}^A(\mathbf{a}^A, \phi) = \mathbf{I} + \sin \phi \mathbf{a}_\times + (1 - \cos \phi) \mathbf{a}_\times \mathbf{a}_\times. \quad (2.3)$$

The shaft-body triad with reference to the body frame is defined by a combination of three rotations in a well defined sequence:

1. a rotation of an angle  $\pi + \iota_{\text{tilt}}$  about  $\mathbf{j}_B$ , representing the fixed tilt of the mast (summing  $\pi$  to the tilt angle makes  $\mathbf{i}_{SB}$  point backwards and  $\mathbf{k}_{SB}$  point upwards as in a conventional main rotor configuration);
2. a rotation of an angle  $\iota_{\text{cant}}$  about  $\mathbf{i}_B$ , representing the cant of the mast;
3. a rotation of an angle  $\iota_{\text{contr}}$  about a given unity vector  $\mathbf{a}_{\text{contr}}$ , representing the tilt control (nacelle angle) in a tilt-rotor vehicle; in other words: the rotation from nominal shaft position (body attached) to commanded shaft position.

In the current implementation  $\mathbf{a}_{\text{contr}}$  can be only set equal to one unity vector between:  $\mathbf{i}_B$ ,  $\mathbf{j}_B$ ,  $\mathbf{k}_B$ .

Using the previously defined *Euler-Rodrigues* formula, the tensor resulting from the combination of the three rotations can be written as:

$$\begin{aligned} \mathbf{R}_{B \rightarrow SB}^B &= \mathbf{R}_{B \rightarrow \text{tilt}}^B \mathbf{R}_{\text{tilt} \rightarrow \text{fixed}}^{\text{tilt}} \mathbf{R}_{\text{fixed} \rightarrow SB}^{\text{fixed}} \\ &= \mathbf{R}_{B \rightarrow \text{tilt}}^B(\mathbf{j}_B^B, \pi + \iota_{\text{tilt}}) \mathbf{R}_{\text{tilt} \rightarrow \text{fixed}}^{\text{tilt}}(\mathbf{i}_B^{\text{tilt}}, \iota_{\text{cant}}) \mathbf{R}_{\text{fixed} \rightarrow SB}^{\text{fixed}}(\mathbf{j}_B^{\text{fixed}}, \iota_{\text{contr}}) \\ &= \mathbf{R}_{B \rightarrow \text{tilt}}^B(\mathbf{j}_B^B, \pi + \iota_{\text{tilt}}) \mathbf{R}_{\text{tilt} \rightarrow \text{fixed}}^{\text{tilt}}(\mathbf{R}_{\text{tilt} \rightarrow B}^{\text{tilt}} \mathbf{i}_B^B, \iota_{\text{cant}}) \cdots \\ &\cdots \mathbf{R}_{\text{fixed} \rightarrow SB}^{\text{fixed}}(\mathbf{R}_{\text{fixed} \rightarrow B}^{\text{fixed}} \mathbf{j}_B^B, \iota_{\text{contr}}), \end{aligned} \quad (2.4)$$

where:

$$\mathbf{R}_{\text{tilt} \rightarrow B}^{\text{tilt}} = (\mathbf{R}_{B \rightarrow \text{tilt}}^B)^T, \quad (2.5a)$$

$$\mathbf{R}_{\text{fixed} \rightarrow \text{B}}^{\text{fixed}} = (\mathbf{R}_{\text{B} \rightarrow \text{fixed}}^{\text{B}})^{\text{T}} = (\mathbf{R}_{\text{B} \rightarrow \text{tilt}}^{\text{B}} \mathbf{R}_{\text{tilt} \rightarrow \text{fixed}}^{\text{tilt}})^{\text{T}}, \quad (2.5\text{b})$$

and as usual we have also the inverse rotation tensor:

$$\mathbf{R}_{\text{SB} \rightarrow \text{B}}^{\text{SB}} = (\mathbf{R}_{\text{B} \rightarrow \text{SB}}^{\text{B}})^{\text{T}}, \quad (2.6)$$

### 2.3.2.4 Rotation from shaft-body triad to shaft-wind triad

The shaft-wind triad is defined by the shaft-body triad, rotated about  $\mathbf{k}_{\text{SB}}$  so that the following conditions are satisfied:

1. the total airspeed vector  $\mathbf{V}$  in the origin point C (rotor hub) lies on the plane defined by  $\mathbf{i}_{\text{SW}}$  and  $\mathbf{k}_{\text{SW}}$ ;
2. the unity vector  $\mathbf{i}_{\text{SW}}$  is directed as the projection of  $\mathbf{V}$  on  $x_{\text{SW}}$ .

A reference frame so defined allows to write the rotor equations under simplified assumptions, since horizontal airspeed (with reference to the shaft) will be always directed as  $\mathbf{i}_{\text{SW}}$ , regardless of the sideslip of the airframe; this is coherent with the assumptions the classical closed form rotor equations are based on.

The position of the pivot point  $P$ , that is the centre of rotation of the nacelle in a tilt rotor configuration, known in the design frame, is expressed in body frame:

$$\mathbf{r}_{OP}^{\text{B}} = \mathbf{R}_{\text{B} \rightarrow \text{D}}^{\text{B}} (\mathbf{r}_{DP}^{\text{D}} - \mathbf{r}_{DO}^{\text{D}}). \quad (2.7)$$

The position of the rotor hub  $C$ , which is located along the mast axis at a distance  $d_{\text{pivot}}$  from the pivot, is expressed in body frame:

$$\mathbf{r}_{OC}^{\text{B}} = \mathbf{r}_{OP}^{\text{B}} + \mathbf{R}_{\text{B} \rightarrow \text{SB}}^{\text{B}} (d_{\text{pivot}} \mathbf{k}_{\text{SB}}^{\text{SB}}). \quad (2.8)$$

The rotor hub position is considered the position where all rotor forces are applied; also, asymptotic airspeed used in the calculation of rotor forces is evaluated in this same point and assumed as uniform over the whole rotor disc.

The total speed in  $C$ , including the component due to rigid body rotation, is calculated as:

$$\mathbf{v}_C^{\text{B}} = \mathbf{v}_O^{\text{B}} + \boldsymbol{\omega}^{\text{B}} \times \mathbf{r}_{OC}^{\text{B}}. \quad (2.9\text{a})$$

$$\mathbf{v}_C^{\text{SB}} = \mathbf{R}_{\text{SB} \rightarrow \text{B}}^{\text{SB}} \mathbf{v}_C^{\text{B}}. \quad (2.9\text{b})$$

where linear and angular velocities evaluated in the body frame origin point  $O$  are used.

The wind speed, known in inertial frame, is expressed in shaft-body frame:

$$\mathbf{v}_{\text{wind}}^{\text{SB}} = \mathbf{R}_{\text{SB} \rightarrow \text{I}}^{\text{SB}} \mathbf{v}_{\text{wind}}^{\text{I}} = (\mathbf{R}_{\text{I} \rightarrow \text{B}}^{\text{B}} \mathbf{R}_{\text{B} \rightarrow \text{SB}}^{\text{B}})^{\text{T}} \mathbf{v}_{\text{wind}}^{\text{I}}. \quad (2.10)$$

The total airspeed at point  $C$  is then:

$$\mathbf{V}^{\text{SB}} = -\mathbf{v}_C^{\text{SB}} + \mathbf{v}_{\text{wind}}^{\text{SB}} . \quad (2.11)$$

We have now all the data required to determine the rotation tensor from the shaft-body triad to the shaft-wind triad. Unity vector  $\mathbf{k}_{\text{SW}}$  is known by definition:

$$\mathbf{k}_{\text{SW}}^{\text{SB}} = \mathbf{k}_{\text{SB}}^{\text{SB}} . \quad (2.12)$$

Unity vector  $\mathbf{i}_{\text{SW}}$  is obtained as:

$$\mathbf{i}_{\text{SW}}^{\text{SB}} = \frac{1}{\sqrt{(\mathbf{V}^{\text{SB}} \cdot \mathbf{i}_{\text{SB}}^{\text{SB}})^2 + (\mathbf{V}^{\text{SB}} \cdot \mathbf{j}_{\text{SB}}^{\text{SB}})^2}} \begin{Bmatrix} \mathbf{V}^{\text{SB}} \cdot \mathbf{i}_{\text{SB}}^{\text{SB}} \\ \mathbf{V}^{\text{SB}} \cdot \mathbf{j}_{\text{SB}}^{\text{SB}} \\ 0 \end{Bmatrix} , \quad (2.13)$$

and the right-handed triad is completed by  $\mathbf{j}_{\text{SW}}$ :

$$\mathbf{j}_{\text{SW}}^{\text{SB}} = \mathbf{k}_{\text{SW}}^{\text{SB}} \times \mathbf{i}_{\text{SW}}^{\text{SB}} . \quad (2.14)$$

then the rotation tensor is written as a DCM:

$$\mathbf{R}_{\text{SB} \rightarrow \text{SW}}^{\text{SB}} = [\mathbf{i}_{\text{SW}}^{\text{SB}} \mid \mathbf{j}_{\text{SW}}^{\text{SB}} \mid \mathbf{k}_{\text{SW}}^{\text{SB}}] , \quad (2.15a)$$

$$\mathbf{R}_{\text{SW} \rightarrow \text{SB}}^{\text{SW}} = (\mathbf{R}_{\text{SB} \rightarrow \text{SW}}^{\text{SB}})^{\text{T}} . \quad (2.15b)$$

### 2.3.2.5 Change of basis for controls

Pilot inputs for cyclic pitch controls define the attitude of the swash plate with reference to a body-fixed azimuth reference; in our case the body fixed azimuth is measured with reference to the shaft-body reference frame, as a right handed angle  $\psi^{\text{SB}}$  about  $\mathbf{k}_{\text{SB}}$ , starting from  $\mathbf{i}_{\text{SB}}$ .

Since rotor force calculations are performed relative to airspeed direction in the shaft-wind reference frame, cyclic pitch controls are to be expressed with reference to this reference frame, with azimuth measured as a right handed angle  $\psi^{\text{SW}}$  about  $\mathbf{k}_{\text{SW}}$ , starting from  $\mathbf{i}_{\text{SW}}$ .

Cyclic pitch as a function of azimuth (see eq. B.4) with reference to the shaft-body frame is defined as:

$$\theta(\psi^{\text{SB}}) = \theta_0 - A_1^{\text{SB}} \cos \psi^{\text{SB}} - B_1^{\text{SB}} \sin \psi^{\text{SB}} . \quad (2.16)$$

The same can be written also with reference to the shaft-wind frame:

$$\theta(\psi^{\text{SW}}) = \theta_0 - A_1^{\text{SW}} \cos \psi^{\text{SW}} - B_1^{\text{SW}} \sin \psi^{\text{SW}} , \quad (2.17)$$



where the azimuth differs from the previous one of the sideslip angle:

$$\psi^{\text{SW}} = \psi^{\text{SB}} + \beta_{\text{SB}} . \quad (2.18)$$

Recalling the identities:

$$\sin(a - b) = \sin a \cos b - \cos a \sin b , \quad (2.19a)$$

$$\cos(a - b) = \cos a \cos b + \sin a \sin b , \quad (2.19b)$$

and rearranging we obtain the control angles with reference to the shaft-wind frame:

$$A_1^{\text{SW}} = A_1^{\text{SB}} \cos \beta_{\text{SB}} - B_1^{\text{SB}} \sin \beta_{\text{SB}} , \quad (2.20a)$$

$$B_1^{\text{SW}} = A_1^{\text{SB}} \sin \beta_{\text{SB}} + B_1^{\text{SB}} \cos \beta_{\text{SB}} . \quad (2.20b)$$

### 2.3.3 Inflow model

#### 2.3.3.1 Inflow solution according to the actuator disc theory

The inflow model described later on defines the rotor uniform self-induced velocity as a function of the asymptotic airspeed  $V$ , the rotor disc angle of attack  $\alpha_{\text{TPP}}$ , the thrust coefficient  $C_{\text{T}}$  and the blade tip speed  $v_{\text{tip}}$ .

The hovering induced velocity is calculated as:

$$u_{\text{h}} = v_{\text{tip}} \sqrt{\frac{C_{\text{T}}}{2}} \quad (2.21)$$

This value is used as reference value for non-dimensional speeds:

$$v^* = \frac{V}{|u_{\text{h}}|} ; \quad (2.22a)$$

$$u^* = \frac{u}{|u_{\text{h}}|} . \quad (2.22b)$$

The non-dimensional induced velocity, outside the vortex ring state region, is given by the actuator disc theory as the minimum real positive root of a polynomial [2]:

$$u^*(v^*, \alpha_{\text{TPP}}) = \min\{u^* \in \Re : p(u^*) = \dots \dots u^{*4} - 2v^* \sin \alpha_{\text{TPP}} u^{*3} + v^{*2} u^{*2} - 1 = 0; u^* \geq 0\} . \quad (2.23)$$

The root of the polynomial is found numerically (see A.1). Note that the zero solution is acceptable if and only if  $C_{\text{T}}$  is zero.

### 2.3.3.2 Interpolation of the empirical inflow model for vortex ring state condition

#### 2.3.3.3 Vortex ring state

Normal and tangential components of the asymptotic speed are defined as:

$$v_t = v^* \cos \alpha_{\text{TPP}} ; \quad (2.24a)$$

$$v_n = v^* \sin \alpha_{\text{TPP}} . \quad (2.24b)$$

If  $1 < v_n < 2$ , the rotor is in a moderate descent condition, which is heavily influenced by the vortex ring state. In this condition the solution from the actuator disc theory is not reliable.

The induced velocity that the rotor would produce in axial flight ( $v_t = 0$ ) at the same normal airspeed is known from an experimental relationship:

$$u_{\text{VRS0}}^* = u_{\text{VRS0}}^*(v_n) \quad (2.25)$$

In order to obtain a realistic value in the flight envelope region affected by the vortex ring state, the empirical value for axial flight is weighted using the values of the polynomial solution on borders of the vortex ring state region as form functions:

$$a = 2 - v_n ; \quad (2.26a)$$

$$v_1 = \sqrt{1 + v_t^2} ; \quad (2.26b)$$

$$v_2 = \sqrt{4 + v_t^2} ; \quad (2.26c)$$

$$u_{\text{VRS}}^* = u_{\text{VRS0}}^* \left( a \frac{u^*(v_1, \alpha_{\text{TPP}})}{u^*(1, \alpha_{\text{TPP}})} + (1 - a) \frac{u^*(v_2, \alpha_{\text{TPP}})}{u^*(2, \alpha_{\text{TPP}})} \right) \quad (2.26d)$$

In order to insure continuity of the solution and to restrict the effect of the interpolation only to the region where vortex ring state decreases the induced velocity, the interpolated value  $u_{\text{VRS}}^*$  is used instead of  $u^*$  only when the value according to the actuator disc theory exceeds it.

In figure 2.2 the solution of the polynomial expression for the induced velocity according to the disc actuator theory is shown; it is easy to see that the values in the part of flight envelope affected by the vortex ring state have no physical meaning and show significant discontinuity; in figure 2.3 the same data is smoothed using the experimental data as described before; the comparison between the two solutions is shown by the difference plot in figure 2.4, that confirms that the empirical correction is limited to the portion of flight envelope affected by the vortex ring state, while the rest of the envelope retains the solution according to the disc actuator theory. In

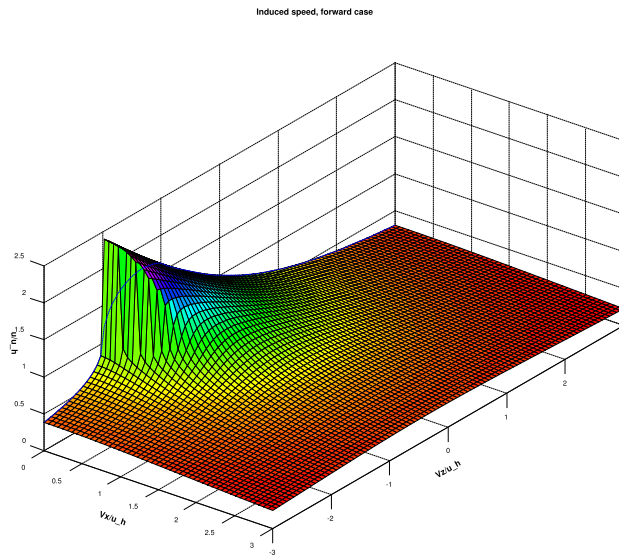


Figure 2.2: Induced velocity from actuator disc theory as a function of tangential and normal speed components

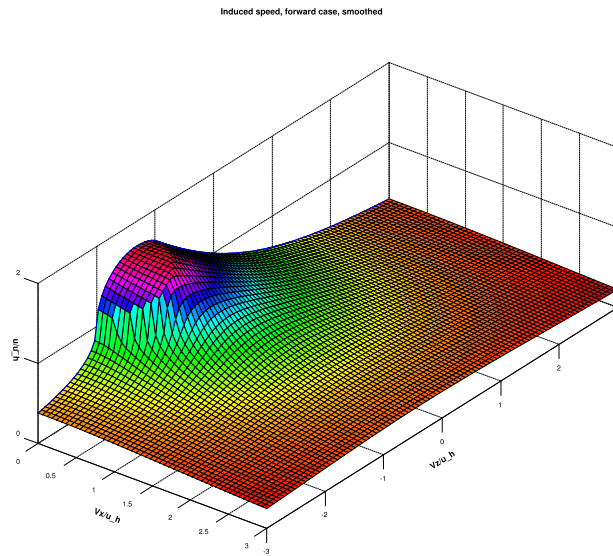


Figure 2.3: Induced velocity from actuator disc theory as a function of tangential and normal speed components, with smoothing of experimental data in the part of envelope affected by the vortex ring state

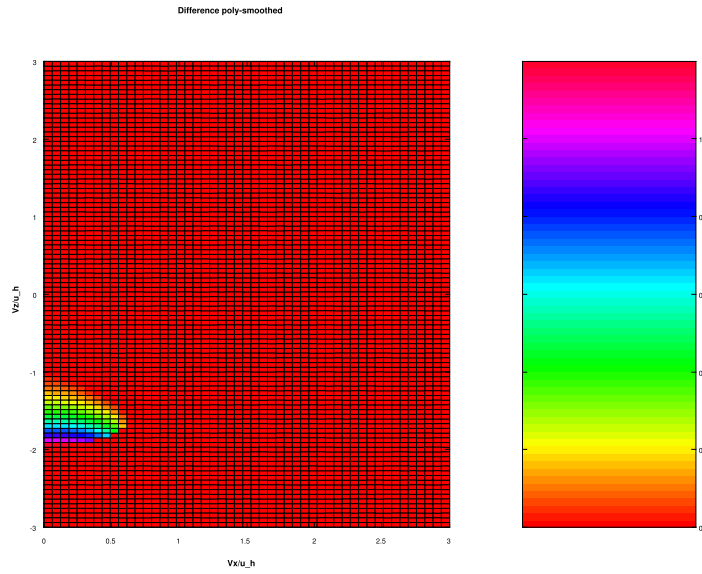


Figure 2.4: Difference between the induced velocity calculated by the new rotor model and the values calculated according to NFpath algorithm

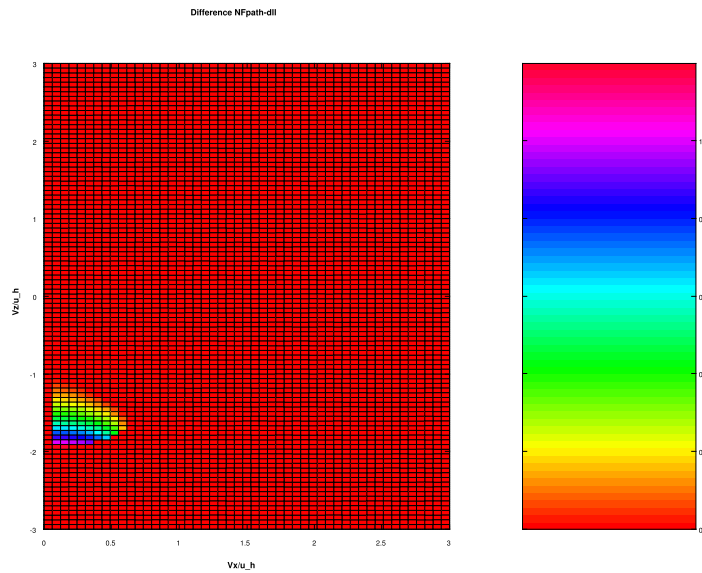


Figure 2.5: Difference between the actuator disc solution and the the mixed experimental-theoretical smoothed solution

figure 2.5 a comparison between the new model and the results from *NFpath* algorithms: it is evident that *NFpath* applies the vortex ring state empirical correction only to part of the region affected by the phenomenon, leaving the rest of the region uncorrected and with discontinuities that can propagate to the rotor model and to the rotorcraft model, possibly creating problems for the use of gradient methods (e.g. trim procedures).

### 2.3.3.4 Ground effect model

In order to evaluate ground effect it is necessary to calculate the hub distance from ground along the mast axis and the absolute value of airspeed parallel to ground:

$$d_{\text{gnd}} = \frac{-z_{\text{gnd}} + (\mathbf{R}_{\text{I} \rightarrow \text{B}}^{\text{I}} \mathbf{r}_{\text{OC}}^{\text{B}}) \cdot \mathbf{k}_{\text{I}}^{\text{I}}}{(\mathbf{R}_{\text{I} \rightarrow \text{SB}}^{\text{I}} \mathbf{k}_{\text{SB}}^{\text{SB}}) \cdot \mathbf{k}_{\text{I}}^{\text{I}}}, \quad (2.27\text{a})$$

$$\sqrt{((\mathbf{R}_{\text{I} \rightarrow \text{B}}^{\text{I}} \mathbf{v}_{\text{C}}^{\text{B}}) \cdot \mathbf{i}_{\text{I}}^{\text{I}})^2 + ((\mathbf{R}_{\text{I} \rightarrow \text{B}}^{\text{I}} \mathbf{v}_{\text{C}}^{\text{B}}) \cdot \mathbf{j}_{\text{I}}^{\text{I}})^2}, \quad (2.27\text{b})$$

where  $z_{\text{gnd}}$  is the vertical distance of  $O$  from ground. Note that if the rotor is upside-down ( $\mathbf{k}_{\text{SB}}$  pointing to ground) or the hub is under terrain level,  $d_{\text{gnd}}$  is set to negative; in this case the algorithm causes OGE to be forced.

Ground distance is evaluated along the mast axis in order to account for the effect of rotorcraft attitude; this differs from the approach used in *NFpath*, where only the vertical ground distance was considered.

Ground effect is taken into account by multiplying the uniform induced velocity, calculated for OGE conditions, by a coefficient  $k_{\text{gnd}}$  that is function of the distance between hub and ground along the shaft axis and of the airspeed parallel to ground.

Defining the function that evaluates the coefficient  $k_{\text{gnd}}$ , special care was used in making sure that this coefficient is a continuous function of the ground distance and airspeed.

The coefficient  $k_{\text{gnd}}$  for axial flight is known as an empirical function of the ground distance (in the form of distance/radius ratio), limited to minimum and maximum boundaries<sup>1</sup>:

$$\begin{aligned} d_{\text{gnd}} < d_{\text{gnd,lo}} &: & k_{\text{gnd},0} &= k_{\text{gnd},0}(d_{\text{gnd,lo}}), \\ d_{\text{gnd,lo}} \leq d_{\text{gnd}} \leq d_{\text{gnd,hi}} &: & k_{\text{gnd},0} &= k_{\text{gnd},0}(d_{\text{gnd}}), \\ d_{\text{gnd}} > d_{\text{gnd,hi}} &: & k_{\text{gnd},0} &= 1, \end{aligned} \quad (2.28)$$

The aim of the following additions to this simple ground effect model is to add a realistic representation of the behaviour of ground effect versus ground

<sup>1</sup>Company confidentiality restrictions apply: detailed information about this topic cannot be disclosed.

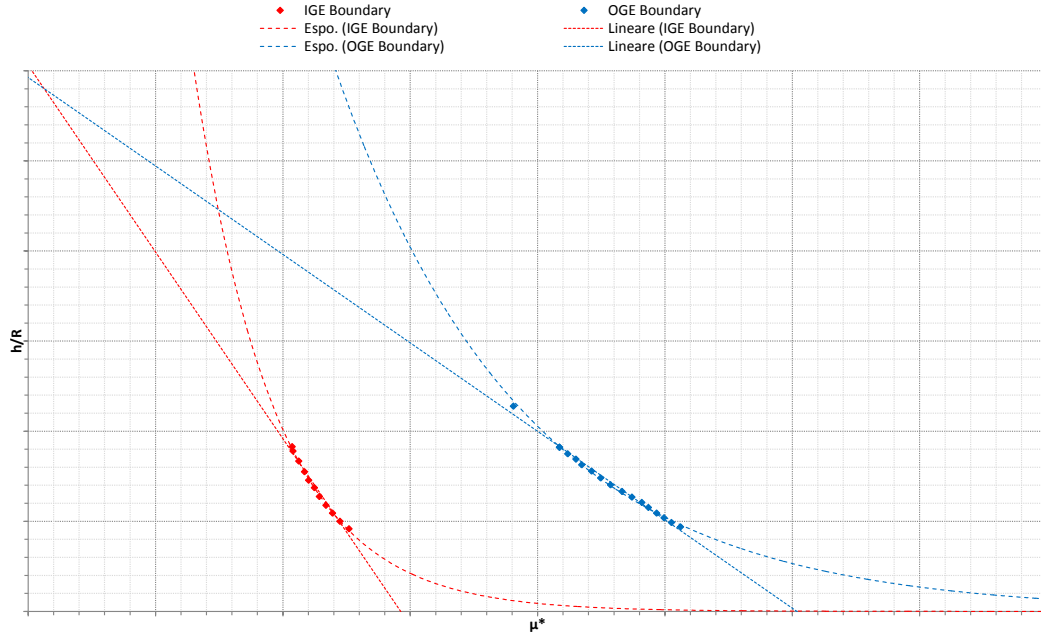


Figure 2.6: Experimental Curtiss-Sun diagram with interpolations

speed, defining a continuous transition between the hover condition (where ground effect is maximum) and high advance ratio motion (where ground effect is absent).

Based on linearisation of experimental data in the form of *Curtiss-Sun* diagrams [9], as shown in figure 2.6, the algorithm calculates an upper boundary ground airspeed for completely developed ground effect as a function of non-dimensional ground distance; for a ground airspeed lesser than this boundary, the coefficient  $k_{\text{gnd}}$  is equal to the one calculated for axial flight. In the same fashion, a lower boundary airspeed for out-of-ground-effect condition is calculated and  $k_{\text{gnd}}$  is assigned as unity for airspeeds greater than this boundary:

$$\mu^* = \mu_{\text{NF}} \sqrt{\frac{2}{C_{\text{T}}}} . \quad (2.29\text{a})$$

$$\mu_{\text{IGE}}^* = c_{\text{IGE},0} + c_{\text{IGE},1} d_{\text{gnd}} , \quad (2.29\text{b})$$

$$\mu_{\text{OGE}}^* = c_{\text{OGE},0} + c_{\text{OGE},1} d_{\text{gnd}} , \quad (2.29\text{c})$$

For airspeeds between the two boundaries a cosine interpolation is used in

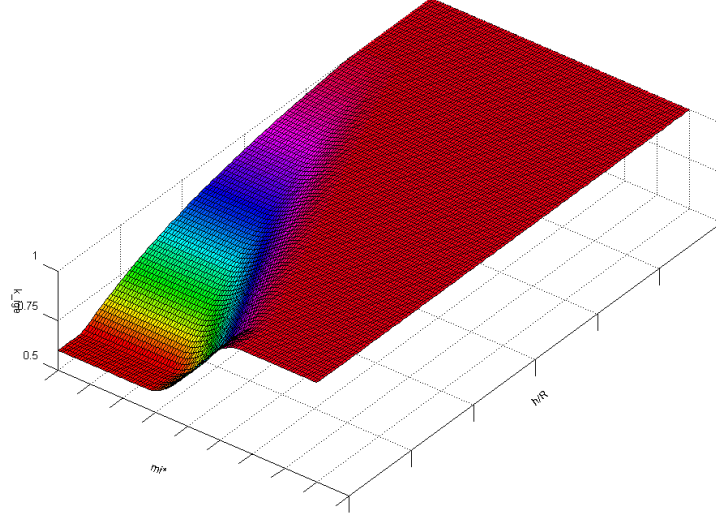


Figure 2.7: Ground effect coefficient

order to ensure continuity:

$$\begin{aligned}
 \mu^* < \mu_{\text{IGE}}^* &: & a &= 1, \\
 \mu_{\text{IGE}}^* \leq \mu^* \leq \mu_{\text{OGE}}^* &: & a &= \frac{1}{2} \left( 1 + \cos \left( \pi \frac{\mu^* - \mu_{\text{IGE}}^*}{\mu_{\text{OGE}}^* - \mu_{\text{IGE}}^*} \right) \right), \\
 \mu^* > \mu_{\text{OGE}}^* &: & a &= 0,
 \end{aligned} \tag{2.30}$$

The described interpolation results in a continuous function, as depicted in figure 2.7:

$$k_{\text{gnd}} = 1 - (1 - a)k_{\text{gnd},0}, \tag{2.31a}$$

$$u = u_{\text{h}} k_{\text{gnd}} \min\{u^*; u_{\text{VRS}}^*\}. \tag{2.31b}$$

The properties of the described ground effect model will be described in detail in section 4.3.

### 2.3.3.5 Accounting for negative thrust

According to the momentum balance equation, the uniform induced velocity will have always the same direction and opposite sign as the thrust. Since in the convention used thrust is positive upwards and induced velocity is positive downwards, numerical values of  $u$  and  $C_T$  will always have the same sign.

In case  $C_T$  is negative, the calculation is performed in the same way as described above, but  $C_T$ ,  $\alpha_{TPP}$ , and  $u_h$  are replaced with their opposites. With these substitutions the resulting value of  $u$  has the correct sign (negative) and vortex ring state is evaluated in the correct normal airspeed range.

### 2.3.4 Rotor equations

Closed-form equations for rotor forces and flapping used in the described model are derived under the assumption that the blade is untwisted. As already noted before, such a formulation is an acceptable approximation of a blade with a moderate linear twist, provided that the pitch of the real blade, measured at 75% of the radius, equals the uniform pitch in the untwisted model, so:

$$\theta_0 = \theta_{75, \text{twisted}} . \quad (2.32)$$

#### 2.3.4.1 Non-linear equation set

A non linear function for the inflow, including a model for vortex ring state and ground effect, has been obtained; recalling the relationship between the angle of the attack of the disc and the longitudinal flapping angle, and the expression of the latter with reference to the non-feathering plane:

$$\alpha_{\text{TPP}} = \alpha_{\text{SW}} + a_1^{\text{SW}} , \quad (2.33a)$$

$$a_1^{\text{SW}} = a_1^{\text{NF}} - B_1 , \quad (2.33b)$$

it is possible to express the induced velocity  $u$  as a non-linear function of the thrust coefficient  $C_T$  and of the longitudinal flapping coefficient  $a_1^{\text{NF}}$ .

In order to complete the problem we still need two more equations for  $C_T$  and  $a_1^{\text{NF}}$ . These equations can be derived in closed form by substituting the truncated Fourier expansion of blade flapping into the differential equation of flapping [23, 5, 21]. A possible expression of these two equations, where inflow distribution has been modelled according to [12], is the following:

$$C_T = \sigma \frac{C_{L/\alpha}}{4} \left( \frac{2}{3} \theta_0 \frac{1 - \mu_{\text{NF}}^2 + \frac{9}{4} \mu_{\text{NF}}^4}{1 + \frac{3}{2} \mu_{\text{NF}}^2} + \lambda_{\text{TPP}} \frac{1 - \frac{1}{2} \mu_{\text{NF}}^2}{1 + \frac{3}{2} \mu_{\text{NF}}^2} \right) , \quad (2.34a)$$

$$a_1^{\text{NF}} = \frac{\frac{2\mu_{\text{NF}}(\frac{4}{3}\theta_0 + \lambda_{\text{TPP}}) - \frac{16\phi}{\Omega\gamma(1-e\beta)^2} - \frac{\phi}{\Omega}}{1 + \frac{3}{2}\mu_{\text{NF}}^2} + \frac{8}{\gamma} \frac{\epsilon}{1 + \frac{3}{2}\mu_{\text{NF}}^2} \frac{\frac{4}{3}(\mu_{\text{NF}}a_0 + 1.1\nu^{\frac{1}{2}}\lambda_i)}{1 + \frac{1}{2}\mu_{\text{NF}}^2}}{1 - \left( \frac{8}{\gamma} \frac{\epsilon}{1 + \frac{3}{2}\mu_{\text{NF}}^2} \right) \left( -\frac{8}{\gamma} \frac{\epsilon}{1 + \frac{1}{2}\mu_{\text{NF}}^2} \right)} . \quad (2.34b)$$

By substituting the following definitions:

$$\lambda_{\text{TPP}} = \frac{V \sin \alpha_{\text{TPP}} - u}{v_{\text{tip}}} , \quad (2.35a)$$



$$\lambda_i = \frac{u}{v_{\text{tip}}}, \quad (2.35b)$$

$$\nu = \frac{1 + \sin \alpha_{\text{TPP}}}{1 - \sin \alpha_{\text{TPP}}}, \quad (2.35c)$$

$$\gamma = \frac{\rho C_{L/\alpha} c R^4}{I_\beta}, \quad (2.35d)$$

$$\epsilon = \frac{M_b}{I_\beta} x_{\text{cg}} e_\beta R^2, \quad (2.35e)$$

in Eqs. 2.34, a set of three algebraic non linear equations with three unknown variables is obtained:

$$C_T = f_1(C_T, a_1^{\text{NF}}, u), \quad (2.36a)$$

$$a_1^{\text{NF}} = f_2(C_T, a_1^{\text{NF}}, u), \quad (2.36b)$$

$$u = f_3(C_T, a_1^{\text{NF}}, u), \quad (2.36c)$$

which can be solved numerically. In the model implementation the equations were divided by reference values in order to improve their conditioning and then solved using Broyden's method (see section A.2).

#### 2.3.4.2 Additional closed-form rotor equations

The average drag coefficient used in the following equations is calculated using the same proprietary algorithm introduced in section 1.2.1.3.

The lateral flapping coefficient is calculated using the following closed form equation, incorporating the effect of roll rate:

$$b_{1\text{NF}} = \frac{\frac{4}{3} \left( \mu_{\text{NF}} a_0 + 1.1 \nu^{\frac{1}{2}} \lambda_i \right) - \frac{16\dot{\theta}}{\Omega \gamma (1-\epsilon)^2} - \frac{\dot{\theta}}{\Omega} - \frac{8}{\gamma} \epsilon a_{1\text{NF}}}{1 - \frac{1}{2} \mu_{\text{NF}}^2}. \quad (2.37)$$

The H-force coefficient is calculated as:

$$h_{\text{cd}} = \frac{C_H}{\sigma} = \frac{1}{4} \mu_{\text{NF}} \left( C_d + C_{l/\alpha} \lambda_{\text{TPP}} \frac{\frac{1}{3} \theta_0 \left( 1 - \frac{9}{2} \mu_{\text{NF}}^2 \right) + \lambda_{\text{TPP}}}{1 + \frac{3}{2} \mu_{\text{NF}}^2} \right), \quad (2.38)$$

It is important to point out that in the present implementation the model doesn't take into account the effect of reverse flow area in the calculations of the H-force, as well as in all the other evaluations. For comparison purposes, it is useful to remember that in *NFpath* the reverse flow correction is implemented only for the H-force evaluation.

The required torque coefficient is calculated by eq. 1.23c, with the “induced K” evaluated as a linear interpolation between the hovering value and the forward flight value in the low speed range.

Dimensional values for thrust and H-force, with reference to the TPP frame, required torque and required power are given by eqs. 1.24.

Control moments about the rotor hub, with reference to the shaft-wind reference frame, are directly proportional to the flapping coefficients:

$$M_{y,SW,C} = \frac{1}{2} N_b M_b x_{cg} e v_{tip}^2 a_{1SW} , \quad (2.39a)$$

$$M_{x,SW,C} = -\frac{1}{2} N_b M_b x_{cg} e v_{tip}^2 b_{1SW} . \quad (2.39b)$$

### 2.3.5 Accounting for rotor sense of rotation

The calculation of rotor forces is set up for rotors rotating counter-clockwise (positive right-handed rotation about  $\mathbf{k}_{SB}$ ); in case a rotor is indicated in the parameters as clockwise rotating, the following adjustments apply:

- $A_1$  is used in place with the opposite sign;
- the sign of resulting values of  $b_{1NF}$ ,  $b_{1SW}$ ,  $M_{x,SW,C}$ , and  $Q_R$  is changed.

### 2.3.6 Change of basis for flapping angles

The longitudinal and lateral flapping angles  $a_{1SW}$  and  $b_{1SW}$ , which are readily obtained by eqs. B.5 from the previously calculated values of  $a_{1NF}$  and  $b_{1NF}$ , are referred to the shaft-wind reference frame. They need to be brought to the rotorcraft-fixed shaft-body frame in order to describe the rotor disc attitude relative to the body. This change of basis, that involves a single rotation along  $\mathbf{k}_{SW}$  can be performed using the same approach used in section 2.3.2.5.

The flapping angles with reference to the shaft body reference frame can be written as:

$$a_{1SB} = b_{1SW} \cos \beta_{SB} + b_{1SW} \sin \beta_{SB} , \quad (2.40a)$$

$$b_{1SB} = -b_{1SW} \sin \beta_{SB} + b_{1SW} \cos \beta_{SB} . \quad (2.40b)$$

### 2.3.7 Change of basis for rotor forces

The longitudinal flapping angle  $a_{1SW}$  can be regarded as the geometrical angle between  $\mathbf{i}_{SW}$  and the intersection of the tip-path plane and the plane defined by  $\mathbf{i}_{SW}$  and  $\mathbf{k}_{SW}$ ; likewise, the lateral flapping angle  $b_{1SW}$  can be seen

as the geometrical angle comprised between  $\mathbf{j}_{\text{SW}}$  and the intersection of the tip-path plane and the plane defined by  $\mathbf{j}_{\text{SW}}$  and  $\mathbf{k}_{\text{SW}}$ .

In these terms, the flapping angles do not define a proper rotation sequence between the tip-path plane triad and the shaft-wind triad. Anyway, since flapping angles are typically small, it is legitimate to consider  $a_{1\text{SW}}$  as a rotation angle along  $\mathbf{j}_{\text{SW}}$  and  $b_{1\text{SW}}$  as a rotation angle along  $\mathbf{i}_{\text{SW}}$ .

Moreover, being both rotations angles small, it is legitimate to consider the rotation resulting from the combination of the two rotations as independent of the sequence; on the basis of this assumption, the rotation tensor between the shaft-wind triad and the tip-path plane triad can be approximated as:

$$\mathbf{R}_{\text{SW} \rightarrow \text{TPP}}^{\text{SW}} = \begin{bmatrix} 1 & 0 & a_{1\text{SW}} \\ 0 & 1 & b_{1\text{SW}} \\ -a_{1\text{SW}} & -b_{1\text{SW}} & 1 \end{bmatrix}, \quad (2.41)$$

thus the rotation tensor between the body triad and the tip-path plane triad is:

$$\mathbf{R}_{\text{B} \rightarrow \text{TPP}}^{\text{B}} = \mathbf{R}_{\text{B} \rightarrow \text{SW}}^{\text{B}} \mathbf{R}_{\text{SW} \rightarrow \text{TPP}}^{\text{SW}} = \mathbf{R}_{\text{B} \rightarrow \text{SB}}^{\text{B}} \mathbf{R}_{\text{SB} \rightarrow \text{SW}}^{\text{SB}} \mathbf{R}_{\text{SW} \rightarrow \text{TPP}}^{\text{SW}}. \quad (2.42)$$

Now we can perform the change of basis on the rotor forces, bringing them to the body frame:

$$\begin{Bmatrix} \mathbf{F}_{\text{R}}^{\text{B}} \\ \mathbf{M}_{\text{R}}^{\text{B}} \end{Bmatrix} = \begin{bmatrix} \mathbf{R}_{\text{B} \rightarrow \text{TPP}}^{\text{B}} & \mathbf{0} \\ \mathbf{0} & \mathbf{R}_{\text{B} \rightarrow \text{SW}}^{\text{B}} \end{bmatrix} \begin{Bmatrix} \mathbf{F}_{\text{R}}^{\text{TPP}} \\ \mathbf{M}_{\text{R}}^{\text{SW}} \end{Bmatrix} \quad (2.43)$$

where:

$$\mathbf{F}_{\text{R}}^{\text{TPP}} = \begin{Bmatrix} H_{\text{TPP}} \\ 0 \\ T_{\text{TPP}} \end{Bmatrix} \quad (2.44a)$$

$$\mathbf{M}_{\text{R}}^{\text{SW}} = \begin{Bmatrix} M_{x,\text{SW},\text{C}} \\ M_{y,\text{SW},\text{C}} \\ -k_{\text{CCW}} - J_{\text{R}}\dot{\Omega} \end{Bmatrix} \quad (2.44b)$$

and:

- $k_{\text{CCW}}$  is 1 for counter-clockwise rotating rotors (positive right-handed rotation along  $\mathbf{k}_{\text{SB}}$ ) and -1 for clockwise rotating rotors (the angular velocity  $\Omega$  and its time derivative are positive with reference to the sense of rotation defined by  $k_{\text{CCW}}$ );
- $J_{\text{R}}$  is the angular moment of inertia of the isolated rotor relative to the shaft axis.

Note that the torque  $Q_R$  is the required torque, positive right-handed about  $\mathbf{k}_{SB}$ ; the previously shown formulas take into account the rotor inertia and angular acceleration in order to determine the value (and the sign) of the torque that the rotor applies to the airframe.

## 2.4 Limitations and foreseen developments

The described model shows all the typical limitations of algebraic rotor models [19]:

- the span-wise parametrization of the blade geometry must be described as a function that can be analytically integrated (in the present implementation geometry parameters are span-wise constant);
- non uniformity of the inflow can only be introduced by a function that can be analytically integrated (presently accomplished according to the theory of Mangler and Squire);
- the rotor is represented by a disc model, with only coning and flapping degrees of freedom;
- the loads are analytically integrated over the disc and averaged in azimuth;
- the rotor disc doesn't have any dynamics of its own and responds immediately to control inputs or aerodynamic perturbation.

The latter limitation is of major importance in understanding the possible uses of the rotor model: the absence of disc own dynamics has the consequence that the model allows only quasi-steady simulation. Rotorcraft rigid body dynamics and rotor dynamics can be regarded as cascading feedback systems, where the rotor dynamics describe the inner loop: then, as a rule of thumb, the quasi-steadiness assumption can be assumed to be acceptable as long as the bandwidth of controls and perturbations acting on the inner loop is at least one order of magnitude lower than the lower edge of rotor bandwidth; since our model is based on a first order truncated representation of flapping only, this frequency can be approximated with the angular revolution frequency  $\Omega/2\pi$ . For a typical medium helicopter this means that a quasi-steady simulation is acceptable up to an input bandwidth in the order of magnitude of 0.5 Hz, which is enough only for gentle manoeuvres and low-gain control systems.

The aforementioned limitation could be possibly mitigated, while preserving the computational advantage of analytically integrated loads, by replacing the set of algebraic equations with a set of ordinary differential equations that describe the dynamics of the disc degrees of freedom (coning and flapping angles), as proposed in [6] and [7].

Another important limitation of the proposed model is the absence of corrections for the reverse flow region; in this region classical closed-form equations account for lift with the wrong sign and, also, the linearised aerodynamic model is not representative of the high incidence conditions that are found in the concerned region. This error, that becomes sensible at high advance ratios, can be corrected in at least two ways:

- lift can be numerically integrated on the reverse flow region and the obtained force can be summed two times to the analytically obtained forces (assuming that the erroneous contribution of lift has opposite sign and about the same absolute value of the correction);
- closed-form equations that analytically account for the reverse flow can be obtained by dividing the disc in three domains (advancing area, retreating area not affected by reverse flow, retreating area affected by reverse flow) and separately integrating on the three domains using the correct lift convention, then summing the contributions, as proposed in [21].

Neither of these proposed approaches was included in the first release of the rotor model here described, because it was decided to focus on the core algorithms, leaving this and other refinements to a possible future revision of the whole set of formulations.

The second proposed approach can be achieved with relative ease by newly deriving the closed-form equations from the flapping moment equation; doing so could also allow at the same time to obtain a fully coherent set of equations (presently the equations come from different sources in the literature), to remove unwanted assumptions (e.g. gravity approximately directed as the shaft) and to add the dependency from parameters that are presently not accounted for (e.g. blade twist, root cut-out, tip loss, pitch-flapping coupling, etc.). A good starting point for removing some of these assumptions can be found in [6].

Additionally, two more limitations must be taken into account:

- the pitch-flapping phase delay is fixed to  $90^\circ$  (that, strictly speaking, is exactly true only for zero flapping hinge offset);

- the closed form equations used are derived under the assumption that the rotor is fully articulated.

Because of these two limitations, the validity of the present implementation of the model for representing hingeless rotors is dubious.

## Chapter 3

# Integration of a complete rotorcraft model

### 3.1 Scope

This chapter describes a rotorcraft simulation model being developed at *AgustaWestland* Flight Mechanics office. The author of the present work contributed to this model by supplying the complete rotor model and the complete input file reader module, while also collaborating to the definition of general architecture, data structure and interfaces, to the programming and integration of other modules and to testing and debugging of the complete model; moreover the author performed a preliminary validation, that will be described in chapter 4.

The aim of the work is to provide a comprehensive rotorcraft model, incorporating features and formulations of well tested legacy codes (e.g. a rotor model derived from *NFpath*) into a modern and flexible framework, constituted by a library that provides a standardised interface to different user software (e.g. off-line analysis pre/postprocessors, real time simulators, etc.).

### 3.2 Methodology and tools

The model was implemented in fully standard *ANSI C* language using the same integrated development environment described in section 2.2. Also in this case the general purpose mathematical software *Freemat* was used as test pre/postprocessor, through the use of scripts exploiting the DLL interface of the model library.

### 3.3 Model description

#### 3.3.1 Structure

The rotorcraft model is composed by a number of component force evaluators, which compute the generalised force vector with reference to the body frame for each component (e.g. main rotor, tail rotor, fuselage, etc.), using speeds calculated by the kinematic equations. These contributions are summed and fed into the dynamic equations in order to obtain the accelerations.

#### 3.3.2 Equations of motion

Through the kinematic equations the linear and angular velocities with reference to the inertial frame are obtained:

$$\begin{Bmatrix} \mathbf{v}_O^I \\ \omega^I \end{Bmatrix} = \begin{bmatrix} \mathbf{R}_{I \rightarrow B}^I & \mathbf{0} \\ \mathbf{0} & \mathbf{R}_{I \rightarrow B}^I \end{bmatrix} \begin{Bmatrix} \mathbf{v}_O^B \\ \omega^B \end{Bmatrix}. \quad (3.1)$$

In order to write the dynamic equations, we first define a mass matrix using the mass, the first moments of inertia  $S_i$  and the second moments of inertia  $J_{ij}$  of the complete rotorcraft, referred to body axes and to their origin  $O$  (which is not necessarily the center of mass):

$$\mathbf{M} = \begin{bmatrix} m\mathbf{I} & \mathbf{S}_O^T \\ \mathbf{S}_O & \mathbf{J}_O \end{bmatrix} = \begin{bmatrix} m & 0 & 0 & S_x & 0 & 0 \\ 0 & m & 0 & 0 & S_y & 0 \\ 0 & 0 & m & 0 & 0 & S_z \\ S_x & 0 & 0 & J_x & J_{xy} & J_{xz} \\ 0 & S_y & 0 & J_{yx} & J_y & J_{yz} \\ 0 & 0 & S_z & J_{zx} & J_{zy} & J_z \end{bmatrix}. \quad (3.2)$$

Then a matrix is obtained from the generalised velocity vector with reference to the body frame with the south-west cross product operator [4]:

$$\mathbf{W}^B = \begin{Bmatrix} \mathbf{v}_O^B \\ \omega^B \end{Bmatrix}, \quad (3.3a)$$

$$\mathbf{W}_{\times sw}^B = \begin{bmatrix} \omega_{\times}^B & \mathbf{0} \\ \mathbf{v}_{\times}^B & \omega_{\times}^B \end{bmatrix} = \begin{bmatrix} 0 & -\omega_z & \omega_y & 0 & 0 & 0 \\ \omega_z & 0 & -\omega_x & 0 & 0 & 0 \\ -\omega_y & \omega_x & 0 & 0 & 0 & 0 \\ 0 & -v_z & v_y & 0 & -\omega_z & \omega_y \\ v_z & 0 & -v_x & \omega_z & 0 & -\omega_x \\ -v_y & v_x & 0 & -\omega_y & \omega_x & 0 \end{bmatrix}. \quad (3.3b)$$



The total generalised force vector is defined as the sum of the component contributions:

$$\mathbf{f}_g = \sum_i \left\{ \begin{array}{c} \mathbf{F}_i^B \\ \mathbf{M}_i^B \end{array} \right\} . \quad (3.4)$$

Then the dynamic equations can be written in form of a set of linear equations:

$$\mathbf{M}\mathbf{a}^B = \mathbf{f}_g - \mathbf{W}_{\times sw}^B \mathbf{M}\mathbf{W}^B . \quad (3.5)$$

where the generalised accelerations vector is:

$$\mathbf{a}^B = \left\{ \begin{array}{c} \dot{\mathbf{v}}_O^B \\ \dot{\boldsymbol{\omega}}^B \end{array} \right\} , \quad (3.6)$$

that can be obtained by solving the linear system; since the mass matrix is symmetric definite positive, the system can be efficiently solved by using Cholesky's decomposition.

### 3.3.3 Component models description

For reference, see the definitions of reference frames in appendix B and the rotations already described in section 2.3.2.

#### 3.3.3.1 Rotors

The rotor model has already been extensively described in chapter 2. Two instances of the same model are used for the main rotor and the tail rotor.

The rotor model provides four control inputs and two rotor state inputs:

- collective pitch;
- longitudinal cyclic pitch;
- lateral cyclic pitch;
- controlled tilt (nacelle position);
- shaft angular rate;
- shaft angular acceleration.

Both the main and tail rotor have the controlled tilt input statically set to zero, since this feature will be used in the future for modelling of non-conventional configurations (tilt rotor).

Since the rotorcraft model doesn't include at present time any model of the engine and of the drivetrain, rotor rotation dynamics are not simulated; then the shaft angular rate is constantly set to the nominal value from the input file, while the shaft angular acceleration is statically set to zero.

### 3.3.3.2 Gravity

The position of the centre of gravity  $G$ , which is known in the design frame, is expressed in body frame:

$$\mathbf{r}_{OG}^B = \mathbf{R}_{B \rightarrow D}^B (\mathbf{r}_{DG}^D - \mathbf{r}_{DO}^D). \quad (3.7)$$

The gravity force, as a function of total mass  $m$ , is known with reference to the inertial frame:

$$\mathbf{g}^I = g \mathbf{k}_I^I. \quad (3.8)$$

Then its expression with reference to the body is a function of the rotation tensor obtained from the attitude Euler angles:

$$\mathbf{g}^B = \mathbf{R}_{B \rightarrow I}^B \mathbf{g}^I. \quad (3.9)$$

Then the generalised force vector for gravity, with moments referred to the reference point  $O$ , is:

$$\begin{Bmatrix} \mathbf{F}_G^B \\ \mathbf{M}_G^B \end{Bmatrix} = \begin{Bmatrix} \mathbf{g}^B \\ \mathbf{r}_{OG}^B \times \mathbf{g}^B \end{Bmatrix}. \quad (3.10)$$

### 3.3.3.3 Aerodynamic surfaces

The component models a semi-wing having its root in the origin  $W$  of the aerodynamic surface local reference frame. The axis  $y_W$  lies spanwise at quarter-chord position. The semi-wing extends of a semi-span  $s$  in the direction of positive  $y_W$  if the parameter  $d_W$  has the value  $+1$ , otherwise in the direction of negative  $y_W$  if  $d_W = -1$ .

The orientation of the reference frame with reference to the body frame is defined first by a rotation about  $\mathbf{k}_B$  of the sweep angle  $\Lambda$ , multiplied by  $d_W$ , followed by a rotation about  $\mathbf{i}_B$  of the anhedral angle  $\Gamma$ , multiplied by  $d_W$  (and decremented of  $\pi/2$  in the case of vertical tail). Then the rotation tensor from body triad to horizontal tail local triad is given by:

$$\begin{aligned} \mathbf{R}_{B \rightarrow W}^B &= \mathbf{R}_{B \rightarrow \text{sweep}}^B \mathbf{R}_{\text{sweep} \rightarrow W}^{\text{sweep}} \\ &= \mathbf{R}_{B \rightarrow \text{sweep}}^B (\mathbf{k}_B^B, d_W \Lambda) \mathbf{R}_{\text{sweep} \rightarrow W}^{\text{sweep}} (\mathbf{i}_B^{\text{sweep}}, d_W \Gamma) \\ &= \mathbf{R}_{B \rightarrow \text{sweep}}^B (\mathbf{k}_B^B, d_W \Lambda) \mathbf{R}_{\text{sweep} \rightarrow W}^{\text{sweep}} (\mathbf{R}_{\text{sweep} \rightarrow B}^{\text{sweep}} \mathbf{i}_B^B, d_W \Gamma), \end{aligned} \quad (3.11)$$

where the intermediate rotation tensors are function of a rotation direction and a rotation angle through the Euler-Rodrigues formula (see section 2.3.2.3).

Similarly, for the vertical tail we have:

$$\begin{aligned}
 \mathbf{R}_{B \rightarrow W}^B &= \mathbf{R}_{B \rightarrow \text{sweep}}^B \mathbf{R}_{\text{sweep} \rightarrow W}^{\text{sweep}} \\
 &= \mathbf{R}_{B \rightarrow \text{sweep}}^B(\mathbf{k}_B^B, d_W \Lambda) \mathbf{R}_{\text{sweep} \rightarrow W}^{\text{sweep}}(\mathbf{i}_B^{\text{sweep}}, d_W \Gamma - \frac{1}{2}\pi) \\
 &= \mathbf{R}_{B \rightarrow \text{sweep}}^B(\mathbf{k}_B^B, d_W \Lambda) \mathbf{R}_{\text{sweep} \rightarrow W}^{\text{sweep}}(\mathbf{R}_{\text{sweep} \rightarrow B}^{\text{sweep}} \mathbf{i}_B^B, d_W \Gamma - \frac{1}{2}\pi),
 \end{aligned} \tag{3.12}$$

The position of the wing root  $W$  with reference to the body frame can be obtained from the design frame position through the usual transformation:

$$\mathbf{r}_{OW}^B = \mathbf{R}_{B \rightarrow D}^B(\mathbf{r}_{DW}^D - \mathbf{r}_{DO}^D). \tag{3.13}$$

The aerodynamic computational point  $A$  is estimated to be at quarter chord, half span:

$$\mathbf{r}_{WA}^W = \begin{Bmatrix} 0 \\ \frac{1}{2}d_W s \\ 0 \end{Bmatrix}. \tag{3.14a}$$

$$\mathbf{r}_{OA}^B = \mathbf{r}_{OW}^B + \mathbf{R}_{B \rightarrow W}^B \mathbf{r}_{WA}^W. \tag{3.14b}$$

The previous expression of the ACP represents an approximation when roll-rate or pitch rate are not null.

The total speed in  $A$ , including the component due to rigid body rotation, is calculated as:

$$\mathbf{v}_A^B = \mathbf{r}_O^B + \omega^B \times \mathbf{r}_{OA}^B. \tag{3.15a}$$

$$\mathbf{v}_A^W = \mathbf{R}_{W \rightarrow B}^W \mathbf{v}_A^B. \tag{3.15b}$$

A change of basis is performed also on the wind speed:

$$\mathbf{v}_{\text{wind}}^W = \mathbf{R}_{W \rightarrow I}^W \mathbf{v}_{\text{wind}}^I = (\mathbf{R}_{I \rightarrow B}^I \mathbf{R}_{B \rightarrow W}^B)^T \mathbf{v}_{\text{wind}}^I. \tag{3.16}$$

The total airspeed at point  $A$  is then:

$$\mathbf{V}^W = -\mathbf{v}_A^W + \mathbf{v}_{\text{wind}}^W. \tag{3.17}$$

The climb angle is:

$$\tau = \tan^{-1} \left( \frac{\mathbf{V}^W \cdot \mathbf{k}_W^W}{\mathbf{V}^W \cdot \mathbf{i}_W^W} \right). \tag{3.18}$$

Then the angle of attack is known by adding the setting angle:

$$\alpha = \tau + \iota; \tag{3.19}$$

A new triad AW is obtained by rotating the aerodynamic surface local triad of the angle of attack, so that  $x_{AW}$  is aligned to the airspeed:

$$\mathbf{R}_{W \rightarrow AW}^W = \begin{bmatrix} \cos \alpha & 0 & -\sin \alpha \\ 0 & 1 & 0 \\ \sin \alpha & 0 & \cos \alpha \end{bmatrix}, \quad (3.20)$$

Aerodynamic coefficients are calculated as a function of the angle of attack in the usual way, using a linearised model or an interpolation.

Then forces and moments can be calculated:

$$\mathbf{F}_{wing}^{AW} = \frac{1}{2} \rho |\mathbf{V}^W|^2 S \begin{Bmatrix} -C_d \\ 0 \\ -C_l \end{Bmatrix}, \quad (3.21a)$$

$$\mathbf{M}_{wing}^{AW} = \frac{1}{2} \rho |\mathbf{V}^W|^2 S c \begin{Bmatrix} 0 \\ C_m \\ 0 \end{Bmatrix}, \quad (3.21b)$$

where  $S$  is the area of the aerodynamic surface and  $c$  the chord.

The generalised force vector for the aerodynamic surface, with moments referred to the reference point  $O$ , is then:

$$\begin{Bmatrix} \mathbf{F}_{wing}^B \\ \mathbf{M}_{wing}^B \end{Bmatrix} = \begin{bmatrix} \mathbf{R}_{B \rightarrow AW}^B & \mathbf{0} \\ \mathbf{0} & \mathbf{R}_{B \rightarrow AW}^B \end{bmatrix} \begin{Bmatrix} \mathbf{F}_{wing}^{AW} \\ \mathbf{M}_{wing}^{AW} \end{Bmatrix} + \dots \\ \dots + \begin{Bmatrix} \mathbf{0} \\ \mathbf{r}_{OA}^B \times (\mathbf{R}_{B \rightarrow AW}^B \mathbf{F}_{wing}^{AW}) \end{Bmatrix}. \quad (3.22)$$

### 3.3.3.4 Fuselage

The position of the fuselage aerodynamic computational point  $Q$  with reference to the body frame can be obtained from the design frame position through the usual transformation:

$$\mathbf{r}_{OQ}^B = \mathbf{R}_{B \rightarrow D}^B (\mathbf{r}_{DQ}^D - \mathbf{r}_{DO}^D). \quad (3.23)$$

The total speed in A, including the component due to rigid body rotation, is calculated as:

$$\mathbf{v}_Q^B = \mathbf{r}_O^B + \omega^B \times \mathbf{r}_{OQ}^B. \quad (3.24)$$

The wind speed is considered with reference to the body frame and summed to get the total airspeed:

$$\mathbf{v}_{wind}^B = \mathbf{R}_{B \rightarrow I}^B \mathbf{v}_{wind}^I = (\mathbf{R}_{I \rightarrow B}^I \mathbf{R}_{B \rightarrow W}^B)^T \mathbf{v}_{wind}^I. \quad (3.25a)$$

$$\mathbf{V}^B = -\mathbf{v}_Q^B + \mathbf{v}_{\text{wind}}^B. \quad (3.25b)$$

The sideslip is defined as:

$$\beta = \tan^{-1} \left( \frac{\mathbf{V}^B \cdot \mathbf{k}_B^B}{\mathbf{V}^B \cdot \mathbf{i}_B^B} \right). \quad (3.26)$$

While the angle of attack is:

$$\alpha = \tan^{-1} \left( \frac{\mathbf{V}^B \cdot \mathbf{k}_B^B}{\sqrt{(\mathbf{V}^B \cdot \mathbf{i}_B^B)^2 + (\mathbf{V}^B \cdot \mathbf{j}_B^B)^2}} \right). \quad (3.27)$$

The six fuselage aerodynamic coefficients  $C_d$ ,  $C_s$ ,  $C_l$ ,  $C_r$ ,  $C_m$  and  $C_y$  are calculated as a function of the angles of attack and sideslip using a linearised model or an interpolation.

A new triad BW is obtained by rotating the body triad so that  $x_{QW}$  is aligned to the airspeed:

$$\mathbf{R}_{B \rightarrow BW}^B = \begin{bmatrix} \cos \alpha \cos \beta & -\sin \beta & -\sin \alpha \cos \beta \\ \cos \alpha \sin \beta & \cos \beta & -\sin \alpha \sin \beta \\ -\sin \alpha & 0 & \cos \alpha \end{bmatrix}, \quad (3.28)$$

Then forces and moments can be calculated in this reference frame:

$$\mathbf{F}_{\text{fus}}^{\text{BW}} = \frac{1}{2} \rho |\mathbf{V}^B|^2 A \begin{Bmatrix} -C_d \\ C_s \\ -C_l \end{Bmatrix}, \quad (3.29a)$$

$$\mathbf{M}_{\text{fus}}^{\text{BW}} = \frac{1}{2} \rho |\mathbf{V}^B|^2 A R \begin{Bmatrix} -C_r \\ C_m \\ -C_y \end{Bmatrix}, \quad (3.29b)$$

where  $A$  is the reference area and  $R$  is the reference length for the coefficients; usually it is assumed that  $A$  is the main rotor area and  $R$  the main rotor radius.

The generalised force vector for the fuselage, with moments referred to the reference point  $O$ , is:

$$\begin{aligned} \begin{Bmatrix} \mathbf{F}_{\text{fus}}^B \\ \mathbf{M}_{\text{fus}}^B \end{Bmatrix} &= \begin{bmatrix} \mathbf{R}_{B \rightarrow BW}^B & \mathbf{0} \\ \mathbf{0} & \mathbf{R}_{B \rightarrow BW}^B \end{bmatrix} \begin{Bmatrix} \mathbf{F}_{\text{fus}}^{\text{BW}} \\ \mathbf{M}_{\text{fus}}^{\text{BW}} \end{Bmatrix} + \dots \\ &\dots + \begin{Bmatrix} \mathbf{0} \\ \mathbf{r}_{OQ}^B \times (\mathbf{R}_{B \rightarrow BW}^B \mathbf{F}_{\text{fus}}^{\text{BW}}) \end{Bmatrix}. \end{aligned} \quad (3.30)$$

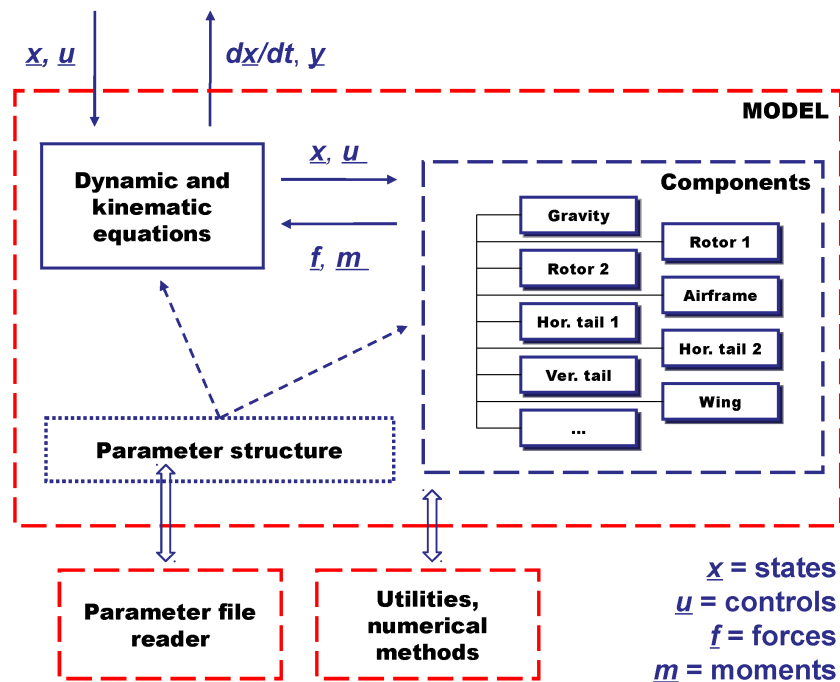


Figure 3.1: Rotorcraft model architecture

### 3.4 Implementation

The general architecture of the model is illustrated in figure 3.1. The rotorcraft model receives states (namely position, attitude Eulers angles, speeds and angular rates) and controls (main rotor collective, longitudinal and lateral cyclic pitch, tail rotor collective) as input; these are passed on to the components modules, which use them to calculate generalised forces; these forces are summed and applied to the motion equations in order to calculate the rotorcraft accelerations, which are returned by the model as output, together with a set of additional outputs (e.g. forces, flapping angles, etc.).

Components are designed in order to be modular; some of them represent more than one instance in the rotorcraft: for example, forces on vertical tail plane and on horizontal tail planes are all calculated by a single aerodynamic surface module.

At present time, the model architecture is statically fixed and represents a conventional rotorcraft, although all the necessary infrastructure in the modules is already in place for a more flexible configuration that will be allowed by future developments.

It should be noted that the rotorcraft model and the component models

communicate according to a one-to-many scheme, with no direct interaction between different components. For this reason no interference is modelled at present time. At the time of writing, a comprehensive interference model, which will combine the contributions of each component into a single airspeed perturbation field, is in its initial development.

### 3.4.1 Parameter structure

The model receives the rotorcraft parameters from an external library, that reads a rotorcraft description file; the file is supplied according to the FMR (Flight Mechanics Rotorcraft) file format specification [1], which is a file format being developed at *AgustaWestland* Flight Mechanics office with the aim of having a single software-independent rotorcraft description file.

Also the internal model parameter structure is modelled after the FMR specification; this will allow in the immediate future to replace the input file reader library with a standardised library, presently in final development, that will provide complete management of the data structure, including the following features:

- read FMR-formatted input files;
- provide a library of standard constants;
- calculate dependent parameters from input parameters;
- allocate memory for the data structure;
- set and retrieve values in the data structure;
- allow for encryption and access protection.

### 3.4.2 External interfaces

In figure 3.2 an overview of the simulation framework is shown. The previously described model is used as simulation back-end; it outputs the rotorcraft accelerations to a front-end module containing procedures to calculate trim conditions, integrate a single time step and linearise the model; this module provides an abstraction layer to external software (e.g. pre/post-processors, real-time simulators) that can use the underlying model through a standardised interface; additionally, it provides the possibility of using other back-end models conforming to the same standard interface. Alternatively, the user can interact with the model through dynamically linked executables

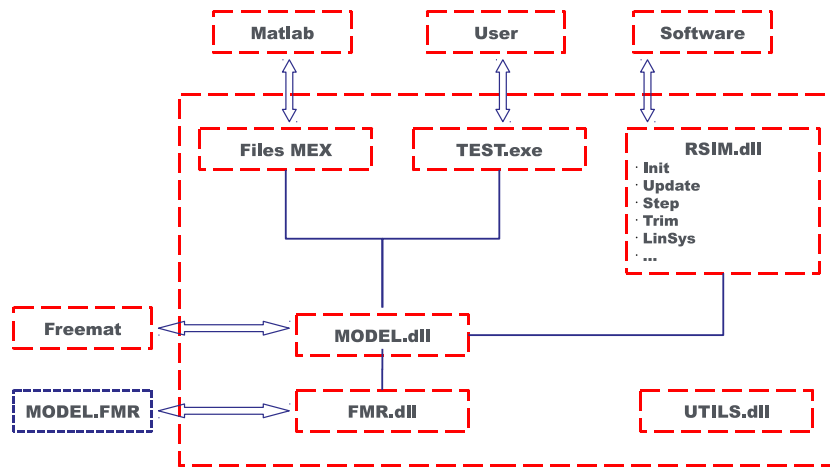


Figure 3.2: Framework architecture

(shown as *test.exe* in the figure) or interact with it via general purpose software such as *Freemat* or *Matlab*, either directly through the DLL interface or using dedicated interface modules (such as *Matlab* MEX files).

### 3.5 Limitations and foreseen developments

From the modelling point of view, the presented rotorcraft shows at the current time three main limitations, that add to the ones already described for the rotor model:

- no interference model is implemented;
- some components are not modelled (e.g. engines, drivetrain, landing gear);
- the rotorcraft configuration is fixed (conventional helicopter).

While the third limitation is relatively easy to eliminate with moderate effort, the other two require a considerable amount of active development. In particular the interference model, at the moment of writing in its inception phase, represents a challenge, since the design objective is to obtain a generic method in which all the components contribute to a unique airspeed perturbation field, abandoning the classical one-to-one interference schemes based on the use of empirical coefficients. Although challenging, achieving such generality is not negotiable for two reasons:



- generality of the interference scheme is a prerequisite for flexible rotorcraft configuration;
- a method not relying on empirical coefficients would be of great use in the analysis of novel rotorcraft designs, especially those with unconventional configurations, where limited experimental or statistical data for interference coefficients is available.

As far as the implementation is concerned, what is still missing is the complete integration of the data structure management library AWFMR and the development in low level language of the procedural functions (trim, step, linearization), which are at the moment prototyped outside of the library in Freemat/Matlab environment.



# Chapter 4

## Numerical results

Several numerical tests, some of which will be described later on, were performed using the described rotorcraft model; some of them involved a comparison to results produced by other software, used as reference, namely:

1. *NFpath*, representing the company's standard proven tool in the field of simplified rotorcraft models (level 1 mathematical model in the Padfields classification [19]);
2. *Camrad*, representing a higher fidelity model not intended for real-time use (level 2 mathematical model in the Padfields classification).

While comparison to *NFpath* has the scope of ensuring the correctness of the newly implemented model using a reference that is homogeneous in the majority of formulations and assumptions, the comparison to *Camrad* serves the aim of verifying coherence of results from an engineering point of view (in terms of orders of magnitude) and having a measure of improvements obtained, keeping in mind the major differences between the models.

*NFpath* has been described extensively in chapter 1.

*Camrad* is a code implementing a comprehensive analytical model of rotorcraft aerodynamics and dynamics, that combines structural, inertial and aerodynamic models [10]. The core of the software is the trim procedure, which uses a non linear solver based on *Newton-Raphson* method to solve the algebraic equations for the trim variables. As in the model described in the present work, the rotor is modelled using the quasi-steady assumption. The rotor model used by *Camrad* is based on the blade-element theory, applied to a hierarchical structure of modelling schemes; the reference data was generated using a rigid blade structural model combined with a uniform inflow model. The code release used was *AICAM 2.0* (release September 2004), which is a version of the original software *Camrad/JA* by *Johnson Aeronautics*, incorporating several customizations by *AgustaWestland*.

Rotorcraft parameter sets supplied to the different software were set up in order to represent as precisely as possible the same physical entities in the different models, but avoiding any tuning that could mask differences in the mathematical models. The parameters used don't represent exactly any real-world rotorcraft, anyway they are representative of a medium-class conventional helicopter such as the *AW139*.

Since the new model doesn't include any implementation of interferences, all the relevant options in *NFpath* and *Camrad* were deactivated (e.g. download, blockage, etc.). This has the consequence that results obtained have a significance only in a fair comparison of different codes using the same conditions, while the physical significance of data is reduced, especially in regions of the flight envelope where interference effects are not negligible (e.g. download at low advance ratios).

## 4.1 Trim analysis

Since the trim procedure provided by the front-end module described in section 3.4.2 was still not available, a prototype trim procedure was implemented in *Freemat* environment; the procedure, given flight speeds, uses Broyden's iterative non linear solver (see section A.2) to equate all linear and angular accelerations to zero, thus, obtaining attitude and controls for trimmed flight under the condition of zero sideslip (yaw angle is fixed).

An horizontal speed sweep trim analysis was performed with each of the three codes, at sea level, standard ISA atmospheric conditions and out of ground effect; the results, summarized in figures from 4.1 to 4.4, show very good agreement between the different codes, with the novel model performing very similarly to *NFpath*, whose physical formulation is almost identical.

A noticeable improvement is found in the values of the coning angle, as a consequence of fixing a bug found in the *NFpath* implementation of the relevant closed form equation.

Roll angle and lateral flapping angle show deviations from *NFpath* values towards *Camrad* values, as a result of the implementation of a fully three-dimensional model with rigorous transformations between different reference frames.

An almost constant offset in shaft power value can be noticed between *Camrad* and the other two codes; the reason for this has not been investigated, however it is likely to be a consequence of different models for drag coefficient and induced power evaluations.

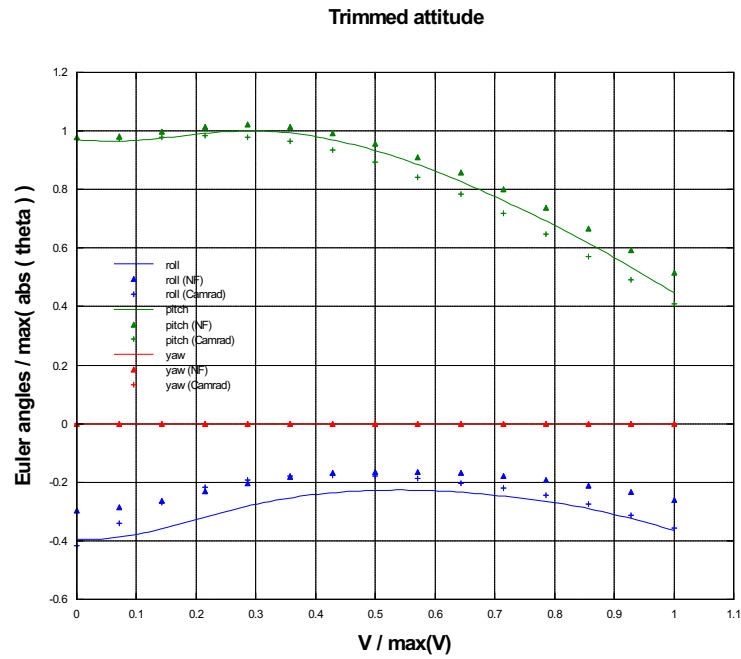


Figure 4.1: Attitude Euler's angles in trim as a function of horizontal speed

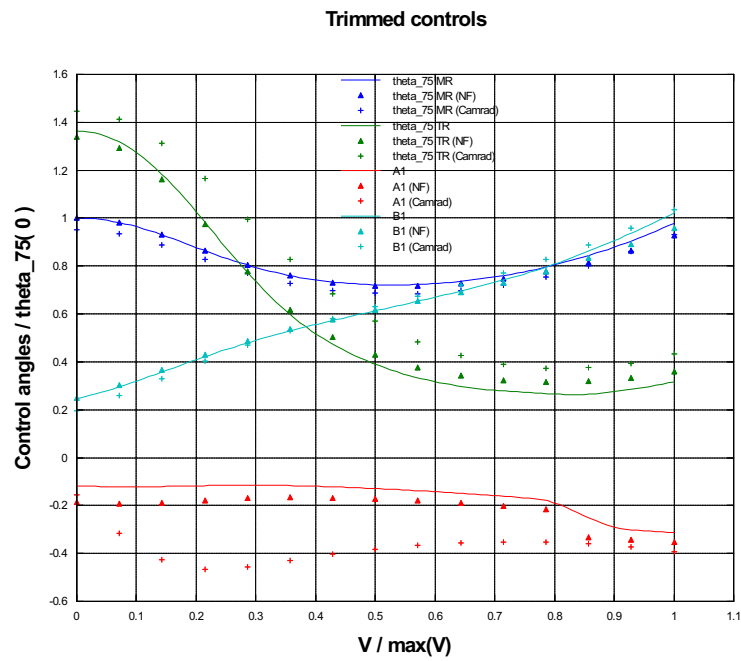


Figure 4.2: Control angles in trim as a function of horizontal speed

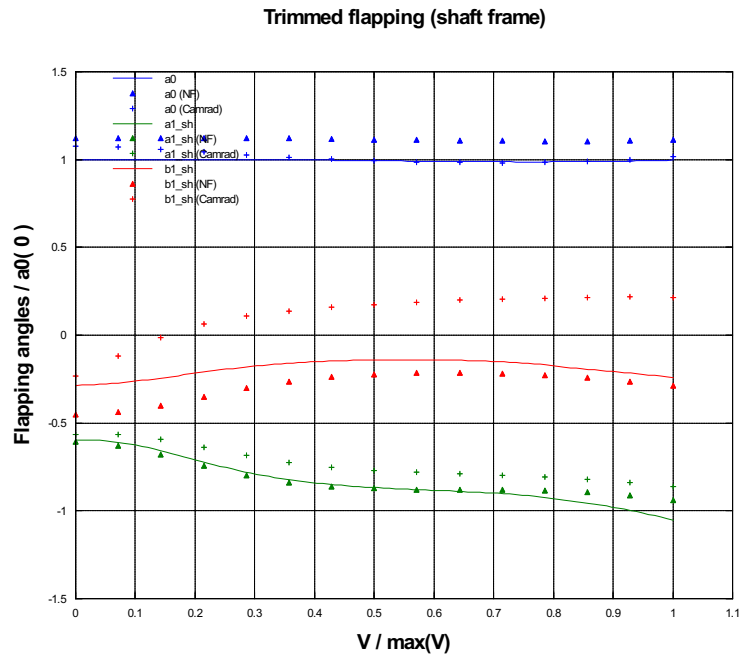


Figure 4.3: Flapping angles in trim as a function of horizontal speed

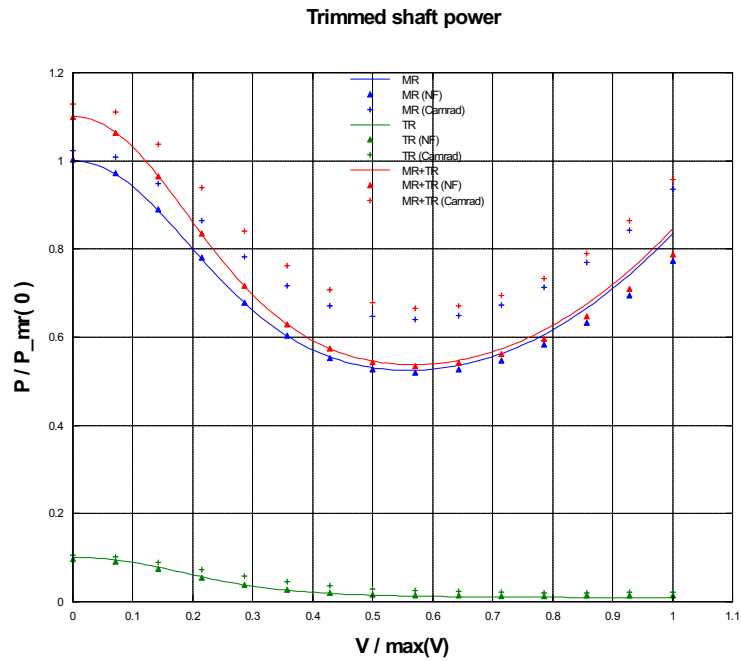


Figure 4.4: Shaft power in trim as a function of horizontal speed

## 4.2 Validation of components

A validation of the components, considering each one independently from the others, was performed using the following procedure:

1. an horizontal speed sweep trim analysis was performed with the reference software (alternatively *NFpath* or *Camrad*) in standard conditions (sea level, standard ISA atmosphere and out of ground effect);
2. for each speed condition, trim values for attitude and controls from the reference software were used to produce a direct snapshot using the model under validation;
3. forces, moments and other relevant quantities for each component of the model under validation were compared and plotted against the respective result generated by the reference model.

Forces and moments are given in body frame. All moments are referred to the same reference point in the rotorcraft; in the analysis presented later on, this reference point was set in the same location as the centre of gravity.

### 4.2.1 Rotors

For the purpose of comparing the different rotor models, the correction for the H-force in *NFpath* was switched off, coherently with the absence of reverse flow corrections in the new model. Since *Camrad* is based on a blade element model, modelling of reverse flow is inherently correct; this can be a cause for discrepancies between results produced by *Camrad* and those from other models not accounting for reverse flow.

The model shows a substantial agreement with *NFpath* results for quantities related to the rotor, as can be seen in figures 4.5 and 4.6.

Comparison versus *Camrad*, as shown in figures from 4.7 to 4.14, results in a very good agreement as far as the forces are concerned; moments show a similar trend, although values deviate, especially in the medium-high speed range. Agreement of flapping angles proves very satisfactory with the exception of the lateral flapping, that shows a noticeable deviation in the low speed range; at higher speed the trend is similar, while keeping a significant offset. Both deviations need to be investigated; however it is reasonable to assume that they can be traced to the different self induction models and to the fact that in the algebraic rotor model the blade flapping motion form is imposed (as 1st order Fourier series). It is also worth considering that, as noted in the experimental results comparison contained in [5], unsatisfactory modelling of

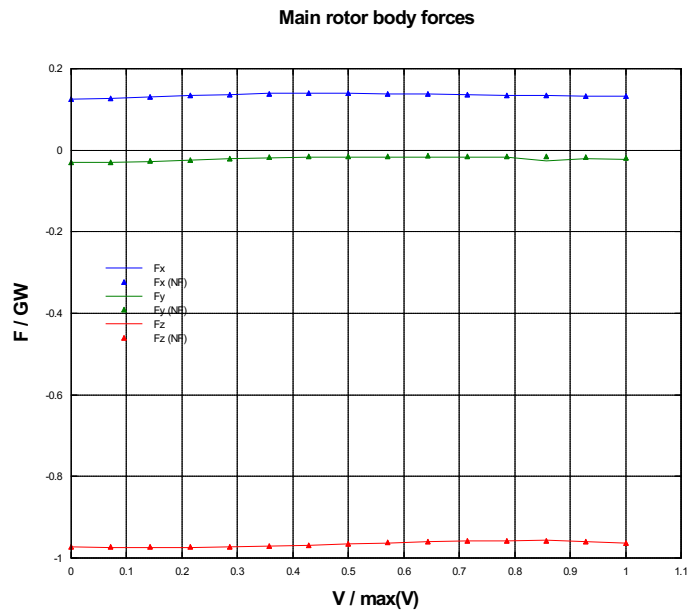


Figure 4.5: Main rotor forces resulting from NFpath trimmed attitude and controls

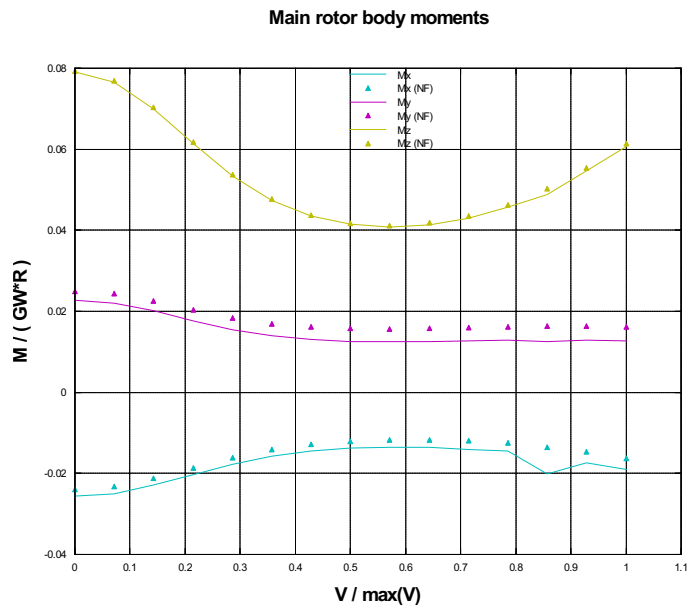


Figure 4.6: Main rotor moments resulting from NFpath trimmed attitude and controls



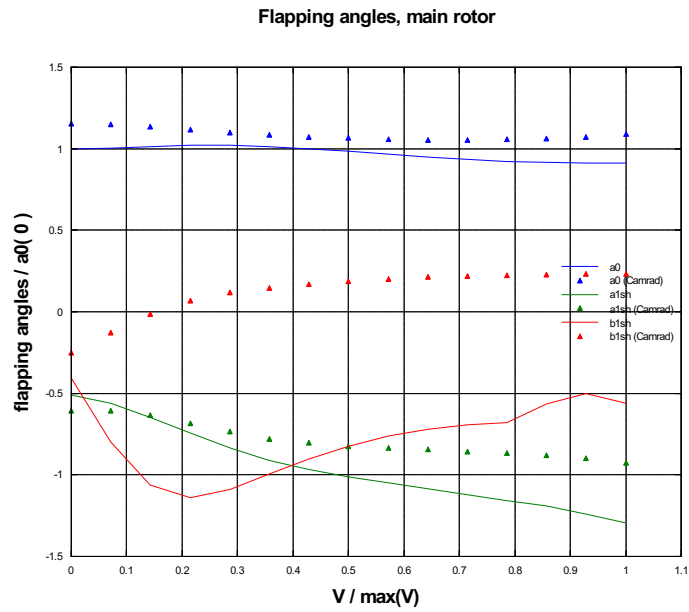


Figure 4.7: Main rotor flapping angles resulting from Camrad trimmed attitude and controls

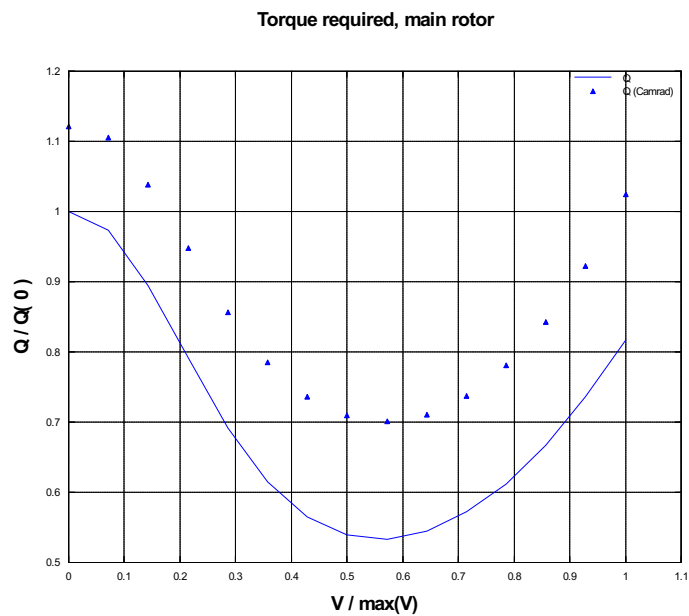


Figure 4.8: Main rotor torque required resulting from Camrad trimmed attitude and controls

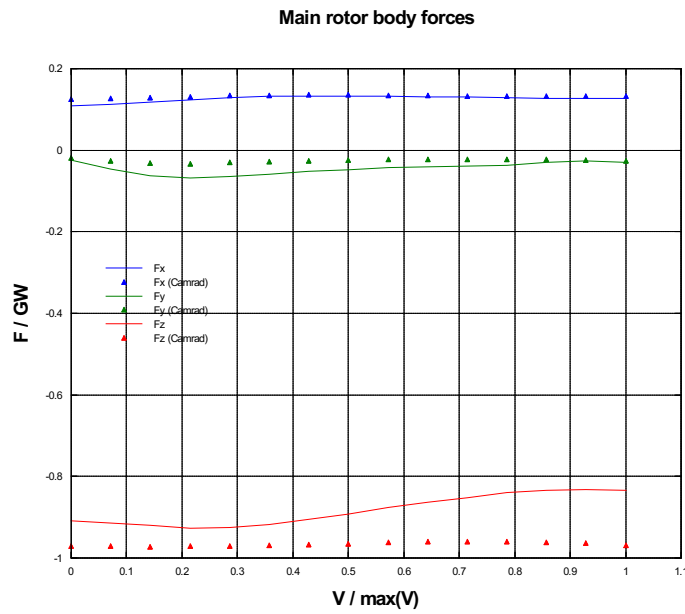


Figure 4.9: Main rotor forces resulting from Camrad trimmed attitude and controls

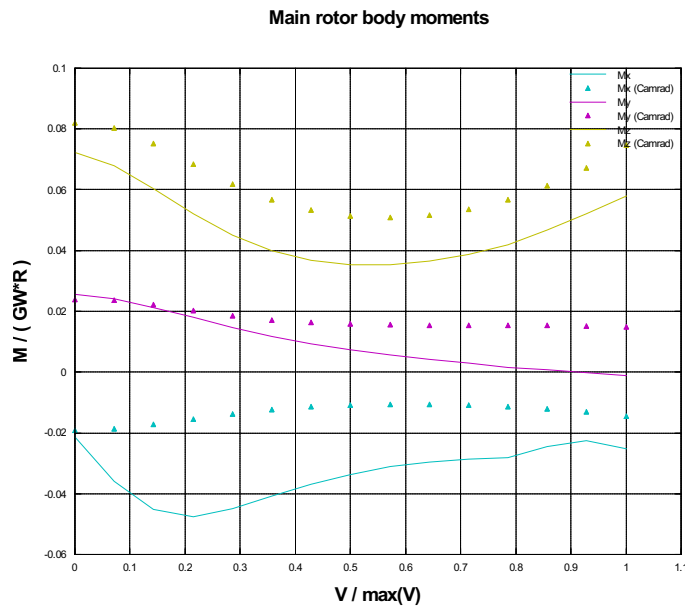


Figure 4.10: Main rotor moments resulting from Camrad trimmed attitude and controls

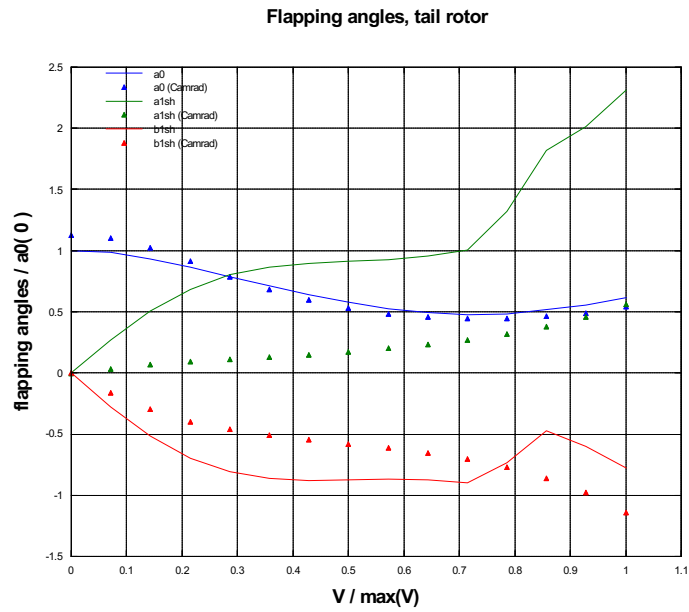


Figure 4.11: Tail rotor flapping angles resulting from Camrad trimmed attitude and controls

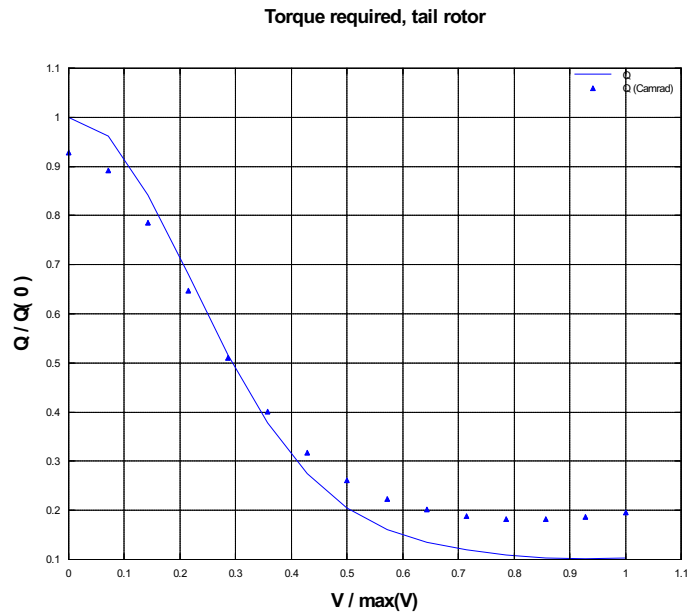


Figure 4.12: Tail rotor torque required resulting from Camrad trimmed attitude and controls

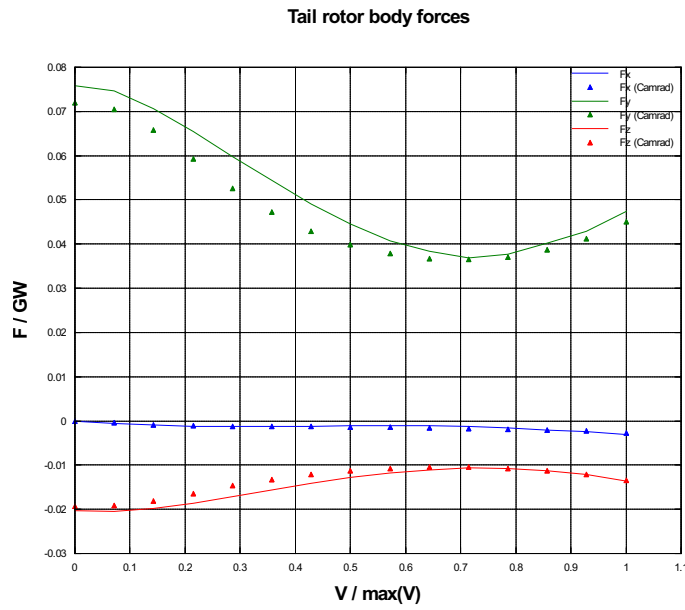


Figure 4.13: Tail rotor forces resulting from Camrad trimmed attitude and controls

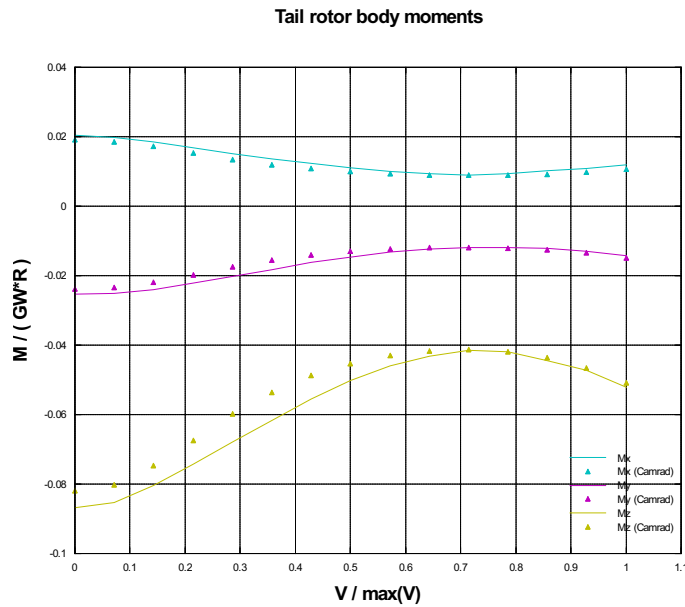


Figure 4.14: Tail rotor moments resulting from Camrad trimmed attitude and controls

lateral flapping is a common deficiency of analytically integrated rotor models and can be traced to the strong dependency of the lateral flapping on the longitudinal induced speed distribution, which in turn is usually affected by several assumptions. Moreover, torque shows an almost constant offset that was already discussed in section 4.1.

#### 4.2.2 Gravity

As expected, gravity forces calculated by the different codes agree perfectly, as shown in figures 4.15 and 4.16.

#### 4.2.3 Fuselage

Limiting to the in-plane longitudinal fuselage forces and moments, outputs show good agreement with *NFpath* results, as depicted in figures from 4.17 to 4.19; the major difference is embodied by the fact that the tested model implements a fully three-dimensional aerodynamic body model characterised by six coefficients and rigorous reference frames rotations, then yawing moment is reproduced and other forces and moments show minor discrepancies.

The goodness of the three-dimensional fuselage aerodynamic model is confirmed by the near overplot in the comparison versus *Camrad*, shown in figures from 4.20 to 4.22.

It is worthwhile to note that the fuselage is one of the components that are more strongly affected by the absence of an interference model: this is easy to see considering that in hover condition, according to the model, the fuselage produces no force at all, while physically it should be subject to a noticeable force in  $z_B$  direction due to the download.

#### 4.2.4 Aerodynamic surfaces

As expected, the simple aerodynamic model for aerodynamic surfaces nearly overplots the reference data from both *NFpath* (figures from 4.23 to 4.26) and *Camrad* (figures from 4.27 to 4.31).

### 4.3 Analysis of the ground effect model

As described in section 2.3.3.4, a novel ground effect model was implemented; the behaviour of this new model has been compared versus *NFpath*. Two trim-to-trim comparisons were run, one at constant ground altitude and varying horizontal speed and one in hover at variable ground altitude. Additionally the variation of thrust coefficient versus horizontal speed at constant

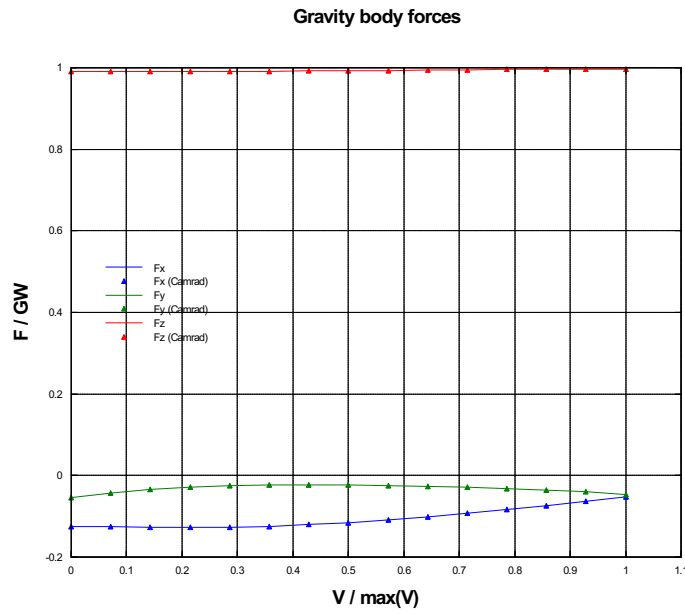


Figure 4.15: Gravity forces resulting from Camrad trimmed attitude and controls

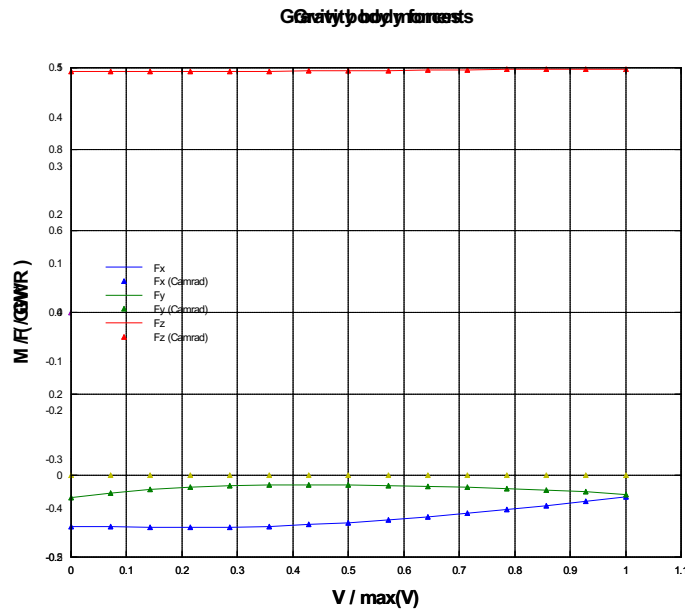


Figure 4.16: Gravity moments resulting from Camrad trimmed attitude and controls

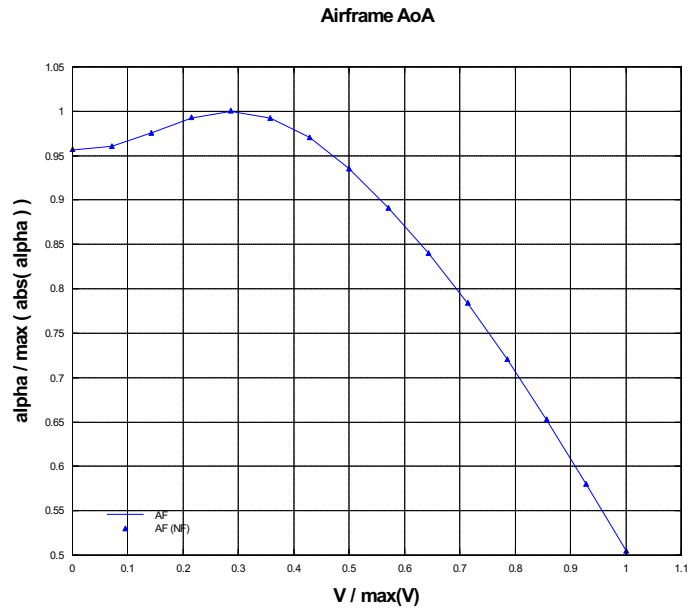


Figure 4.17: Fuselage angle of attack resulting from NFpath trimmed attitude and controls

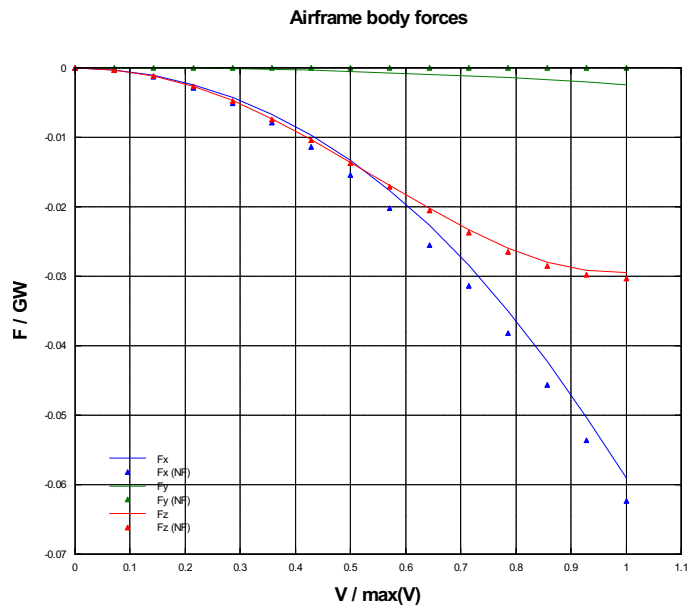


Figure 4.18: Fuselage forces resulting from NFpath trimmed attitude and controls

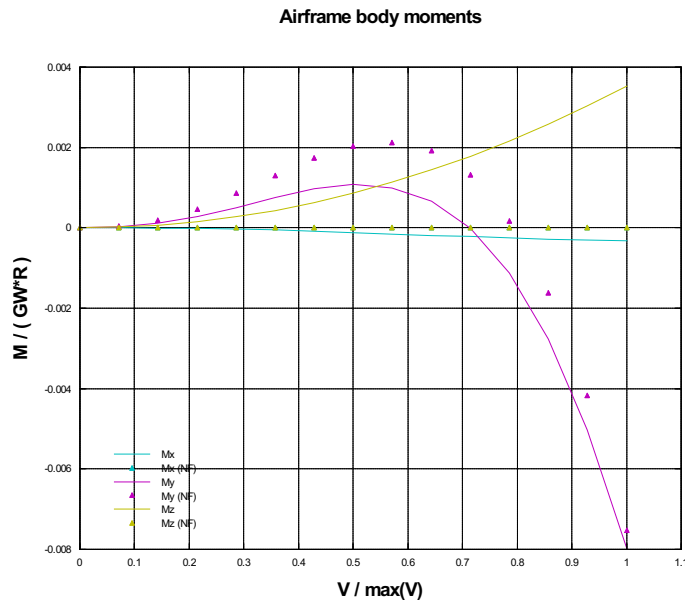


Figure 4.19: Fuselage moments resulting from NFpath trimmed attitude and controls

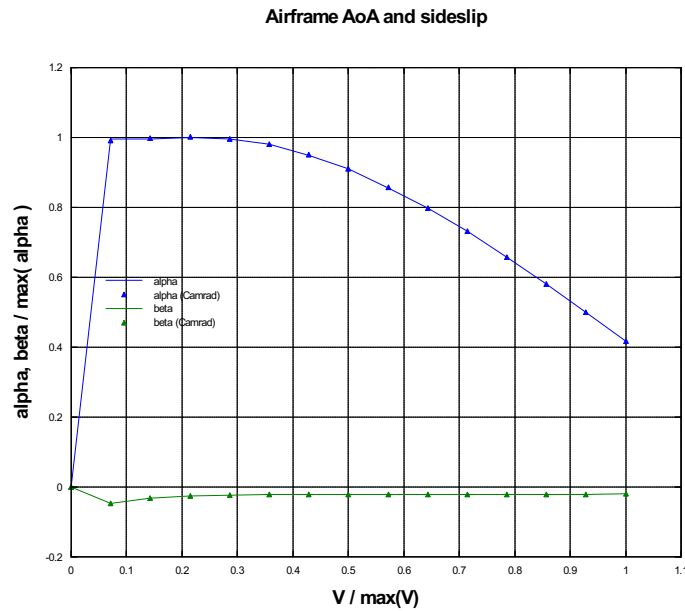


Figure 4.20: Fuselage Angle of attack resulting from Camrad trimmed attitude and controls



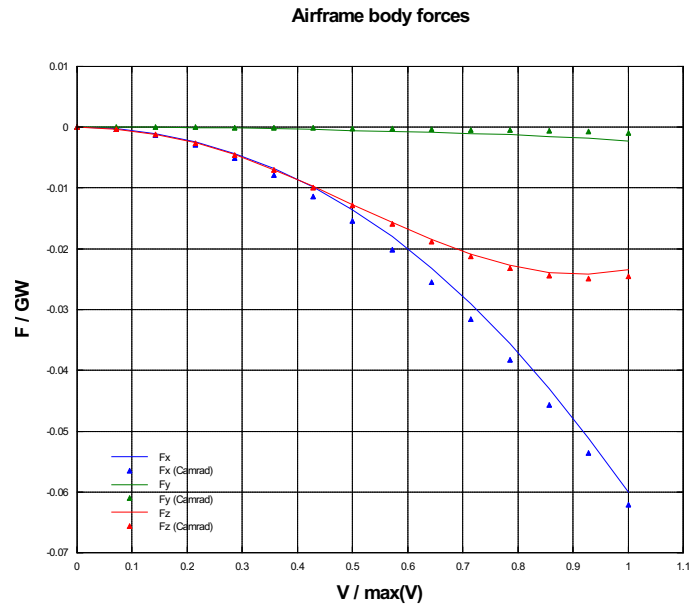


Figure 4.21: Fuselage forces resulting from Camrad trimmed attitude and controls

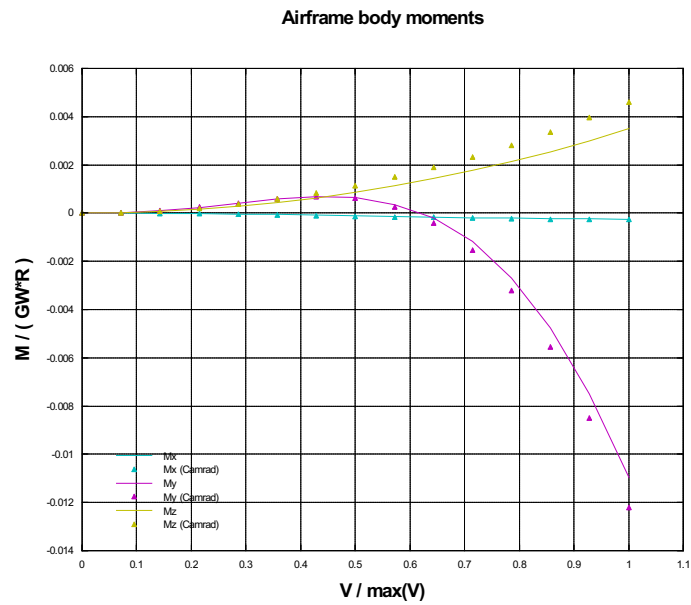


Figure 4.22: Fuselage moments resulting from Camrad trimmed attitude and controls

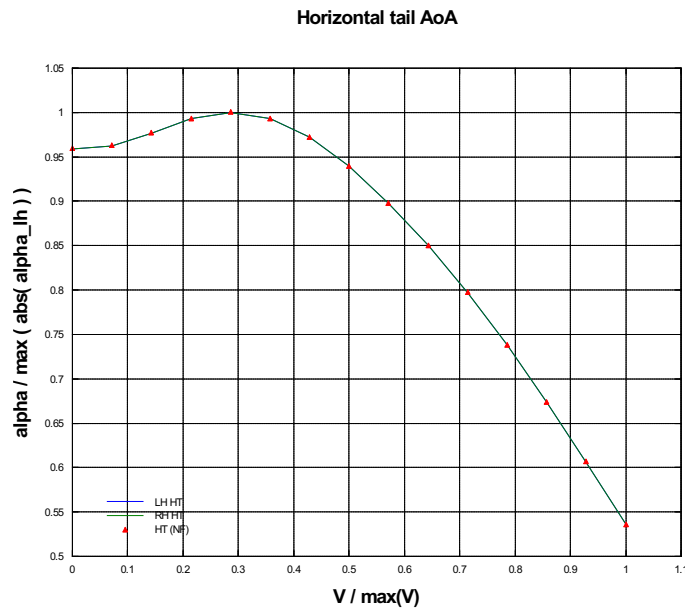


Figure 4.23: Horizontal tail angle of attack resulting from NFpath trimmed attitude and controls

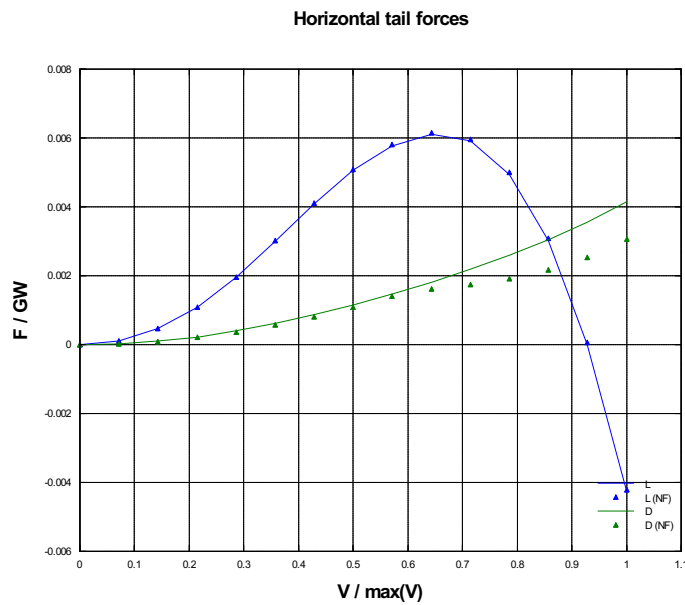


Figure 4.24: Horizontal tail lift and drag resulting from NFpath trimmed attitude and controls

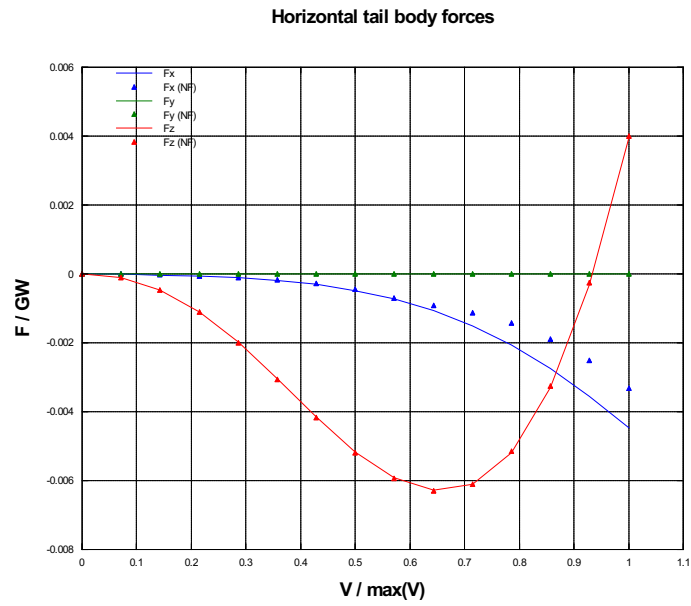


Figure 4.25: Horizontal tail forces resulting from NFpath trimmed attitude and controls

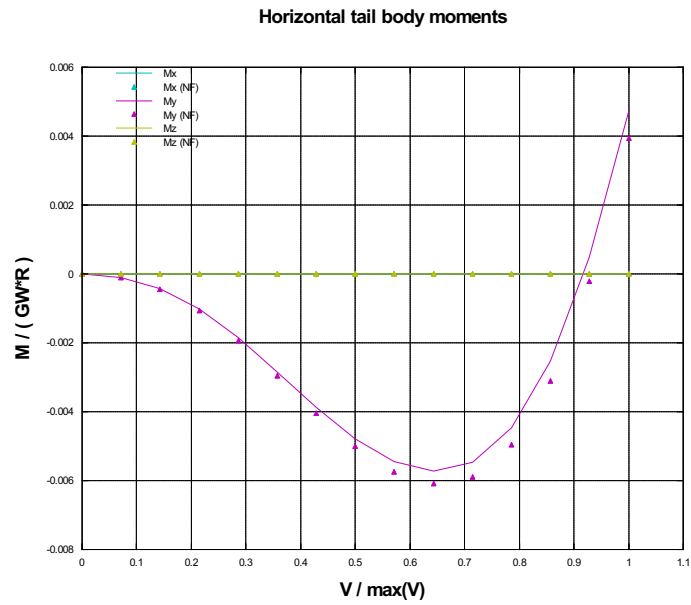


Figure 4.26: Horizontal tail moments resulting from NFpath trimmed attitude and controls

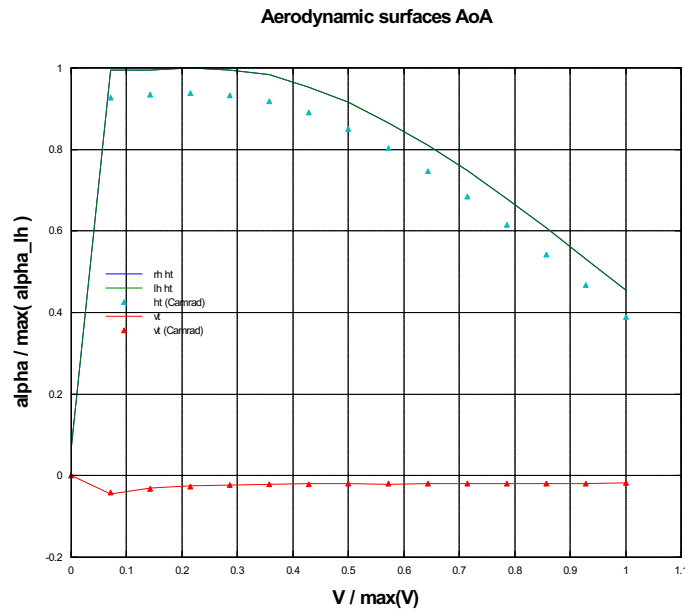


Figure 4.27: Horizontal and vertical tail angle of attack resulting from Camrad trimmed attitude and controls

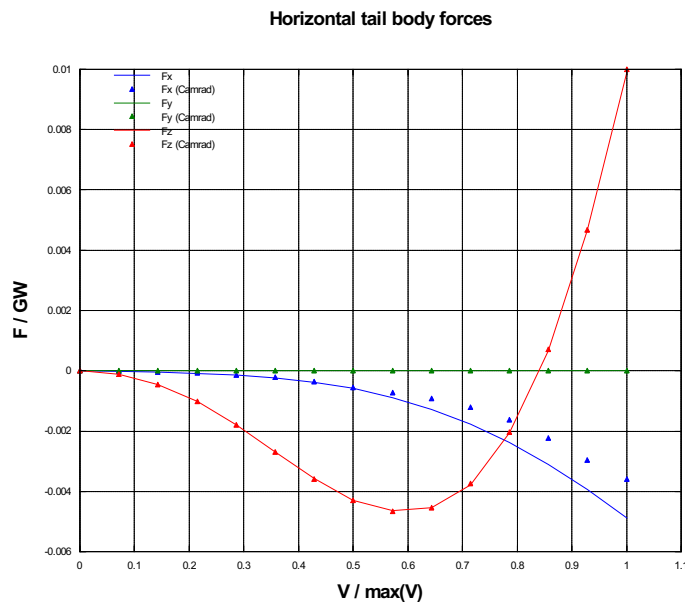


Figure 4.28: Horizontal tail forces resulting from Camrad trimmed attitude and controls

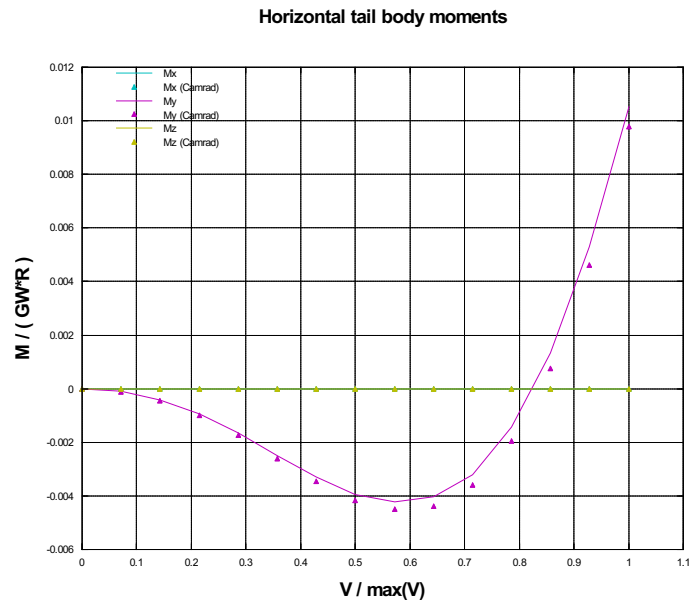


Figure 4.29: Horizontal tail moments resulting from Camrad trimmed attitude and controls

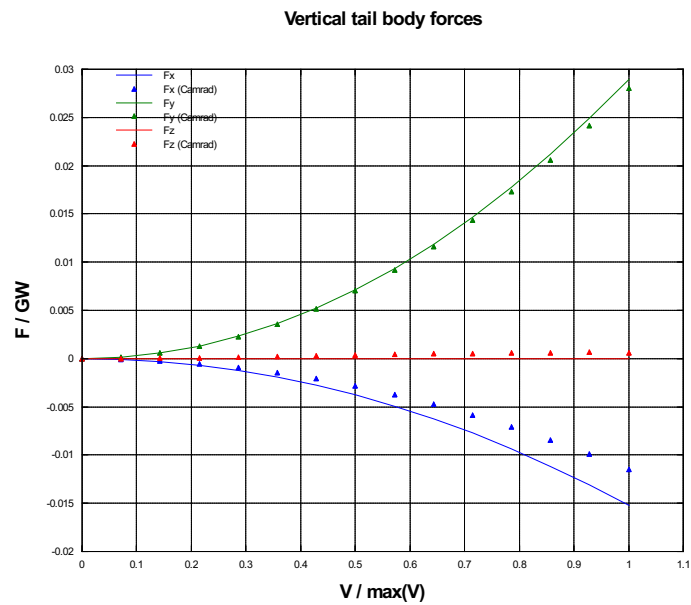


Figure 4.30: Vertical tail forces resulting from Camrad trimmed attitude and controls

attitude and controls was analysed; well start by reviewing this latter analysis, since it gives the rationale for accepting the model.

### 4.3.1 Constant attitude and controls analysis

As described in section 1.2.1.1, *NFpath* evaluates the ground effect based on an experimental curve that relates induced velocity to ground distance; the coefficient introducing the ground effect is linearly interpolated between hover and a fixed speed, which is assumed to be the upper limit for ground effect. As a result, the decrease of ground effect because of horizontal speed is immediate as soon as the rotorcraft begins to move; moreover the speed boundaries and the altitude boundaries of the ground effect region are independent of each other.

Based on the descriptions of the ground effect phenomena found in literature [9, 21], this kind of modelling can be substantially improved; particularly, the sensible effect of accelerating a rotorcraft from hover in ground effect condition is often described as a smooth increase of thrust as the vehicle begins to move, then an abrupt thrust decrease followed by another smooth increase as the vehicle accelerates outside of the ground effect speed region.

The simple model presented in section 1.2.1.1 seems to reproduce correctly this effect, at least from a qualitative point of view. This can be seen clearly in figure 4.32, where the trend for the thrust coefficient versus advance ratio, with constant attitude and controls, is shown.

The trend in the cited figure appears also very similar to the ones appearing in analogous experimental diagrams appearing in [9]; unfortunately this comparison can be assessed only from a qualitative point of view. It was impossible to reproduce the experimental rotor described in the cited reference using the newly implemented model, because of two reasons: the data describing the rotor in the article is incomplete; the described rotor is hingeless, therefore it would be incorrectly represented by the current model.

### 4.3.2 Horizontal speed sweep trim analysis

A trim-to-trim speed sweep comparison of the in-ground-effect behaviour of the model compared to the original *NFpath* code output confirms the qualitative considerations above and confirms that continuity of results is achieved on all the outputs of the model. Results are shown in figures from 4.33 to 4.37.

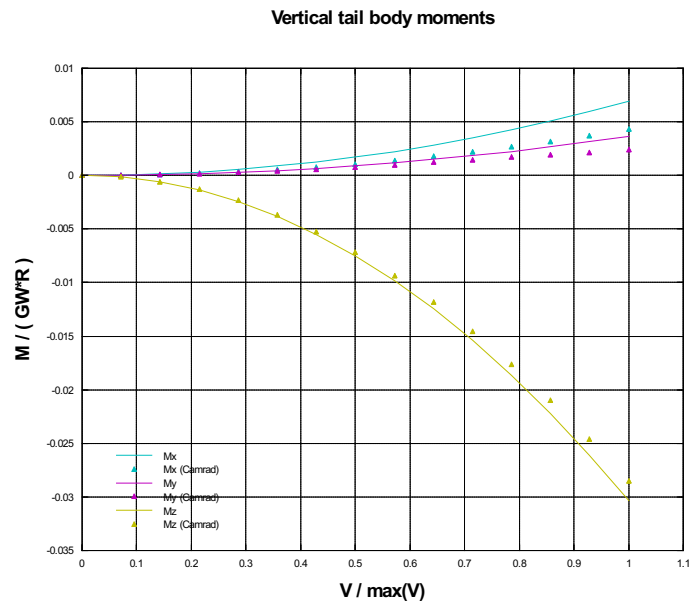


Figure 4.31: Vertical tail moments resulting from Camrad trimmed attitude and controls

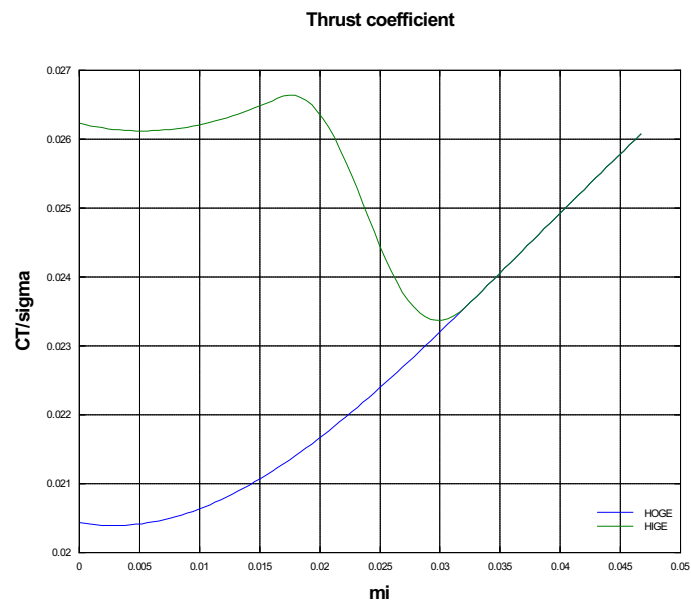


Figure 4.32: Thrust coefficient versus advance ratio at constant attitude and controls

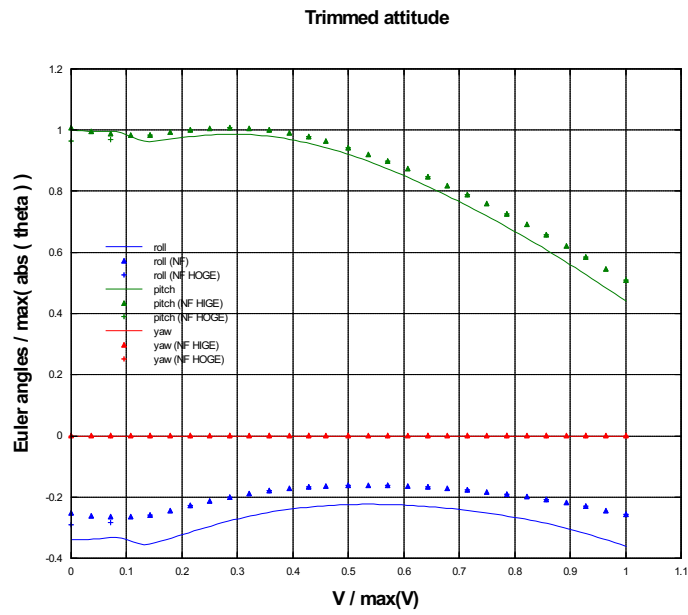


Figure 4.33: Trimmed attitude versus horizontal speed in ground effect

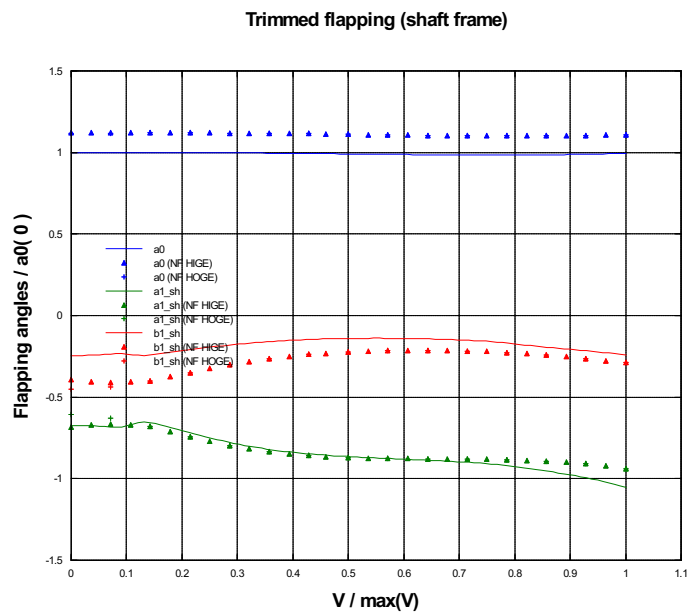


Figure 4.34: Trimmed flapping angles versus horizontal speed in ground effect



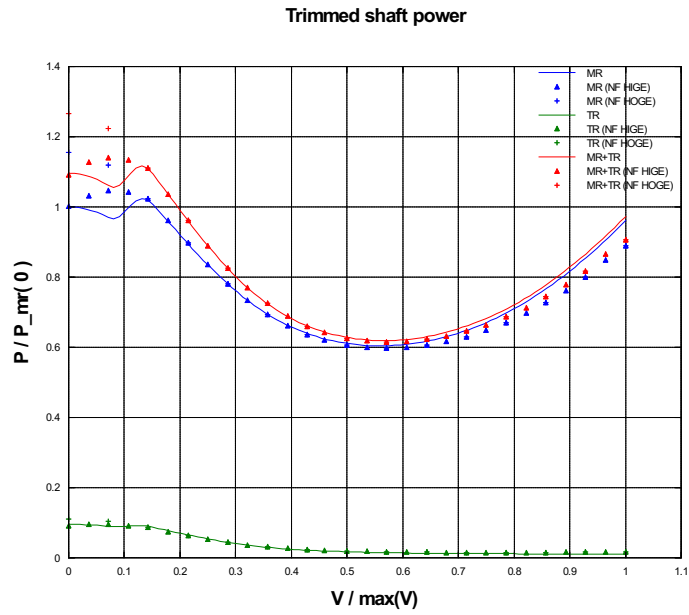


Figure 4.35: Trimmed shaft power versus horizontal speed in ground effect

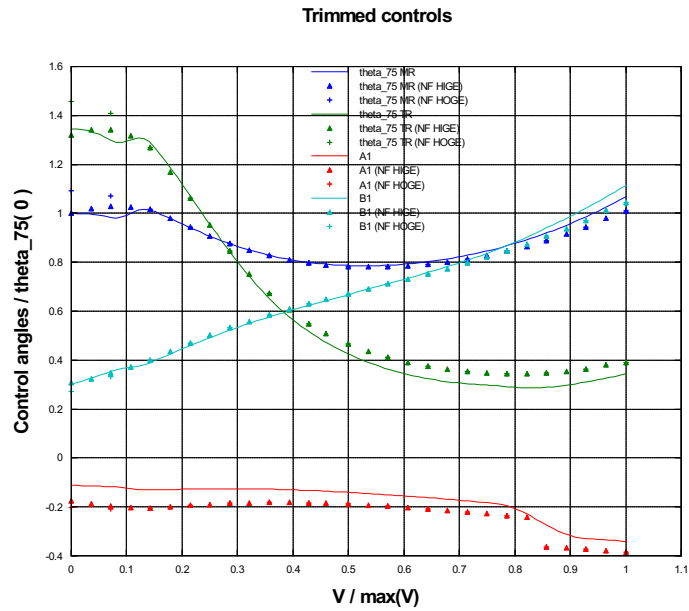


Figure 4.36: Trimmed controls versus horizontal speed in ground effect

### 4.3.3 Ground altitude sweep trim analysis

Another trim-to-trim comparison was performed, this time with a ground altitude sweep. As expected, the model behaves just like *NFpath*, because it shares with it the same experimental curve describing the relationship between induced velocity and ground altitude in hover. As in other analyses, the only significant deviations are found in the coning angle, for the reason explained in section 4.1, and also in the roll angle and in the lateral cyclic pitch control, because of the different, more precise kinematics in the new model. Results are shown in figures from 4.38 to 4.42.

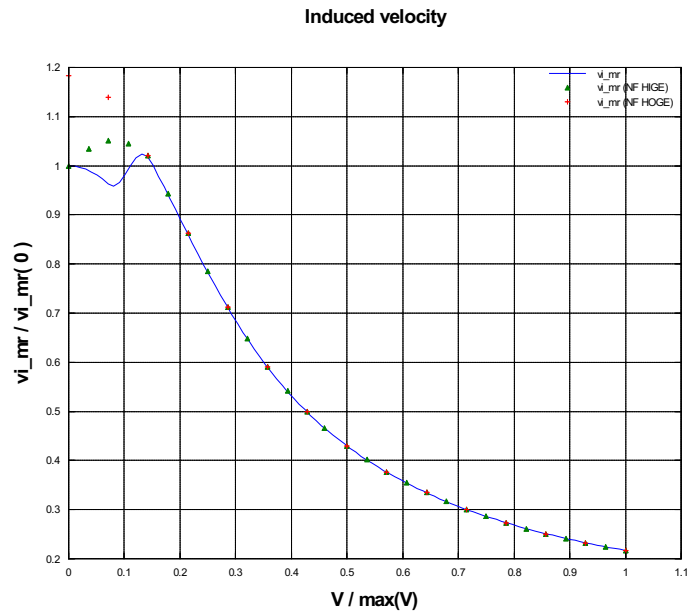


Figure 4.37: Trimmed induced velocity versus horizontal speed in ground effect

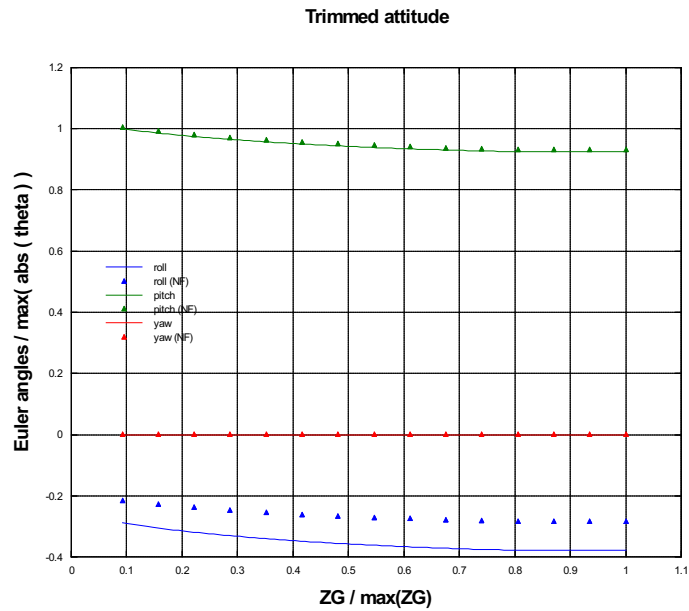


Figure 4.38: Trimmed attitude versus ground altitude, hovering

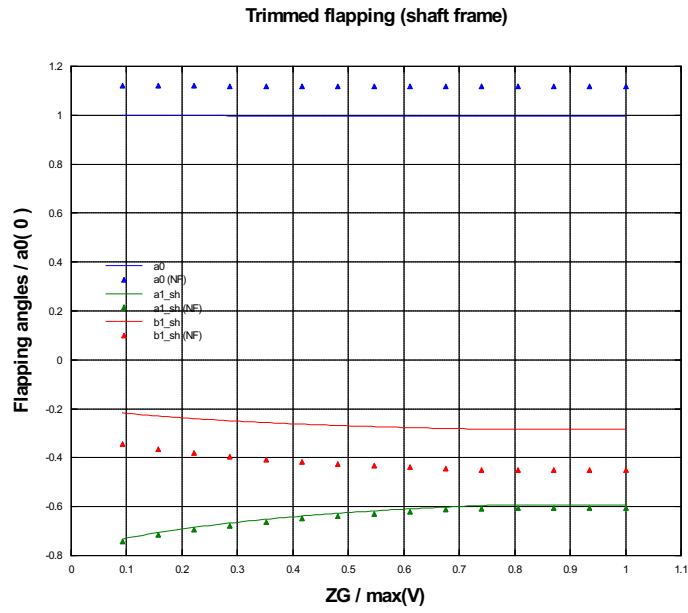


Figure 4.39: Trimmed flapping angles versus ground altitude, hovering

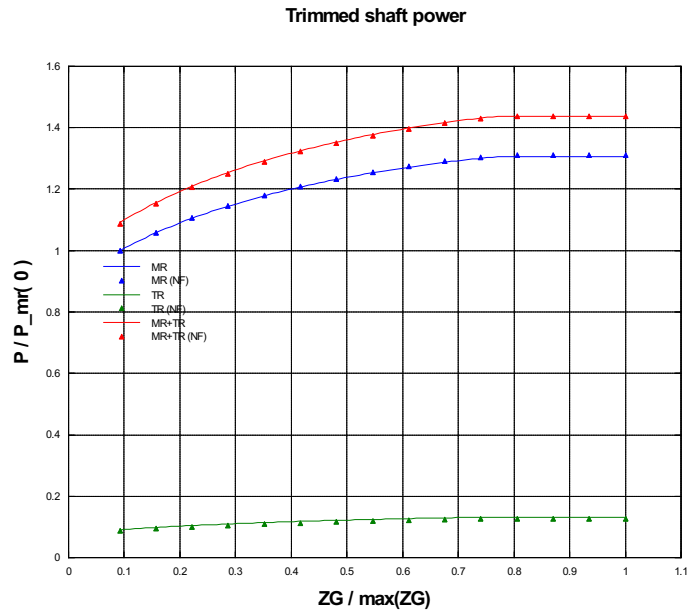


Figure 4.40: Trimmed shaft power versus ground altitude, hovering

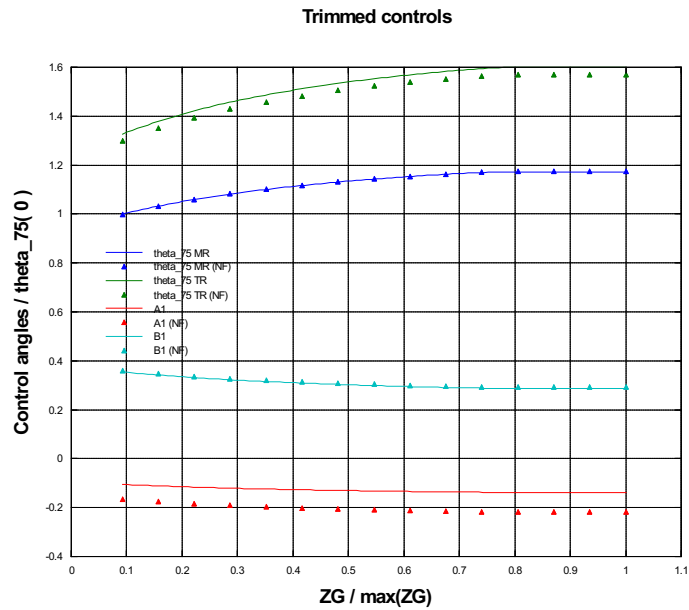


Figure 4.41: Trimmed controls versus ground altitude, hovering

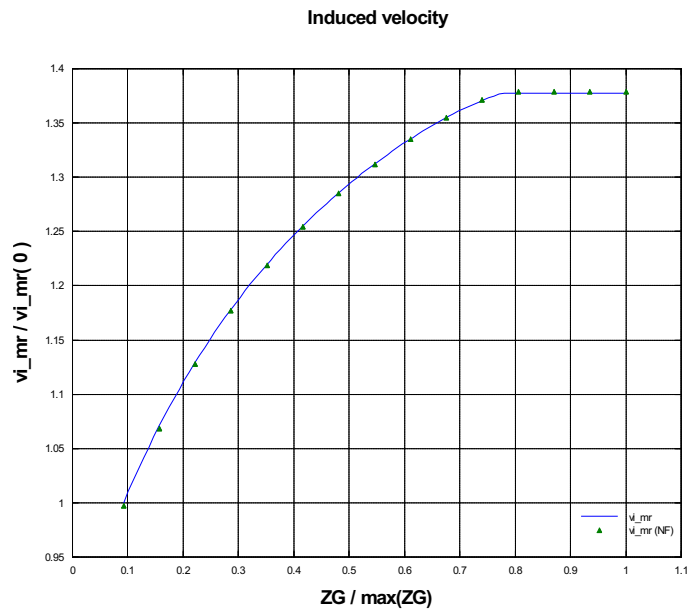


Figure 4.42: Trimmed induced velocity versus ground altitude, hovering



## Conclusions

Through an accurate review of the algorithms used in the well proven *NFpath* code and their comparison to the available literature, a reliable starting point for further development of a simplified rotor model was obtained. The result was a set of equations describing the model and their supporting hypotheses.

The equations were used to newly implement a numerical model, still retaining most of the original limitations, such as the restriction of motion to the longitudinal plane. The re-implemented numerical model was tested against the original code, in order to confirm the coherency of the formulations with the original code.

Starting from the previously obtained set of equations, a new generalised model was developed. The main innovation was to consider a fully three-dimensional motion; in order to accomplish this result, it was necessary to correct the closed form equations so that also the effects of roll rate are taken into account; then the equations need to be solved in a shaft-wind reference frame, rotated of the sideslip angle, so that the azimuth of relative speed is fixed in this reference frame. The introduction of the shaft wind reference frame and the removal of the hypothesis of small attitude angles required to establish a set of reference frame transformations for arbitrary attitude angles. Also the model for ground effect was improved. The model was implemented as modular code in *C* language, with particular care to ensure numerical robustness.

The rotor model was then integrated in a complete rotorcraft simulation model; the author partly contributed also to the general architecture of this complete rotorcraft model and to its implementation. The complete rotorcraft model was designed to be modular; each module represents a force evaluator for each rotorcraft subsystem, whose contributions are then summed.

Both the isolated rotor model and the complete rotorcraft model were the object of an extensive test campaign, with the aim of robustness verification and preliminary validation; all the tests were run in parallel with the original *NFpath* code and with a blade element simulation provided by the *CAMRAD* code; this comparison allowed the assessment of the validity of the new model and of the achieved improvements.

In the light of the results of these comparisons, it is possible to say that the model of the rotor effectively reproduces rotor forces and proved to be robust. While the comparison to *NFpath* shows coherence against a proven code of the same class, the tests against *CAMRAD* confirm that the generalisation and innovations introduced in the new formulations are reliable. The same satisfactory evaluation is valid also for the complete rotorcraft model; though important features such as an interference model are still missing, the overall validity of the model was confirmed. Also the goodness of the code architecture was confirmed, making this model a good starting point for further development.

The possible future enhancements should focus on the limitations that the model still retains because of the original assumptions and formulations that were used. In the case of limitations related to hypotheses, there is little room for further generalisation, because most of the limitations are directly connected with the choice of an algebraic rotor model. On the other side, a new formulation of the set of closed form equations could be obtained with no major conceptual difficulties, but requiring long analytical manipulations; this effort would lead to a well defined set of coherent equations that would replace the current one, derived from many different heterogeneous sources in the literature. In this process many additional parameters (e.g. blade twist, root cut-out, pitch-flapping coupling) could be introduced, while reverse-flow region and gravity effects could be accurately modelled. A further step forward could be accomplished by transitioning from a set of algebraic equations to a set of ordinary differential equations accounting for time derivatives of flapping coefficients; this approach would eliminate the assumption of quasi-steadiness of the rotor, thus making the model more reliable for the simulation of unsteady and fast manoeuvres.



# Appendix A

## Numerical methods

### A.1 Polynomial solution for the inflow

As introduced in section 2.3.3.1, the general solution for the uniform induced velocity, according to the disc actuator theory, is given by the minimum real positive root of the following 4th order polynomial [2]:

$$p(u^*) = u^{*4} - 2v^* \sin \alpha_{\text{TPP}} u^{*3} + v^{*2} u^{*2} - 1 = 0 . \quad (\text{A.1})$$

Since coefficients are functions of other variables, analytical solution of the polynomial, though theoretically feasible, is not practical for a software implementation; then the desired solution will be found numerically.

In order to efficiently and robustly find a numerical solution for the polynomial, it is necessary to bracket the solution itself [20], that means: there is the need to know two values  $u_1^*$ ,  $u_2^*$  that satisfy:

- $p(u_1^*)p(u_2^*) < 0$ , that means that the polynomial evaluates in the two brackets with different sign;
- the domain interval defined by the two variables contains one and only one root of the polynomial.

In order obtain the required brackets, analysis of the polynomial function is required; for ease of discussion we can perform the analysis graphically, referring to the diagrams from figure A.1 to figure A.6, that show the value of the polynomial as a function of induced velocity, airspeed and incidence. For negative and moderately positive incidences, finding the desired solution is straightforward, since the value of the polynomial decreases monotonically with the induced speed and there is only one positive root for each combination of airspeed ad incidence.

As soon as the positive incidence approaches the value for vertical descent, multiple positive roots appear and the polynomial is no more monotonically

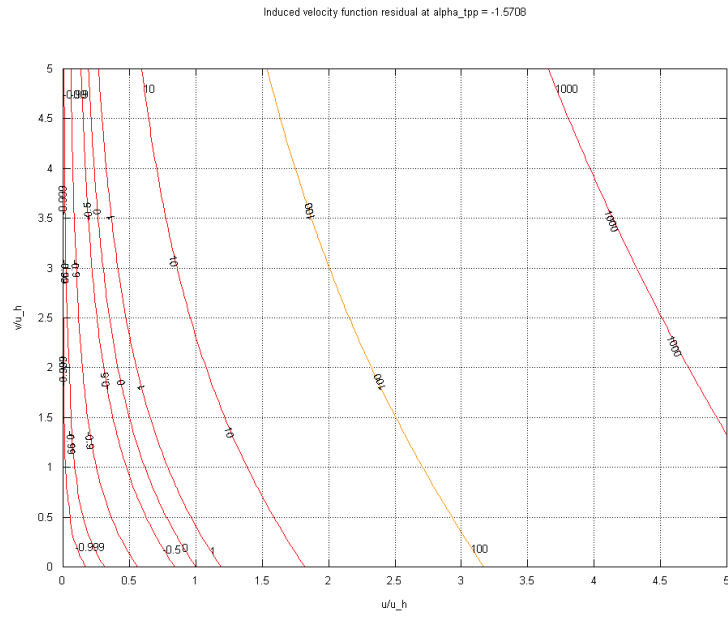


Figure A.1: Induced velocity polynomial residual for  $\alpha_{\text{TPP}} = -\pi/2$

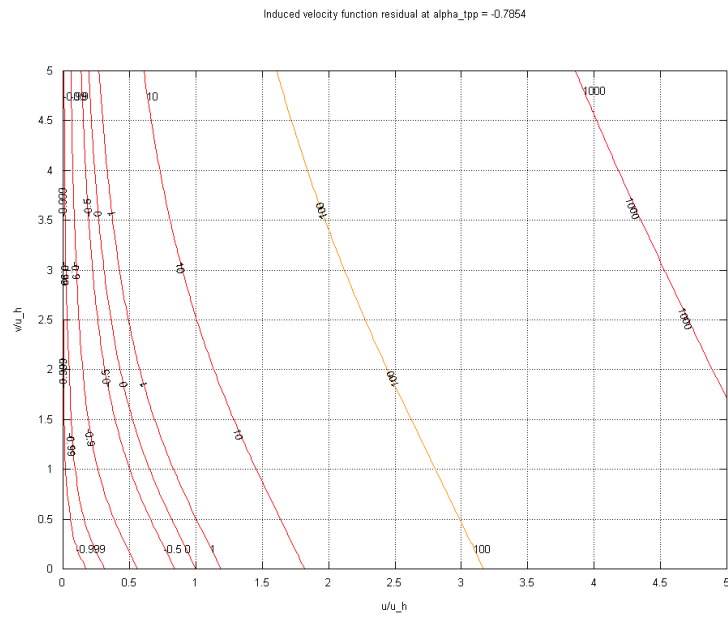


Figure A.2: Induced velocity polynomial residual for  $\alpha_{\text{TPP}} = -\pi/4$

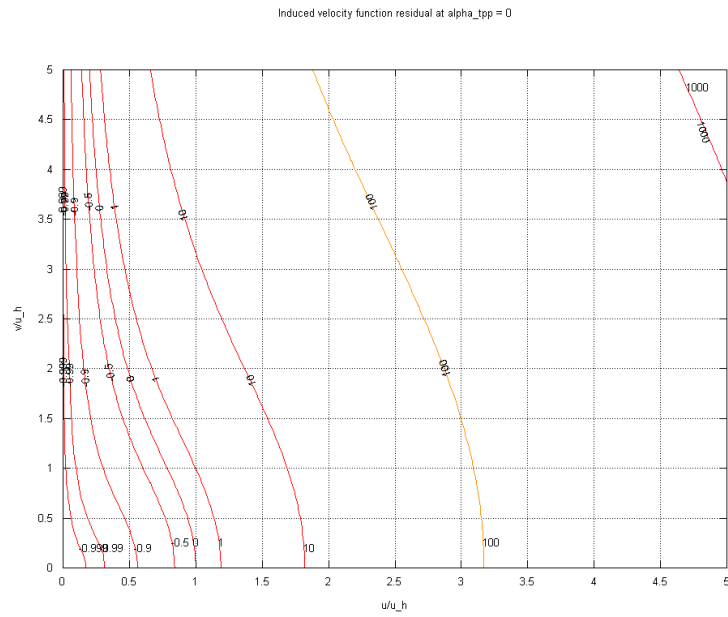


Figure A.3: Induced velocity polynomial residual for  $\alpha_{\text{TPP}} = 0$

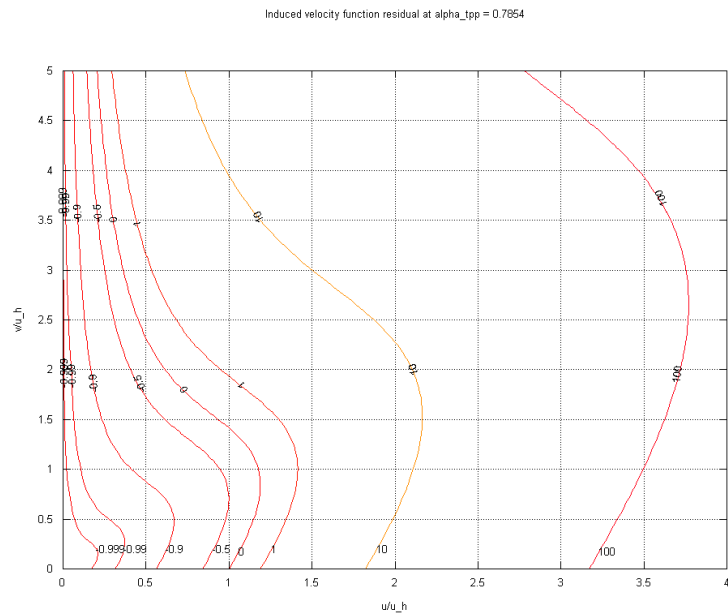


Figure A.4: Induced velocity polynomial residual for  $\alpha_{\text{TPP}} = \pi/4$

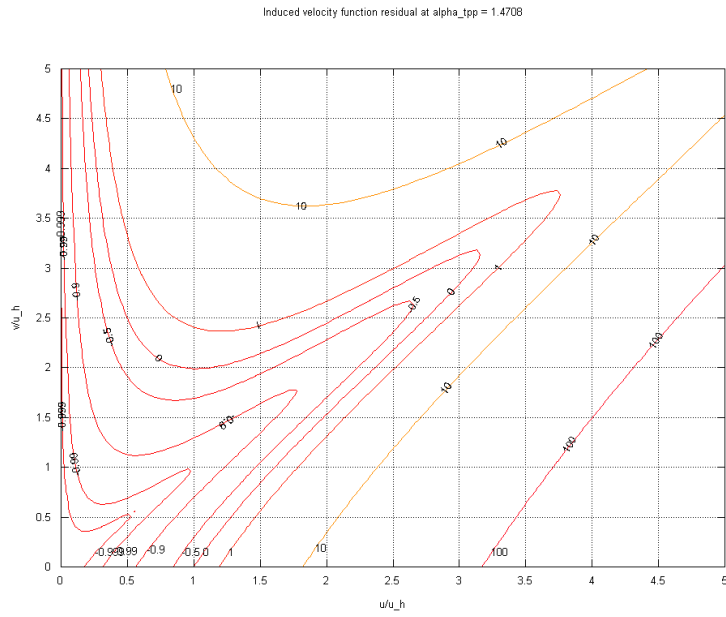


Figure A.5: Induced velocity polynomial residual for  $\alpha_{\text{TPP}} = \pi/2 - 0.1$

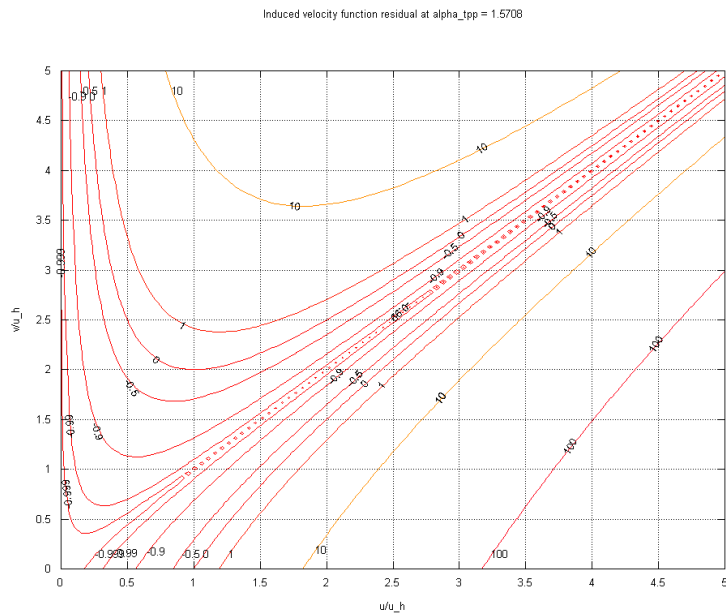


Figure A.6: Induced velocity polynomial residual for  $\alpha_{\text{TPP}} = \pi/2$

decreasing with induced speed; here lies the difficulty in finding suitable brackets for searching the minimum real positive root.

This can be in fact easily accomplished by observing that, if the polynomial evaluates positive in  $u^* = 1$ , then the minimum real positive root lies in the interval  $[0, 1]$ ; if instead it evaluates negative the minimum real positive root exceeds the unity.

While the first interval is a valid bracket for root finding, we still miss an upper limit for the second interval. This can be found remembering that, according to the actuator disc theory, maximum induced speed is found as:

$$\max(u^*) = -\frac{1}{2} \frac{v_v}{u_h} + \frac{1}{2} \sqrt{\frac{v_v^2}{u_h^2} + 4}, \quad (\text{A.2})$$

evaluated for  $v_v/u_h = -2$ . This maximum represents the value obtained prolonging the branch of the induced speed curve for axial flight in climb, hover or slow descent to the lower boundary of the vortex ring state vertical speed range; although this solution doesn't represent a physical solution, it represents the maximum that the induced velocity calculated according to the disc actuator theory can never exceed.

Finally, a procedure for finding the minimum real positive root of the polynomial is found:

1. the polynomial is evaluated in  $u^* = 1$ ;
2. if  $p(1) = 0$ , then  $u^* = 1$ ;
3. if  $p(1) > 0$ , then  $u^* \in [0, 1]$ ;
4. if  $p(1) < 0$ , then  $u^* \in [1, 3.4142]$ ;

Since we know the bracket in which to look for the root and the searched root is real, the search is performed using a robust combination of bisection and Newton-Raphson methods, based on the *rtsafe* algorithm described in [20], modified in order to specialize for polynomial root finding.

Given a polynomial and its first derivative:

$$p(x) = a_n x^n + a_{n-1} x^{n-1} + \dots + a_2 x^2 + a_1 x + a_0, \quad (\text{A.3a})$$

$$\frac{dp}{dx}(x) = n a_n x^{n-1} + (n-1) a_{n-1} x^{n-2} + \dots + 2 a_2 x + a_1, \quad (\text{A.3b})$$

we look for a real unique root  $r$  in a given bracket:

$$\exists! r \in [a, b] : p(r) = 0, \quad (\text{A.4a})$$

$$a < b; p(a)p(b) < 0 . \quad (\text{A.4b})$$

Defining  $r_k$  as the numerical approximation of  $r$  at the  $k$ -th iteration, at each iteration the algorithm checks if the Newton step would lead outside of the bracket:

$$\left( (r_k - b_k) \frac{dp}{dx}(r_k) - p(r_k) \right) \left( (r_k - a_k) \frac{dp}{dx}(r_k) - p(r_k) \right) \geq 0 \quad (\text{A.5})$$

or if the convergence is too slow:

$$2|p(r_k)| > h_k \left| \frac{dp}{dx}(r_k) \right| \quad (\text{A.6})$$

If any of the two conditions is verified, a bisection is applied:

$$h_{k+1} = \frac{1}{2}(b_k - a_k) , \quad (\text{A.7a})$$

$$r_{k+1} = a_k + h_{k+1} , \quad (\text{A.7b})$$

otherwise a Newton step is performed:

$$h_{k+1} = \frac{p(r_k)}{\frac{dp}{dx}(r_k)} , \quad (\text{A.8a})$$

$$r_{k+1} = r_k - h_{k+1} , \quad (\text{A.8b})$$

If the step  $h_k$  is lower than the desired tolerance, the iteration is halted and  $r_k$  is assumed as the numerical solution. Otherwise the bracket is updated:

$$\begin{aligned} p(r_{k+1}) < 0 : a_{k+1} = r_{k+1}; b_{k+1} = b_k , \\ p(r_{k+1}) > 0 : a_{k+1} = a_k; b_{k+1} = r_{k+1} . \end{aligned} \quad (\text{A.9})$$

and a new iteration is started.

## A.2 Broyden's method

Broydens method has been selected for use as solver of the non linear equations set in the rotor model, as described in section 2.3.4.1, as well as for the prototype trim procedure used for analyses section 4.1. This method is particularly suited for an efficient solution of set of equations where the analytical derivatives are not known, since it is Jacobian-free; a numerical approximation of the Jacobian is calculated only for the initialization and later, if needed, as a reset in case of convergence problems.

The basics of the method are illustrated in [22]; some modifications were derived from the implementation described in [20].

Given a system of non linear equations:

$$\mathbf{f}(\mathbf{x}) = 0 , \quad (\text{A.10})$$

we define  $\mathbf{x}_k$  as the numerical approximation of the solution at the  $k$ -th iteration and  $\mathbf{f}_k$  as the residual:

$$\mathbf{f}_k = \mathbf{f}(\mathbf{x}_k) , \quad (\text{A.11})$$

then the foundation of the method lies in the solution of a linear system and in the update of the solution and of the matrix  $\mathbf{Q}_k$  at each iteration:

$$\mathbf{Q}_k \mathbf{s}_{k+1} = \mathbf{f}(\mathbf{x}_k) , \quad (\text{A.12a})$$

$$\mathbf{x}_{k+1} = \mathbf{x}_k + \mathbf{s}_{k+1} , \quad (\text{A.12b})$$

$$\mathbf{Q}_{k+1} = \mathbf{Q}_k + \frac{\mathbf{f}_{k+1} \mathbf{s}_{k+1}^T}{\mathbf{s}_{k+1}^T \mathbf{s}_{k+1}} , \quad (\text{A.12c})$$

with  $\mathbf{Q}_0$  that is initialised as the numerical centred difference Jacobian matrix of  $\mathbf{f}(\mathbf{x}_0)$ .

Convergence can be detected on the solution (by comparing a norm of  $\mathbf{s}_k$  to the tolerance on the solution) or on the residual (by comparing a norm of  $\mathbf{f}_k$  to the tolerance on the residual).

Some additional features in order to improve robustness of the method were implemented. In order for a step to be acceptable, we set the condition:

$$\mathbf{f}_{k+1}^T \mathbf{f}_{k+1} < \mathbf{f}_k^T \mathbf{f}_k . \quad (\text{A.13})$$

In case the condition is not satisfied, the step is not accepted and the following actions are taken before trying a new step:

- if  $\mathbf{Q}_k$  was calculated as an update to the previous step, a new  $\mathbf{Q}_k$  is calculated as the numerical Jacobian in  $\mathbf{x}_k$ , and a new  $\mathbf{x}_{k+1}$  is calculated with it;
- if  $\mathbf{Q}_k$  is already the numerical Jacobian in  $\mathbf{x}_k$ , the new  $\mathbf{x}_{k+1}$  is calculated halving the advance  $\mathbf{s}_{k+1}$ .

By repeating the second action for a sufficient number of times, it is guaranteed that a value for  $\mathbf{s}_{k+1}$  will be found, which is little enough in order for  $\mathbf{x}_{k+1}$  to satisfy the condition for the acceptance of the step. Then the regular iteration scheme can be resumed.





# Appendix B

## Reference systems

Each reference frame is described by three unitary vectors  $\mathbf{i}$ ,  $\mathbf{j}$ ,  $\mathbf{k}$ ; coordinates along the respective axes are named  $x$ ,  $y$ ,  $z$ ; the reference frame is identified by a subscript.

### B.1 Inertial frame

The origin of the inertial frame is an arbitrary fixed point in space. Axis  $z_I$  is directed as as the gravity acceleration:

$$\mathbf{k}_I = \frac{\mathbf{g}}{|\mathbf{g}|} . \quad (\text{B.1})$$

Vector  $\mathbf{i}_I$  points toward an arbitrary direction (possibly North) normal to  $\mathbf{k}_I$ , and  $\mathbf{j}_I$  completes a right-handed triad.

Contrary to this definition, in *NFpath* formulations, vertical quantities referred to the inertial frame are positive upwards.

### B.2 Design frame

The design frame and its origin  $D$ , which is fixed relative to the airframe, are defined by the STA-BL-WL coordinate system according to the customary convention:  $\mathbf{i}_D$  is directed to the aft of the vehicle,  $\mathbf{j}_D$  is positive to the right and  $\mathbf{k}_D$  is positive upwards.

### B.3 Body frame

The origin  $O$  of the body frame is an arbitrary point fixed to the airframe; this point is assumed as reference for position, velocities, accelerations, forces, and moments acting on the vehicle. Vector  $\mathbf{i}_B$  is directed longitudinally towards

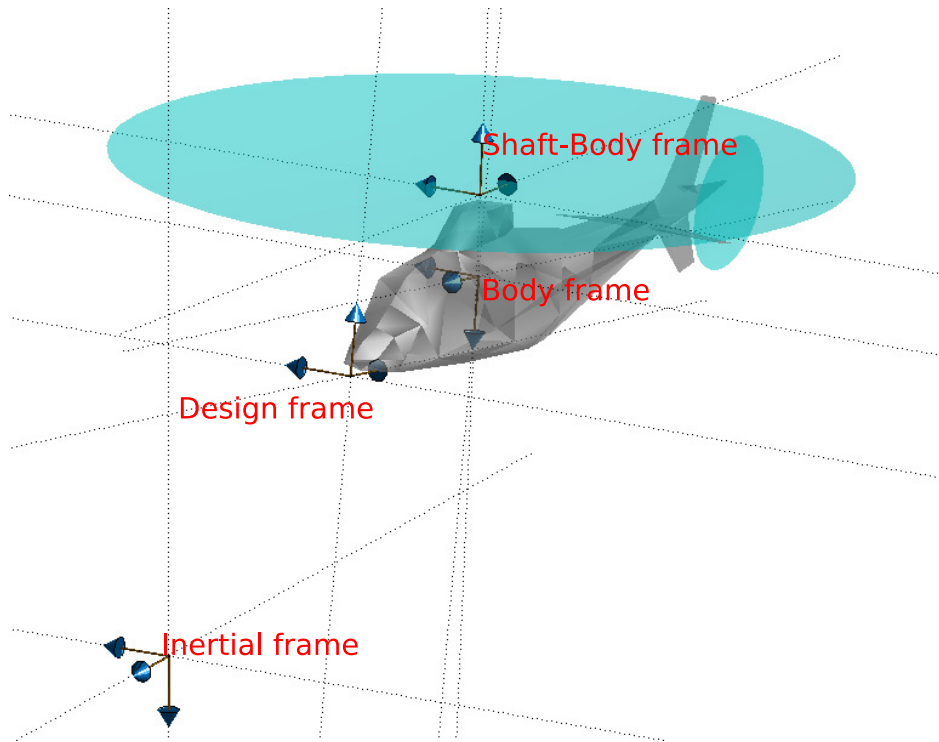


Figure B.1: Overview of the main reference frames

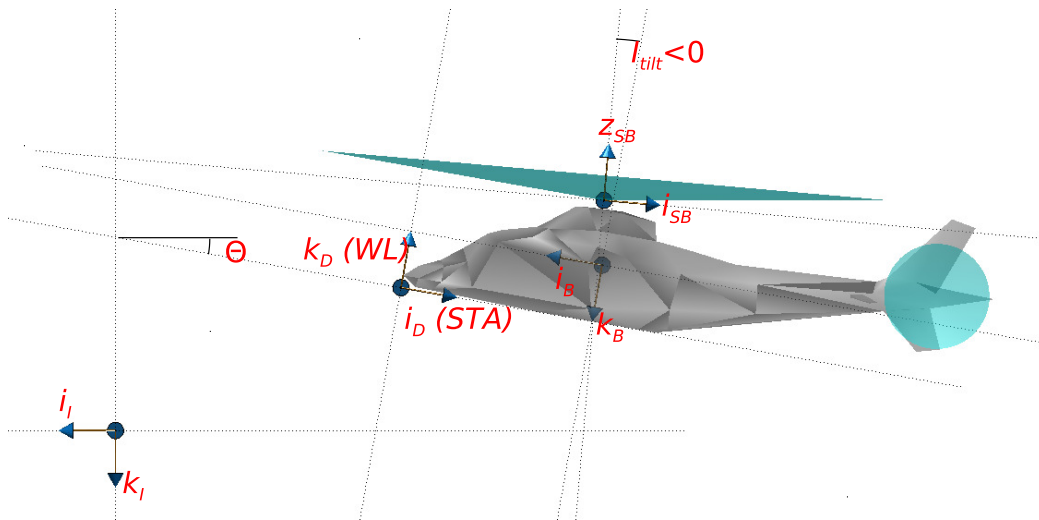


Figure B.2: Main reference frames, lateral view

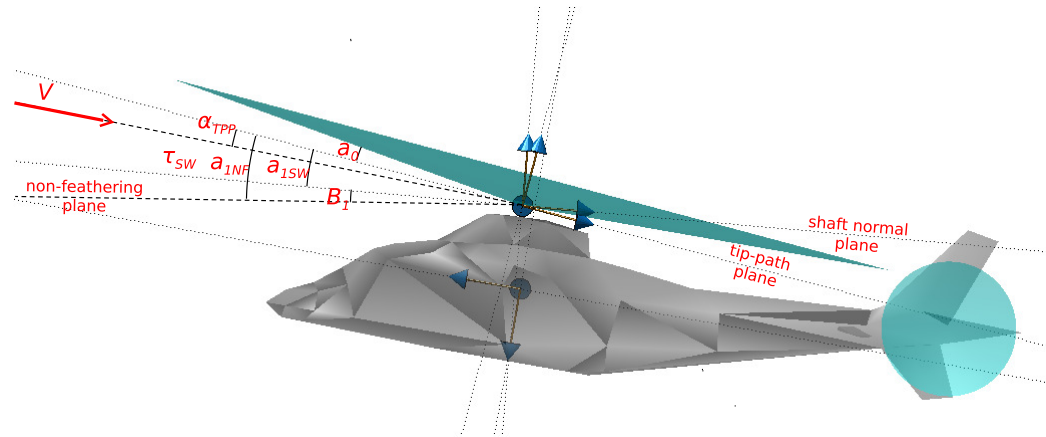


Figure B.3: Flapping angles, lateral view

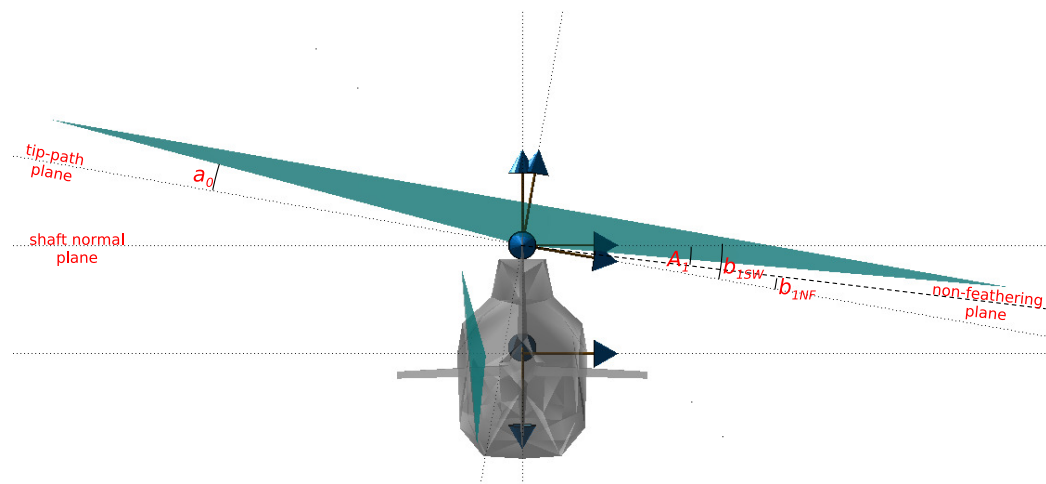


Figure B.4: Flapping angles, rear view

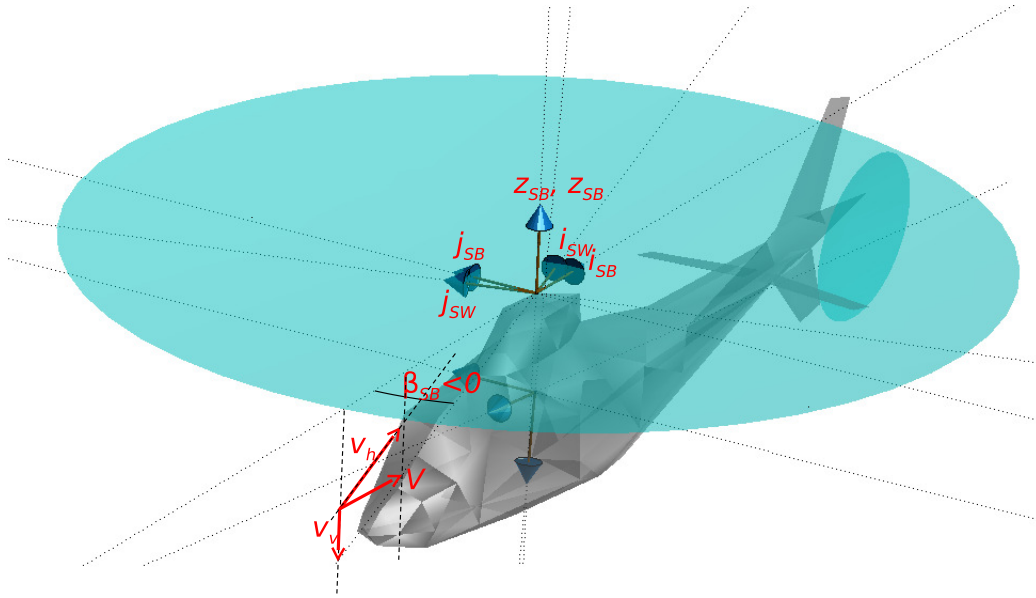


Figure B.5: Relationship between shaft-body and shaft-wind reference systems

the front of the vehicle (typically in the plane of symmetry),  $\mathbf{j}_B$  is normal to  $\mathbf{i}_B$  and directed to the right and  $\mathbf{k}_B$  completes a right-handed triad, being directed downwards.

For the sake of simplicity, in this document the design frame and the body frame share the same orientation of axis, with  $\mathbf{i}$  and  $\mathbf{k}$  having inverted signs in the respective frames. Thus the body triad with reference to the design frame will be assumed to satisfy:

$$\mathbf{i}_D = -\mathbf{i}_B, \quad (\text{B.2a})$$

$$\mathbf{j}_D = \mathbf{j}_B, \quad (\text{B.2b})$$

$$\mathbf{k}_D = \mathbf{k}_B. \quad (\text{B.2c})$$

In *NFpath* the origin of the body frame, that is the reference point for moments, is located at the intersection of the rotor shaft axis with the plane parallel to  $\mathbf{i}_B$  and  $\mathbf{j}_B$  containing the centre of gravity.

## B.4 Shaft-body frame

The shaft-body frame identifies the reference rotor configuration accounting for tilt angle, cant angle and nacelle tilt angle (for tilt-rotors). The origin  $P$

of the shaft frame is located along the rotor mast axis, at the nacelle pivot hinge; for conventional rotorcraft  $P$  is an arbitrary point along the rotor mast axis, possibly the rotor hub centre.

The unity vector  $\mathbf{k}_{SB}$  is directed as the mast axis, pointing upwards, while vector  $\mathbf{i}_{SB}$  points backward. The third vector  $\mathbf{j}_{SB}$  completes a right-handed triad.

## B.5 Shaft-wind frame

The origin  $C$  of the shaft-wind is the hub centre. All rotor forces are assumed to be applied to this point.

The unity vector  $\mathbf{k}_{SW}$  is directed as the mast axis, pointing upwards, and is identical to  $\mathbf{k}_{SB}$ . The unity vector  $\mathbf{i}_{SB}$  is normal to  $\mathbf{k}_{SW}$  and lies on the plane defined by  $\mathbf{k}_{SW}$  and the asymptotic airspeed vector  $\mathbf{V}$ . The direction of  $\mathbf{i}_{SW}$  is the same as the direction of the projection of  $\mathbf{V}$  on a plane normal to  $\mathbf{k}_{SW}$ . The unity vector  $\mathbf{j}_{SW}$  completes a right-handed triad.

The shaft wind triad is defined so that the airspeed vector  $\mathbf{v}$  always lies on the right half-plane defined by  $\mathbf{i}_{SW}$  and  $\mathbf{k}_{SW}$ . This property is of great importance for the calculation of forces acting on the rotor, since it allows using the classical closed-form equations, which are always defined for a forward advancing rotor.

## B.6 Shaft frame

In the *NFpath* code the shaft-wind frame and its rotation with reference to the shaft-body frame are not defined; however, if we assume that the rotorcraft advances and take into account the hypothesis that motion is restricted to the longitudinal symmetry plane, we can consider the shaft-wind frame to coincide with the shaft-body frame; in this case the unique frame will be called simply shaft frame and it will be indicated with subscript  $S$ .

## B.7 Tip-path plane frame, flapping and blade pitch

Blade flapping motion is approximated as first order truncated Fourier series having coning and flapping angles as coefficients:

$$\beta(\psi) = a_0 - a_1 \cos \psi - b_1 \sin \psi . \quad (\text{B.3})$$

The coning and flapping angles can be referred either to the shaft-body frame, or to the shaft wind frame; the blade azimuth  $\psi$  is measured from the direction of  $\mathbf{i}_{SB}$  or  $\mathbf{i}_{SW}$ , according to the reference frame being considered.

When the flapping hinge eccentricity  $e_\beta$  is zero, the trajectory of the blade tips defined by the previous series lies on a plane that is called tip-path plane (TPP). The same definition of TPP will be retained also for non-zero eccentricity values, which are typically in the order of a few percent of the rotor radius, since the blade tip trajectory is nonetheless a good approximation of a plane.

The unity vector  $\mathbf{i}_{\text{TPP}}$  has the same direction and sign as the projection of the asymptotic airspeed on the TPP,  $\mathbf{k}_{\text{TPP}}$  is normal to the TPP and pointing upwards relative to the rotor and  $\mathbf{j}_{\text{TPP}}$  completes a right-handed triad.

Similarly the blade pitch is defined as a first order truncated Fourier series:

$$\theta(\psi) = \theta_0 - A_1 \cos \psi - B_1 \sin \psi . \quad (\text{B.4})$$

The following relationships are assumed as valid, even if they are strictly true only for rotors with zero flapping hinge eccentricity:

$$a_1^{\text{NF}} = a_1^{\text{SW}} + B_1 ; \quad (\text{B.5a})$$

$$b_1^{\text{NF}} = b_1^{\text{SW}} - A_1 . \quad (\text{B.5b})$$

that means that the force-motion phase delay on the blade is assumed to be always exactly  $90^\circ$ .

# Nomenclature

## Symbols

Unless otherwise stated, SI units are implied.

$a_0$	Coning angle
$a_1$	Longitudinal flapping angle
$A$	Rotor disc area
$A_1$	Lateral cyclic pitch
$b_1$	Lateral flapping angle
$B_1$	Longitudinal cyclic pitch
$c$	Blade chord
$C_d$	Drag coefficient
$C_l$	Lift coefficient
$C_{L/\alpha}$	Slope of the lift/AoA curve for the blade profile
$C_H$	H-force coefficient
$C_T$	Thrust coefficient
$e_\beta$	Flapping hinge eccentricity
$\mathbf{g}, g$	Gravity acceleration vector, absolute value
$h_{cd}$	H-force coefficient (alternative definition)
$H$	H-force
$\mathbf{i}_A, \mathbf{i}_A, \mathbf{i}_A$	Unit vectors for reference frame A
$I_\beta$	Blade flapping moment of inertia
$\mathbf{J}_O$	Second moment of inertia matrix, pole O
$m$	Total rotorcraft mass
$M_b$	Blade mass
$N_b$	Number of blades
$P$	Power
$Q$	Shaft torque
$R$	Rotor radius
$R_{A \rightarrow B}^C$	Rotation tensor from frame A to frame B, measured in frame C
$\mathbf{S}_O$	First moment of inertia matrix, pole O
$t_{cd}$	Thrust coefficient (alternative definition)

$T$	Thrust
$u$	Induced velocity
$u_h$	Induced velocity, hovering condition
$v_h$	Horizontal speed, inertial
$v_{\text{tip}}$	Blade tip speed
$v_v$	Vertical speed, inertial, positive upwards
$\mathbf{V}, V$	Asymptotic speed vector, absolute value
$x_{\text{cg}}$	Radius of the blade centre of mass, divided by $R$
$z_g$	Height over ground
$\alpha$	Angle of attack
$\alpha_{\text{TFP}}$	Angle of attack of the rotor disc
$\beta$	Flapping angle
$\beta_{\text{SB}}$	Sideslip angle
$\gamma$	Lock's number
$\epsilon$	Hinge offset factor or influence angle
$\theta$	Blade pitch
$\theta_0$	Collective pitch, untwisted blade
$\theta_{75, \text{twisted}}$	Collective pitch, measured at 75% span of the real blade
$\Theta$	Attitude Euler's pitch angle
$\iota$	Setting angle
$\lambda$	Inflow parameter
$\lambda_i$	Induced inflow parameter
$\mu$	Advance parameter
$\nu$	Parameter for the inflow distribution
$\rho$	Air density
$\sigma$	Rotor solidity ratio
$\tau$	Climb angle
$\Phi$	Attitude Euler's roll angle
$\psi$	Blade azimuth
$\Psi$	Attitude Euler's azimuth angle
$\Omega$	Rotor angular speed

## Acronyms and abbreviations

AoA	Angle of Attack
CFD	Computational Fluid Dynamics
DOF	Degree of Freedom
fus	Fuselage
HT	Horizontal tail



I	Inertial (reference frame)
MR	Main Rotor
NF	Non-Feathering (plane)
SB	Shaft-Body (reference frame)
SW	Shaft-Wind (reference frame)
TPP	Tip-Path Plane
TR	Tail rotor
VT	Vertical Tail



## Bibliography

- [1] AgustaWestland. *AgustaWestland Flight Mechanics Rotorcraft (AWFMR) Rev. 19*, 2010.
- [2] M. Arra. *L'elicottero*. Hoepli, Milano, 2001.
- [3] S. Basu. *Freemat v4.0 documentation*, 2009.
- [4] C. Bottasso. Three dimensional rotations. Lecture notes, 2006.
- [5] A. R. S. Bramwell, G. Done, and Balmford D. *Bramwell's helicopter dynamics*. Butterworth Heinemann, Oxford, UK, 2001.
- [6] R. T. N. Chen. A simplified rotor system mathematical model for piloted flight dynamics simulation. Technical Report TM-78575, NASA, 1979.
- [7] R. T. N. Chen. Effects of primary rotor parameters on flapping dynamics. Technical Report TP-1431, NASA, 1980.
- [8] C. C. Critzos, H. H. Heyson, and R. W. Jr. Boswinkle. Aerodynamic characteristics of NACA 0012 airfoil section at an angle of attack from  $0^\circ$  to  $180^\circ$ . Technical Report TN-3361, NACA, 1955.
- [9] H. C. Jr. Curtiss, M. Sun, W. F. Putman, and E. J. Jr. Hanker. Rotor aerodynamics in ground effect at low advance ratios. *Journal of the American Helicopter Society*, 29(1), 1984.
- [10] W. Johnson. *CAMRAD/JA A Comprehensive model of rotorcraft aerodynamics and dynamics - Volume II (Users manual)*. Johnson Aeronautics, Palo Alto, CA, USA, 1988.
- [11] B. W. Kernighan and D. M. Ritchie. *Il linguaggio C - Principi di programmazione e manuale di riferimento*. Pearson Prentice Hall, Milano, second edition, 2004.
- [12] K. W. Mangler and H. B. Squire. The induced velocity field of a rotor. Technical Report 2642, Aeronautical Research Council, 1950.

- [13] M. Maniscalchi. Codice NFpath - manuale utente. Technical Report 200-90-015/03, Agusta, 2003.
- [14] L. Masellis. Development of a simplified rotor model. In *Proceedings of the Seventh Pegasus-AIAA Student Conference*, 2011.
- [15] Microsoft, Redmond, WA, USA. *MSDN Library for Visual Studio 2008 Express Editions*.
- [16] F. Nannoni. Pgm. NFtrim - manuale teorico. Technical report, Agusta.
- [17] F. Nannoni. Sizing e prestazioni di un velivolo ad ala rotante. Presentation, Agusta, 2002.
- [18] F. Nannoni and A. Stabellini. Simplified inverse simulation for preliminary design purposes. In *Proceedings of the Fifteenth European Rotorcraft Forum*, 1989.
- [19] G. D. Padfield. *Helicopter flight dynamics*. Blackwell Publishing, Oxford, UK, second edition, 2007.
- [20] W. H. Press, S. A. Teukolsky, W. T. Vetterling, and B. P. Flannery. *Numerical recipes in C*. Cambridge University Press, Cambridge, UK, second edition, 1992.
- [21] R.W. Prouty. *Helicopter performance, stability, and control*. Krieger Publishing Company, Malabar, FL, USA, 2005. Reprint with corrections.
- [22] A. Quarteroni, R. Sacco, and F. Saleri. *Matematica numerica*. Springer, Milano, second edition, 2000.
- [23] J. B. Wheatly. An aerodynamic analysis of the autogiro rotor with a comparison between calculated and experimental results. Technical Report TR-487, NACA, 1934.